SAPIENZA
UNIVERSITÀ DI ROMA

UNIVERSITÀ DI ROMA "LA SAPIENZA"

Ph.D in Mathematical Models for Engineering, Electromagnetics and Nanosciences – XXXI Cycle

Curriculum: Electromagnetism

Design and Measurements of the High Gradient Accelerating Structures

Dottorando: Mostafa Behtouei

Supervisor: Prof. Luigi Palumbo

Co-Supervisor: Dr. Bruno Spataro

February 2019

Contents

List of Figures

List of Tables

List of Symbols

ϵ	absolute permittivity of vacuum (8.854 $\times 10^{-12}$ F/m)
σ	electrical conductivity (rad/sec)
RF	radio frequency
SW	standing wave
TW	traveling wave
$TM\ modes$	transverse magnetic modes
$TE\ modes$	transverse electric modes
MHz	mega hertz (10^6 Hz or cps)
GHz	giga hertz (10^9 Hz or cps)
P	power loss
U	stored energy
ω_r	resonant frequency (f), (rad/sec)
Q	quality factor of the cavity
Q_0	unloaded quality factor
Q_L	loaded quality factor
Γ	reflection coefficient
T	transmission coefficient
α	attenuation
dB	decibels
ν_g	group velocity
ν_p	phase velocity
β	propagation constant
k	wavenumber
k_c	cutoff wavenumber
k_z	wavenumber at the direction of propagation

λ	wavelength (m)
λ_c	cutoff wavelength (m)
λ_r	resonant wavelength (m)
Z	impedance
J_m	Bessel functions of the first kind
J'_m	derivative of the Bessel functions of the first kind
R_s	RF surface resistance
δ	skin depth
P_{LW}	power losses in the walls
P_{LE}	power losses in in the end caps of the cavity
G	geometric factor
R	shunt Impedance
b	radius of the cavity
ℓ	length of the cavity
a	iris (aperture) radius
V_{acc}	voltage of acceleration
c	velocity of light
E_z	axial electric field
E_ϕ	azimuthal electric field
E_r	radial electric field
H_z	axial magnetic field
H_ϕ	azimuthal magnetic field
H_r	radial magnetic field
h	iris thickness
LNF	National Laboratory of Frascati
ϕ	phase advance
FEM	Finite Element Method
R_{eff} or ZTT	effective shunt impedance
TTF or T	transit time factor
ff_1	field flatness (maximum field in central cell/ field field in the last cell)

ff_2	field flatness (maximum field in central cell/ field field in the first cell)
s_{11}	reflection coefficient in decibel
ΔT	RF pulsed heating
C_ϵ	specific heat
t	pulse length
k	thermal conductivity
ρ	density
S_c	poynting vector
PC	personal computer
$GPIB$	Generated Purpose Interface Bus
VNA	Vector Network Analyzer
TIG	Tungsten Inert Gas
EBW	Electron Beam Welding
$HFSS$	High Frequency Structures Simulator
$SuperFish$	2D High Frequency Structures Simulator
P_{01}	normalization constant proportional to the power flow of the TM_{01} mode
η_0	impedance of free space (≈ 377)
α_e	electric polarizability of the aperture
α_m	magnetic polarizability of the aperture
$\bar{P}_e$	infinitesimal electric polarization currents (electric moment)
$\bar{P}_m$	infinitesimal magnetic polarization currents (magnetic moment)
E_k	Kilpatrick field (MV/m)
t_F	filling time factor
$SPARC$	Frascati Linac Coherent Light Source
$SBAI$	Basic Science Applied for Engineeing
$INFN$	Italian National Institute for Nuclear Physics

E_{sF} and H_{sF}	scattered fields (radiation fields) due to the polarizability of the iris
Z_{01}	wave impedance of the TM_{010} mode
SMA	SubMiniature version A (antenna)
$\bar{E}_{\mp}$	electric field radiated from the sources propagating in the negative (positive) z direction
$\bar{H}_{\mp}$	magnetic field radiated from the sources propagating in the negative (positive) z direction
A_{01}^{-} and A_{01}^{+}	amplitudes of the radiation fields due to iris as a dipole
$\delta(x)$	dirac delta function
S_{11p}	perturbed reflection coefficient
S_{11p}	unperturbed reflection coefficient

Acknowledgments

I would like to thank Prof. Luigi Palumbo, who has given me the great possibility to start this thesis work under his supervision and Dr. Bruno Spataro (INFN-LNF) for his continuous support of my Ph.D study and related research, for all his helpful comments, suggestions and enthusiastic support. His guidance helped me in all the time of research and writing of this thesis. I could not have imagined having a better advisor and mentor for my Ph.D study. I want to express my gratitude to Dr. Luigi Faillace from INFN-LNF for stimulating and instructive discussions. I would also to acknowledge Prof. Zirilli from Department of Mathematics for his useful suggestions. Thanks to all people from INFN-LNF and the University of Rome "La Sapienza", in particular Prof. Andrea Mostacci for his help in offering me the resources in running the program and technical support.
Special thanks to all my friends who helped me throughout my Ph.D program specially Giovanni Castorina and Luca Ficcadenti.
Last but not the least, it is my privilege to thank my wife, Marjan. Her support, quiet patience, encouragement and unwavering love were undeniably the bedrock upon which the ten years of my life have been built. I owe my deepest gratitude to my parents for supporting me spiritually throughout my life in general.

Chapter 1

Introduction

Electric field can be delivered to a charged particle through a particle accelerator. The beam inside the accelerators gains its energy from either constant electric field or a harmonic time-varying electric field. The first one was electrostatic accelerator in which particle acquires an energy equal to the product of its electric charge times the potential drop, and led to a unit of energy called the electron volt (eV). The maximum energy obtainable was the limitation of this accelerator because the maximum energy is obtained from the product of the charge times the potential difference, and from practical point of view this potential difference is limited by electric breakdown. The later is called RF accelerators and the limitation can be bypassed by localizing a harmonic time-varying electric field to the beam, technically speaking to the bunches. When the field has the correct polarity these bunches will be arrived to take maximum energy of the field and the restriction of energy gain will be removed and the bunches are accelerated into the structures where the electromagnetic cavity resonators excite a particular electromagnetic mode through a high-frequency external power source. For a stable and sustained energy gain the beam must maintain synchronism and phase properly with the fields. The latter requirement has led to the name resonance accelerators, which includes the linac, cyclotron, and synchrotron distinguishing from their orbit in an RF accelerator , the straight line, spiral and circle, respectively. The first formal proposal and experimental test of an RF linac was made by Rolf Wideroe in 1928, but linear accelerators that were useful for nuclear and elementary particle research did not appear until after the development of microwave technology in World War II when high frequency power generators, developed for radar application, became available. Then modern linacs were born

by proposing an accelerator based on a linear array of drift tubes enclosed in a high-Q cylindrical cavity by Luis Alvarez .

The present thesis work contained to the design and measurements of the RF High gradient structures. Generally speaking the design of an accelerating structure is a complex task, and it is not possible to have a procedure that fits in all related applications. Conventionally, the starting point to design a structure is from the specification stating the desired performance of the cavity. Then, some constraints will appear which limit the possibilities of implementation. The next issue to consider at the higher order mode frequencies is the side effects the cavity will have and there also are some parameters which must be chosen to optimize the overall design.

In chapter 2 of this thesis in order to properly understand and be able to choose between a standing-wave or a traveling-wave structure, we briefly introduce the main parameters usually used to characterize Linacs and we will explain why the periodic accelerating structure are used in particle accelerators by the statement has been brought by Floquet to the literature. As the dispersion relation of a structure contains the detailed information needed to determine its suitability for particle acceleration, such as phase and group velocities as a function of frequency, we have decided to dedicate chapter 3 to have a comparison between analytical and numerical methods to estimate group velocity. The concept of group velocity is fundamental in high accelerating periodic structures. It can be obtained from resonant-frequency change due to the cavity perturbation. In the framework of the Compact Light XLS project, we are studying a TW band accelerating structure operating at frequency f=23.988 GHz or f=35.982 GHz in order to linearize longitudinal space phase. Numerical electromagnetic simulations were carried out by using the numerical code HFSS in the frequency domain. In chapter 4 we calculated analytically the shunt impedance, quality factor (Geometric factor) and R/Q independent of the frequency for TM modes for a single cylindrical "pill-box" cavity as these modes in a chain of cylindrical "pill-box" cavities provide accurate model for the accelerating fields in more realistic accelerating structures and the properties of a single cylindrical resonator were simple to treat analytically, and it was as a starting point for accelerating structures. In chapter 5 and 6 the design and measurements of the RF High gradient structure have been done. As the achievement of ultra high accelerating gradients is mandatory in order to fabricate compact accelerators at 11.424 GHz for scientific and industrial applications,

an extensive experimental and theoretical program to determine a reliable ultra high gradient operation of the future linear accelerators is under way in many laboratories. In particular, systematic studies on the 11.424 GHz frequency accelerator structures, R & D on new materials and the associated microwave technology are in progress to achieve accelerating gradients well above 120 MeV/m. To determine the maximum sustainable gradients in normal conducting RF powered particle beam accelerators operating at X-band with extremely low probability of RF breakdown, an electroformed SW structures has been fabricated and characterized by SLAC and INFN with collaboration of other institutes around the world at 11.424 GHz, coated with Au-Ni and with different surface roughness. We designed a gold plate RF High gradient structure operating at the X-band coated with Au-Ni . Bench measurements have been performed in the Department of SBAI of the University of Rome "La Sapienza". The Slater Method for the SW cavity has been employed in order to quantify the electric field inside the structure.This method is a resonant method that only allows to measure the amplitude of the field. A perturbing object (1 mm in length and 1 mm in diameter) is attached to an horizontal fish lens that lays on the same direction as the axis of the structure. By using a step-by-step motor, it is possible to pull the wire through the structure and measure the perturbations caused by the small bead. The measurement setup is referred to as "bead-pull". The frequency shift in the structure has been measured. All the data, obtained by using a VNA, are stored in a PC via a GPIB. Comparing the results with the results exposed from HFSS we report the features that have been quantified, showing good agreement. In chapter 7 we introduced two theoretical approaches for reflection coefficient calculation in a pill-box cavity. The first one in the chapter has been accomplished by circuit theory and the later by modified Bethe's theory. A method to find the overall Q of a resonant circuit is used for a cavity coupled to an external transmission line or waveguide usually contains the RF generator and Q calculation led to the shunt impedance calculation and considering a wave that is emitted from the generator into the guide, the reflection coefficient produced by the cavity load impedance has been calculated. The results was a good agreement comparing with the numerical results. The other analytical approach is based on a theory which states that the aperture is equivalent to an electric or/and magnetic dipole moments. These dipole moments are respectively proportional to the normal electric and magnetic field of the incident wave. The theory originally stated by Bethe, developed by Collin and

modified by S. De Santis, A. Mostacci and L. Palumbo for small hole compared to the wavelength. We applied the theory for TM_{01} mode cavities coupled by a small hole with a thickness size comparable to the wavelength. The amplitudes of forward and backward waves due to polarizabilites have been determined and we found equations for reflection and transmission coefficients. At the end it should be mentioned that for the future work we are studying on the emittance growth of electron beams due to the cylindrical asymmetry of an rf gun.

Chapter 2

General Description of Periodic Structures

2.1 Linear RF structures

A linear particle accelerator is a device in which the charge particles accelerate on a linear path through an array of the cavities (cells) . These kind of devices are called RF liner accelerators or often shortened to Linac and usually operate in a frequency range of 100 MHz up to several GHz. At lower energies they can be used as an injectors to synchrotrons while at high energies are used as colliders. The main advantages of linear accelerators can be summarized as follows:

- An efficient transverse focusing can be achieved by reaching high energy;
- There is no crucial limiting factor such as electric breakdown in linear accelerator as in electrostatic accelerators, where we have got the maximum energy beam of the order of MeV;
- In comparison with circular machines there is an easier procedure for the beam injection and extraction;
- capability of delivering high energy and focused beams;
- As the geometric dimensions are proportional to the electromagnetic field wavelength, increasing the frequency means decreasing the size of accelerating devices. Therefore, high frequency devices have small dimensions.

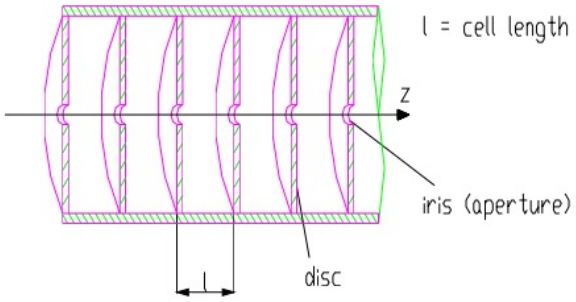

Figure 2.1: Iris-loaded structure

2.2 General Principles of RF Linear Accelerators

Electromagnetic power generated by a klystron or a magnetron usually feeds an RF accelerating structure. The metallic waveguide brings the RF power to the Linac by a complicated system such as circulators in which reflected power can be avoided to go backwards and harm the source. In general there are two types of accelerating structures:

1-Traveling-wave (TW) structures

In these RF waveguide accelerators the electromagnetic field travels with a phase velocity of the injected beam and the beam is synchronized with the traveling wave following linear energy gain along the structure. The reason an iris or metallic disk is used along the waveguide axis is because any electromagnetic field pattern would always have a phase velocity greater than the speed of light, and it would never be locked to any particle beam and this velocity needs to be smaller than the speed of light. In order to avoid this issue, it is necessary to load the TW structure with the irises, usually with a certain period L. The electromagnetic field is need to be damped at the end of the Linac in a matched impedance load. Figure (2.1) shows such a disc-loaded structure.

2.Standing-wave (SW) structures

This structure is constructed from some cavities which are aligned longitudinally and coupled together either electrically or magnetically. The structure is not open and it is closed because it needs to be built up a resonant stationary wave inside it. This resonant RF power is trapped inside the Linac and there is no need to be damped unlike the case of TW Linacs and theoretically all injection power can be used to accelerate the beam.

2.3 Characteristic parameters of a Linac

In this section to understand and distinguish a difference between a standing-wave and a traveling-wave structure we introduce the main parameters usually used to characterize Linacs ([1], [2], [3], [33]). These parameters are used to represent accelerating devices by means of electric circuits [4].

1. Average electric field: E_0, average electric field on axis in the direction of the beam propagation at a given time when $E(t)$ is max. How much field is available for acceleration.

$$E_0 = \frac{1}{L}\int_0^L E(0,0,z)dz. \tag{2.1}$$

2. Shunt impedance: Z, ratio of the average electric field squared (E_0^2) to the power (P) per unit length (L) dissipated on the walls surface, as shown in Eq.2.2. How well the RF power is concentrated in the useful region.

$$Z = E_0^2 \,.\, \frac{L}{P} \quad or \quad Z = E_0^2 \,.\, \frac{dL}{dP}. \tag{2.2}$$

3. Quality factor: Q, ratio of the stored energy (U) to the power lost on the wall (P) in one RF cycle.

$$Q = \frac{2\pi.f}{P} \,.\, U. \tag{2.3}$$

4. Transit time factor: T, ratio of the energy gained in the time varying RF field to that in a DC field. Measure of the reduction in energy gain caused by the sinusoidal time variation of the field in the gap.

$$T = \frac{|\int_{-L/2}^{+L/2} E_z(z) \,.\, e^{-j(\frac{\omega z}{\beta c})dz}|}{\int_{-L/2}^{+L/2} |E_z(z)|dz}. \tag{2.4}$$

Transit time factor describes the reduction of the voltage that a real particle experiences relative to a fictitious particle with infinite speed. It is instructive again to look at the simple pillbox cavity with the z - independent E_z , where the expression for TTF simply becomes:

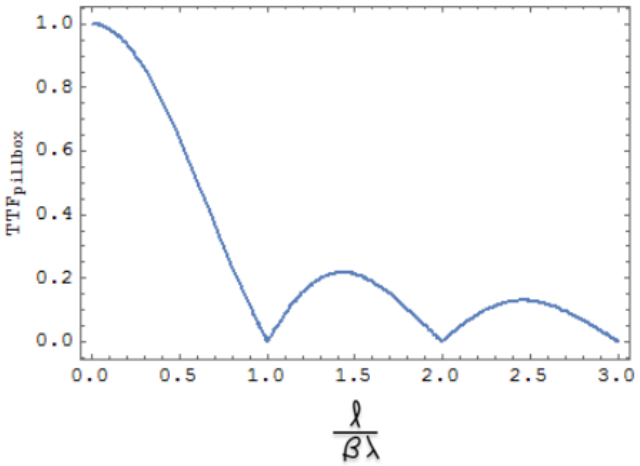

Figure 2.2: The transit time factor of a pillbox cavity as a function of its length ℓ

$$TTF_{pillbox} = \frac{|sin(\frac{\chi_{01}\ell}{2a})|}{\frac{\chi_{01}\ell}{2a}}. \tag{2.5}$$

Eq. (2.5) can be plotted as we shown in Fig. (2.2). Note that TT = 1 for very small gaps, and decreases for larger gaps. It reaches zero when the transit time of the charged particle is an entire RF period, i.e., when $\ell = \beta\lambda$.

5. Effective shunt impedance: ZT^2, while the shunt impedance measures if the structure design is optimized, the effective shunt impedance measures if the structure is optimized and adapted to the velocity of the particle to be accelerated.

$$ZTT = (E_0T)^2 \cdot \frac{L}{P}. \tag{2.6}$$

The peak surface electric field and magnetic field are important constraints in cavity design. In normal conducting cavities, too large peak surface electric field can result in electric breakdown. The Kilpatrick criterion is often used as the basis for the peak surface electric field limit in normal conducting cavities.

In superconducting cavities high electric field causes field emission, which produces electrons in the cavity volume that absorb RF energy and create additional power loss. The surface magnetic fields correspond to surface currents that produce resistive heating.

6. Frequency: Operating frequency as working point of an accelerating structure when designing a linac is one of the main parameters to be chosen.To make it possible to choose

this parameter we have to know the variation of the cavity parameters with the frequency. As an example, the shunt impedance for the unit length, Z_{SH}/m is proportional to square root of frequency, which means higher frequency lead to the higher shunt impedance and it provides higher efficiency in beam acceleration. It should also be noted that the probability of RF breakdowns as a consequence of the intense superficial electric field changes inversely with the frequency and it means, the probability of RF breakdowns diminishes with increasing frequency. This is explained by the Kilpatrick experimental relationship:

$$f(MHz) = 1.64E_k^2 \; Exp(-\frac{8.5}{E_k}), \tag{2.7}$$

where E_k(MV/m) is called the Kilpatrick field and f(MHz) is the frequency of the field. The equation above establishes an upper limit for the superficial field (E_k) at a given frequency. Beyond the Kilpatrick field value, the chance of breakdowns at that frequency starts to rapidly raise, resulting in damages of the material the Linac is made out of.
There is another parameter for the Linac RF design which is called Kilpatrick factor and it is defined as the ratio of the superficial electric field E_s, that the structure can actually support, to the value of the Kilpatrick field for the same frequency. Usually, this ratio is less than 2 although in some cases is possible to reach higher values.

7. Group velocity ν_g and filling time factor t_F

$$\nu_g = \frac{P}{U}, \tag{2.8}$$

$$t_F = \int_0^L \frac{dz}{\nu_g(z)}, \tag{2.9}$$

where P and U are the power flux through the structure with length L and the stored energy per unit length, respectively. For not having the small efficiency of acceleration it would be convenient to have small values of the group velocity, usually in the order of 0.01c and 0.02c. Also, the same reason for the filling time factor keeping it within reasonable values. The equation above for filling time represents the time the electromagnetic energy needs to fill the whole structure, is only used for traveling-wave accelerators. In the case of standing-wave Linacs, where the electromagnetic energy builds up in time with a zero group velocity, the parameter t_F is defined as

$$t_F \propto \frac{Q}{U}. \tag{2.10}$$

2.4 Dispersion Curve

The difference between traveling-wave and standing-wave particle accelerators is not crucial from a theoretical point of view . Superposition of two traveling waves in opposite direction constructs a standing wave. The construction interference between forward waves and reflected waves from the iris allows the wave propagation along the axis in an iris loaded structure, see Fig.(2.1). It follows that it is possible to enclose the structure between two metallic plates placed at symmetry plane locations so that the stationary field pattern, at a given time, is the exact representation of the traveling one [33]. In this configuration, electromagnetic parameters of the TW structure, such as phase or group velocity of the desired accelerating mode and the shunt impedance per unit length can be measured by using the equivalent stationary instantaneous mode of n resonant cavities coupled together. It should be noted that for the standing and traveling waves the definition of phase advance of the electromagnetic field is different. In a TW Linac, the phase-shift is determined by the phase increase, or decrease, of the field traveling from the center of a cell to the subsequent one, while for a SW structure, it refers to the field configuration, since the phase difference is either 0 or π. Figure (2.3) shows the dispersion curve for n-coupled cavities, with n = 3.

2.5 Comparison of "effective shunt impedance" between TW and SW structures

Figure (2.4) [5] illustrates the behavior of the shunt impedance per unit length as a function of different phase shift between each cell. To each phase-shift corresponds a different accelerating mode.

As it is evident, the value of the effective shunt impedance for TW structures is almost twice that for SW accelerators except for the π mode in which case the two values match. Another important parameter is the pulse length from the generator that feeds an accelerating structure. In a TW structure, the excited electromagnetic field needs a time t_F ,

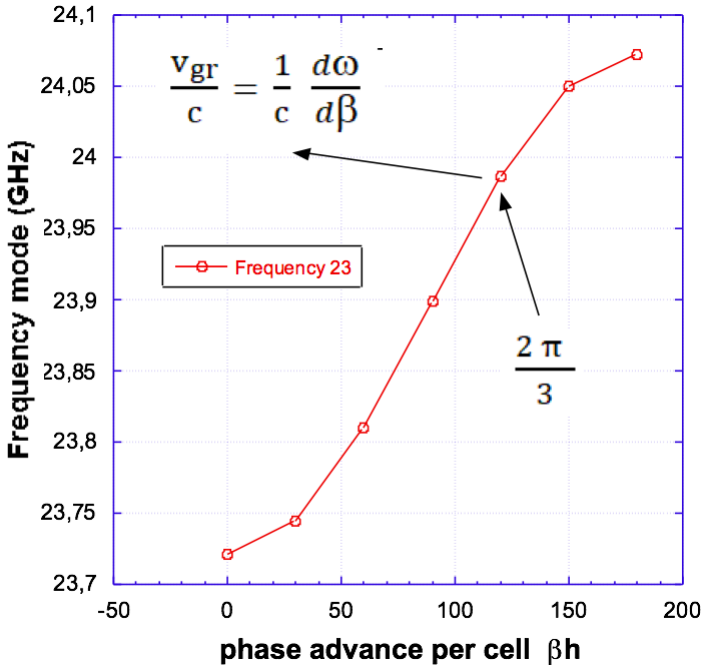

Figure 2.3: Dispersion curve of a 3 cell cavities

the filling time factor defined as L/Vg (Vg= group velocity, L=length of the Linac) while in a SW structure the field distribution "builds up" in a longer time due to subsequent reflections. It follows that, since the beam is usually injected into the Linac after the filling time, all the power used for the transient is not used to accelerate it, that means it is lost. Then, it is reasonable that for "long pulse" operation the unused power is small compared to the total RF power, so that the choice of the type of structure only depends on the kind of particle to be accelerated or the desired phase-shift. On the other hand, in "short pulse" operation the lost transient power is a large amount of the total one, so a TW structure, with a small filling time, is preferred to an SW one.

2.6 Scaling structure design

One should ask what is the most important parameters to choose to design a linac, the response is operating frequency. With the knowledge of the variation of the cavity parameters with the frequency we can choose a frequency in which the linac should be operate. As it has shown in Table (2.1), scaling the cavity dimension b (cavity radius) with frequency all other parameters vary proportional or inversely or in some case has a non linear dependence and vary faster than the frequency.

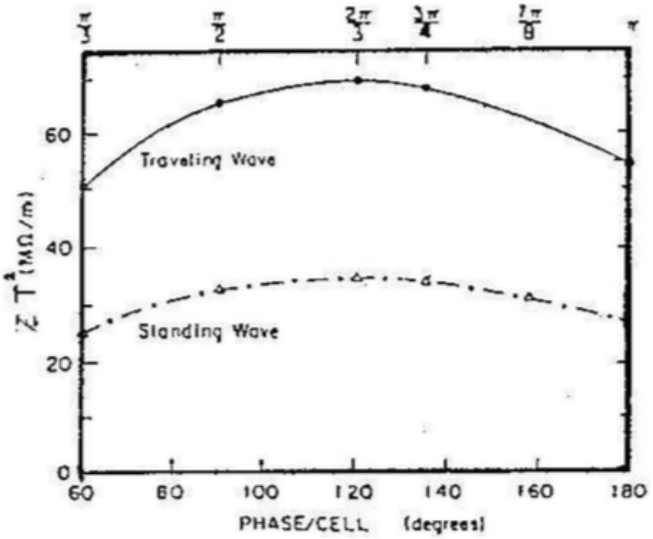

Figure 2.4: Diagram of the effective shunt impedance per unit length as a function of the phase shift, for both TW and SW structures.

Parameters	Frequency scaling
Cavity dimension(b)	f^{-1}
Quality factor(Q_0)	$f^{-1/2}$
Geometric factor(G)	f^0
Stored Energy (U)	f^{-2}
Shunt Impedance (R)	$f^{1/2}$
R over Q (R/Q)	f^1
RF surface resistance (R_s)	$f^{1/2}$
RF power loss in 1 meter [MW]	$f^{-1/2}$

Table 2.1: Scaling Frequency

2.7 Periodic accelerating Structures

The main reasons which the periodic accelerating structure are used are because: the wave must have an electric field component along the direction of particle motion and this condition can be satisfied by a transverse magnetic wave propagating in a uniform waveguide. The particle and the wave must have the same velocity to maintain synchronism and the uniform waveguide can not satisfy this condition because the phase velocity is larger than the speed of light. To solve this problem a periodic structure is used because the reflections from the periodic loading elements reduce the phase velocity compared with the uniform guide. A periodic structure has the property that its modes are composed of a Fourier sum of waves, some of which are suitable for synchronous-particle acceleration. Also beside a periodic waveguide there is another periodic structure is named coupled-cavity, a periodic array of coupled resonant cavities, in which the iris is located between every two cavities. In other word, an array of pillbox cavities are coupled through the irises. There is an analytic description for the dispersion curve and cavity coupling constant based on some theorems, for example, Bethe's theory of coupling of cavities through apertures, the Slater perturbation theorem, and the Floquet theorem. Floquet theorem [Appendix B] stated that in a given mode of an infinite periodic structure, the fields at two different cross sections that are separated by one period differ only by a constant factor, which in general is a complex number and it means that when a structure of infinite length is displaced along its axis by one period, it can not be distinguished from original self. For a mode with eigenfrequency ω (there are intervals of ω called stopbands where the constant is real with magnitude less than 1. For the stopband regions the modes are evanescent. On the other hand, for a passband region in which waves will propagate, within which in the loss-free case the complex constant $e^{j\beta_0 d}$). Based on Floquet theorem the field for a passbands can be written as follows [4]:

$$\bar{E}(\bar{r}, z + d) = e^{-j\beta d}\bar{E}(\bar{r}, z), \tag{2.11}$$

because $E_d(r, z)$ is periodic, it can be expanded in a Fourier series as

$$E_d(r, z) = \Sigma_{n=-\infty}^{+\infty} a_n(r)\ e^{\frac{-j2\pi nz}{d}}, \tag{2.12}$$

where $E_d(r, z)$ is a periodic function with the same period d as the structure and βd is

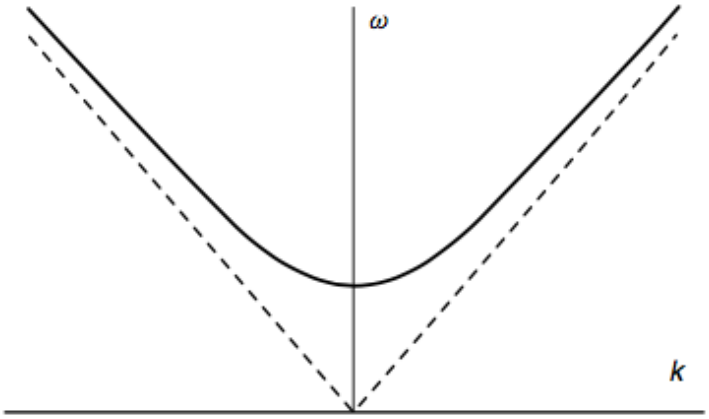

Figure 2.5: Dispersion curve (Brillouin diagram) for uniform waveguide.

called phase advance per period. Making Fourier expansion for most common accelerating TM_{010} mode. The radial solution is found by satisfying the wave equation requiring $E(r,z,t) = E_d(r,z)\ e^{j(\omega t - k_0 z)}$ as the following,

$$a_n''(r) + \frac{a_n'(r)}{r} - K_n^2 a_n(r) = 0, \tag{2.13}$$

for $K_n^2 > 0$, the solution is,

$$E_z = \Sigma_{-\infty}^{+\infty} E_n J_0(K_n r)\ e^{i\omega t - k_n t}, \tag{2.14}$$

where

$k_n = k_0 + \frac{2\pi n}{d}$,

and

$K_n^2 = (\frac{\omega}{c})^2 - (k_0 + \frac{2\pi n}{d})^2$.

Each term in Eq. (2.14) is called space harmonics and as we have n term we could say that there are n space harmonics, each of which is denoted by the index n. We refer to the principle wave as the one with $n = 0$. The space harmonics have the same frequency but different wavenumbers, and each has a constant amplitude E_n independent of z.The propagation constant is

$$\beta_n = \beta_0 + \frac{2\pi n}{d} = \frac{\omega}{v_p} + \frac{2\pi n}{d}. \tag{2.15}$$

As the uniform waveguide has a dispersion relation, shown in Fig. (2.5) given by

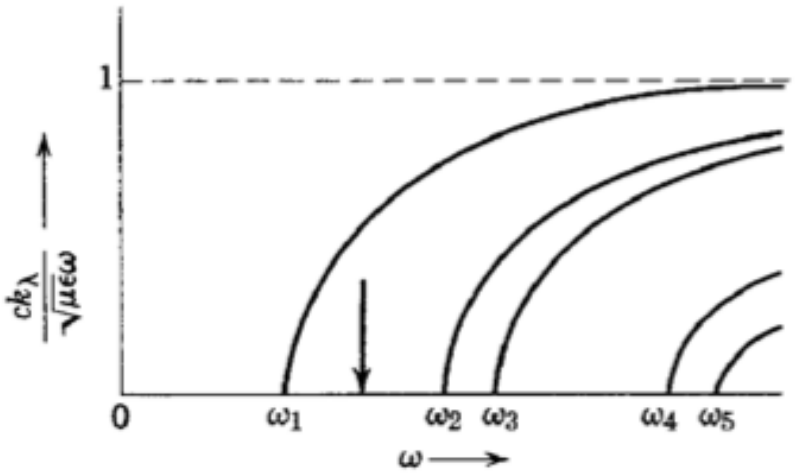

Figure 2.6: Wave number k_λ versus frequency ω for various modes λ. ω_λ is the cutoff frequency [6].

$$\omega^2 = (k_\lambda c)^2 + (k_0 c)^2, \tag{2.16}$$

where k_λ is the cutoff wavenumber for the modes, related to the cutoff angular frequency by $\omega_c = Kc$. For frequencies less than the cutoff frequency, k_λ is imaginary and such modes cannot propagate (cutoff modes). The behavior of the axial wave number as a function of frequency is shown in Fig. (2.6) . As we observe at any given frequency only a finite number of modes can propagate. It is often convenient to choose the dimensions of the guide so that at the operating frequency only the lowest mode can occur.
Then the phase velocity is expressed as

$$\nu_p = \frac{\omega}{k_0} = \frac{c}{\sqrt{1 - (\frac{k_\lambda c}{\omega})^2}} > \ c. \tag{2.17}$$

It should be noted that according to the equation above the phase velocity becomes infinite exactly at cutoff.
When $K_n^2 > 0$, the other nonzero components of the TM_{01} solution are

$$E_r(r, z, t) = j \ \Sigma_{-\infty}^{+\infty} E_n \frac{k_n}{K_n} J_1(K_n r) \ e^{i\omega t - k_n t}, \tag{2.18}$$

$$B_\theta(r, z, t) = j \ \Sigma_{-\infty}^{+\infty} E_n \frac{\omega}{K_n c^2} J_1(K_n r) \ e^{i\omega t - k_n t}, \tag{2.19}$$

when $K_n^2 < 0$, the Bessel functions J_0 and J_1 are replaced with modified Bessel functions I_0 and I_1. By making an assumption that the synchronous space harmonic waves only act on the beam, we can obtain the integrated effect on a beam particle which is synchronous with one of the space-harmonic waves. The effects of the non synchronous are ignored because we assumed its average and it is not other than zero.

For the pillbox cavity, there are two types of modes, transverse-electric (TE_{mnp}) and transverse-magnetic (TM_{mnp}) which are resonant modes of the pillbox and there are infinite number of them. Periodic shape or almost periodic arrays of coupled accelerator cavities are two common types of accelerator cavities in which their characteristics are more interested. There exists a family of normal modes for coupled oscillators, each mode behaving like an independent harmonic oscillator with its own characteristic resonant frequency. Generally speaking, any normal mode can be excited when there will be a right frequency with a suitable driving force with a phase difference from one individual oscillator participating in the motion to the next oscillator. Each of the individual cavity modes of an array of coupled cavities generates its own family of normal modes and lies within a definite frequency band called a passband, which is centered near the resonant frequency of the uncoupled cavity mode. Each passband includes all the normal modes associated with a single cavity mode, such as the familiar TM_{010} mode of the pillbox cavity. Each normal-mode can be described in terms of a characteristic wave that can propagate through the cavity array with a characteristic frequency, and a characteristic wavelength or wavenumber. For a finite length array there are a finite number of modes, equal to the number of coupled oscillators. Fig. (2.7) shows the dispersion curve of the lowest passband of an infinite periodic corresponding to the TM_{010}. There are an infinite number of waves at any frequency within a passband that each of them corresponding to a different space harmonic with the following description as we described before:

- the space harmonic with the number $n = 0$ are the waves propagating in the $+z$ direction correspond to the range from $0 < k_z < \pi/d$, where d is the spatial period.
- n = 1 correspond to the range from $2\pi/d < k_z < 3\pi/d$.
- n = 2 correspond to the range from $2\pi/d < k_z < 3\pi/d$ and so on.
- for the nth space harmonic all the information is presented if the plot is restricted to the range $0 < k_z < \pi/d$. The reason is because the curve has a symmetry.

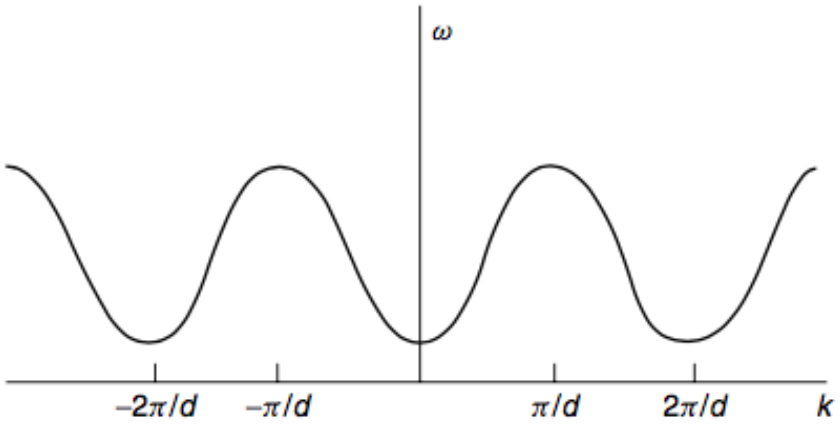

Figure 2.7: Dispersion curve of the lowest passband of an infinite periodic structure.

For a periodic structure, the dispersion curves express the frequency as a periodic function of wavenumber k_z. Each cycle or zone in k_z space represents the behavior of ω versus k_z for the nth space harmonic. At any given frequency, each space-harmonic component of a normal mode has a unique phase velocity, corresponding to the slope of the line from the origin to that point on the dispersion curve. All space-harmonic components have the same group velocity, corresponding to the same tangent on the dispersion curve [4].

Chapter 3

A Comparison of Analytical and Numerical methods to estimate Group Velocity

The concept of group velocity is fundamental in high accelerating periodic structures. It can be obtained from resonant-frequency change due to the cavity perturbation. In the framework of the Compact Light XLS project, we are studying an accelerating structure operating at frequency f=23.988 GHz or f=35.982 GHz in order to linearize longitudinal space phase. In this chapter of the thesis we compare analytical and numerical solutions of the group velocity. Numerical electromagnetic simulations were carried out by using the numerical code HFSS in the frequency domain.

The use of high accelerating periodic structure is required to compensate the non-linearity distortions due to the RF curvature during acceleration and compensation [10]. The design of an X-band accelerating section for linearizing the longitudinal phase space in the Frascati Linac Coherent Light Source (SPARC: Sorgente Pulsata Auto-amplificata di Radiazione Coerente) (Fig. (3.1)) has been accomplished. The structure, operating on the standing wave mode, was a 9 cells structure fed by a central coupler and it has been designed to obtain a 42 MV/m accelerating gradient [11]. We present an analytical and numerical studying of the group velocity on the traveling wave K-band accelerating structure in the framework of the XLS project. The structure will be operated at frequency f=23.988 GHz or f=35.982 GHz in order to linearize longitudinal phase space.

The concept of group velocity have been brought to the literature by Rayleigh [12] for the transverse sound waves propagating in thin elastic rods and the energy propagation under dispersive partial differential equations has been described by this quantity [13,14]. The group velocity of a wave is the velocity of the envelope of the wave packet. The wave packet can be considered to be a Gaussian wave packet with a carrier wave of wavenumber, k_0,

$$g(x) = e^{-\frac{1}{2}(\frac{x-x_0}{\sigma_x})^2}\ e^{jk_0x}, \tag{3.1}$$

where k_0 is the carrier wavenumber. The Fourier transform of this wave packet is

$$\tilde{g}(k) = \frac{\sigma_x}{2\sqrt{\pi}} e^{-\frac{\sigma_x^2}{2}(k-k_0)^2}\ e^{jx_0(k-k_0)}, \tag{3.2}$$

the time evolution of this equation is the wave packet at any time which is constructed by the superposition principle,

$$A(x,t) = \int_{-\infty}^{\infty} \tilde{g}(k) e^{j(kx-\omega(k)t)} dk, \tag{3.3}$$

where $\tilde{g}(k)$ is the Fourier transform of the wave packet at time $t = 0$. Linearizing the angular frequency which is accomplished by Taylor series approximation , $\omega(k) \approx \omega_o + (k - k_0)\frac{d\omega}{dk}$ and substituting into $A(x,t)$ one can obtain:

$$A(x,t) = e^{i(k_0x-\omega_0)} \int_{-\infty}^{\infty} \tilde{g}(k) e^{j(k-k_0)(x-\frac{d\omega}{dk}t)} dk. \tag{3.4}$$

The physical interpretation of this equation has become one of the most important concept in physics and engineering. The first term describes a wave propagating with the velocity of ω_0/k_0 and the second term a wave packet which propagates with $\frac{d\omega}{dk}$ .The previous is called phase velocity and is used for non-dispersive media and the later has known as group velocity which is not other than the envelope of the wave packet travels with this velocity while propagating through space.

The maximum sustainable gradient in an accelerating structure depends on the rf power flow through the structure [60]. The constraints due to rf breakdown in vacuum strongly influence the design of high gradient accelerating structures. For the gradient versus BDR (breakdown rate) and pulse length the equation below can be used [61],

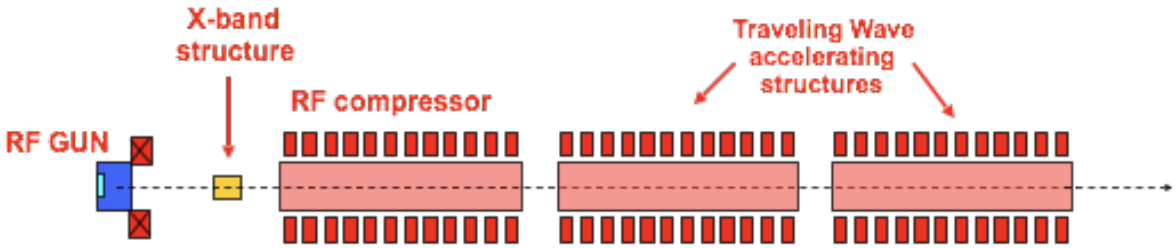

Figure 3.1: Schematic layout of the photo-injector of SPARC phase II.

$$\frac{E_a^n \,.\, t_p^5}{BDR} = const, \tag{3.5}$$

where E_a denotes the accelerating gradient and t_p is pulse length. The author of the article has mentioned that the choice of n=30 for the power exponent is based on the analysis of the available experimental data only, and no assumption is made about the underlying physical mechanism.

Yariv and Yeh has been demonstrated that in the homogeneous lossless media, the group velocity is equivalent to the energy velocity [62] and L. Brillouin has shown that for the material dispersion with the sufficiently small loss also this result can be applied [63],

$$\nu_g = \nu_E \tag{3.6}$$

where the group velocity as a definition is the derivative of angular frequency respect to wave number k, $\nu_g = \nabla_k \omega$ and the energy velocity is defined,

$$\nu_E = \frac{< S >}{< U >} \tag{3.7}$$

where S is denoted for the time-averaged Poynting vector and U is the time averaged energy density. Keeping constant the input power we have,

$$\nu_g \;.\; < U >=< S >= const. \tag{3.8}$$

This means increasing the group velocity, stored energy decreases and decreasing the group velocity, stored energy increases. The accelerating gradient is defined as E_0T ($E_a = E_0T$) where the value E_0 is an average axial electric field over the cell length and T denotes for transit time factor. Recalling hat the stored energy per meter for the TM_{010} mode of an unperturbed pillbox cavity is,

$$U = \frac{\pi\epsilon_0}{2}\ b^2\ E_0^2\ J_1^2(\chi_{01}). \tag{3.9}$$

where ϵ_0 is vacuum permittivity and $J_1(\chi_{01})$ is the Bessel function of the first kind, b is the cavity radius and l denotes for cavity length. Replacing $E_a = E_0 T$ into the equation above and with some manipulation we have,

$$E_a = \frac{T}{bJ_1(\chi_{01})}\sqrt{\frac{2U}{\pi\epsilon_0}}. \tag{3.10}$$

Substituting equation above into the Eq. (3.5) we can obtain BDR,

$$\frac{(\frac{T}{bJ_1(\chi_{01})}\sqrt{\frac{2U}{\pi\epsilon_0}})^n\ .\ t_p^5}{BDR} = const, \tag{3.11}$$

finally substituting the Eq. (3.8) into the equation above, considering T=1 for TW section and some manipulation we have a group velocity dependence for breakdown rate (BDR),

$$BDR = (\frac{C}{bJ_1(\chi_{01})}\sqrt{\frac{2S}{\pi\epsilon_0\nu_g}})^n\ .\ t_p^5, \tag{3.12}$$

where

C: constant,

S: Poynting vector,

b: cavity radius,

ℓ: cavity length,

$J_1(\chi_{01})$: Bessel function of the first kind,

ν_g: group velocity,

ϵ_0: vacuum permittivity,

t_p: pulse length.

or in terms of the input power we can write,

$$BDR = (\frac{C}{bJ_1(\chi_{01})}\sqrt{\frac{2P_{in}}{\pi\epsilon_0\nu_g}})^n\ .\ t_p^5 \tag{3.13}$$

The energy W stored in the entire section at the end of the filling time can be expressed as [64],

$$W = P_{in}\frac{Q}{\omega}(1 - e^{-2\tau}) \tag{3.14}$$

where for a constant-impedance section where the attenuation is uniform we have,

$$\tau = \frac{\omega \ell}{2\nu_g Q} = \alpha \ell \tag{3.15}$$

replacing $Q = \omega W/P_{dis}$ into the Eq. (3.14) where P_{dis} is the power dissipated along the structure we have,

$$P_{dis} = P_{in}(1 - e^{-2\tau}) \tag{3.16}$$

The attenuation factor τ of a constant impedance or constant gradient TW section is defined,

$$\frac{P_{out}}{P_{in}} = e^{-2\tau}. \tag{3.17}$$

Power dissipated along the structure can also be obtained from $P_{dis} = P_{in} - P_{out}$ and considering equation above which we will have the same expression as Eq. (3.16).
So breakdown rate with considering the stored energy for the entire section can be written,

$$BDR = (\frac{C}{bJ_1(\chi_{01})}\sqrt{\frac{2P_{dis}}{\pi\epsilon_0\nu_g(1 - e^{-2\tau})}})^n \ . \ t_p^5 \tag{3.18}$$

where we have used the Eq. (3.16) which is valid when we consider whole structure.
As the normalized peak power per unit length is

$$P_{norm} = \frac{P_{in}/\ell}{dP/dz} = \frac{1}{1 - e^{-2\tau}} \tag{3.19}$$

Then we have,

$$BDR = (\frac{C}{bJ_1(\chi_{01})}\sqrt{\frac{2P_{dis}P_{norm}}{\pi\epsilon_0\nu_g}})^n \ . \ t_p^5 \tag{3.20}$$

The other explanation for the importance of group velocity ν_g is because at TW structure it relates with filling time factor t_F, the time the electromagnetic energy needs to fill the whole structure and it is given as,

$$t_F = \int_0^L \frac{dz}{\nu_g(z)}. \tag{3.21}$$

For not having the small efficiency of acceleration it would be convenient to have small values of the group velocity, usually in the order of 0.01c and 0.02c. Also, the same reason for the filling time factor keeping it within reasonable values.

The electromagnetic waves in a periodic structures as an array of coupled cavities with a central hole in each end wall propagate with the group velocity because there is no monochromatic waves in nature in which the wave travels with the phase velocity. There is an analytical description for the dispersion curve based on Bethe's theory of coupling cavities through apertures, the Slater perturbation theorem, and the Floquet theorem [4]. The cavities will be perturbed by the irises as they act like electric-dipole moment and the interaction energy of the dipoles will change the stored energy. The procedure of shape perturbation is as follows:

Maxwell's curl equations can be written for the two cases as

$$\nabla \times \bar{E}_0 = -j\omega_0 \mu \bar{H}_0, \tag{3.22}$$

$$\nabla \times \bar{H}_0 = j\omega_0 \epsilon \bar{E}_0, \tag{3.23}$$

$$\nabla \times \bar{E} = -j\omega \mu \bar{H}, \tag{3.24}$$

$$\nabla \times \bar{H} = j\omega \epsilon \bar{E}, \tag{3.25}$$

where $\bar{E}_0$, $\bar{H}_0$ and $\bar{E}$, $\bar{H}$ are the fields of the original cavity and perturbed cavity, respectively. ω_0 is the resonant frequency of the original cavity and ω is the resonant frequency of the perturbed cavity.

Now multiply the conjugate of Eq. (6.12) by $\bar{H}$ and multiply Eq. (6.15) by $\bar{E}_0^*$

$$\bar{H} \ . \ \nabla \times \bar{E}_0^* = j\omega_0 \mu \bar{H}_0 \ . \ \bar{H}_0^*, \tag{3.26}$$

$$\bar{E}_0^* \ . \ \nabla \times \bar{H} = j\omega \epsilon \bar{E}_0^* \ . \ \bar{E}, \tag{3.27}$$

subtracting these two equations and using the vector identity we have,

$$\nabla \ . \ (\bar{E}_0^* \times \bar{H}) = j\omega_0 \mu \bar{H} \ . \ \bar{H}_0^* - j\omega \epsilon \bar{E}_0^* \ . \ \bar{E}. \tag{3.28}$$

Similarly, by multiply the conjugate of Eq. (3.23) by $\bar{E}$ and multiply Eq. (3.24) by $\bar{H}_0^*$ and subtracting the equations and using the vector identity we have,

$$\nabla \cdot (\bar{E} \times \bar{H}_0^*) = -j\omega\mu\bar{H}_0^* \cdot \bar{H} + j\omega_0\epsilon\bar{E}_0^* \cdot \bar{E}. \tag{3.29}$$

Now adding $Eq.(3.28)$ and $Eq.(3.29)$,integrate over the volume V,

$$\int_V \nabla \cdot (\bar{E}_0^* \times \bar{H} + \bar{E} \times \bar{H}_0^*)d\nu = -j(\omega - \omega_0)\int_V (\epsilon\bar{E} \cdot \bar{E}_0^* + \mu\bar{H} \cdot \bar{H}_0^*)d\nu, \tag{3.30}$$

using the divergence theorem we obtain,

$$\int_V \nabla \cdot (\bar{E}_0^* \times \bar{H} + \bar{E} \times \bar{H}_0^*)d\nu = \oint_S (\bar{E}_0^* \times \bar{H} + \bar{E} \times \bar{H}_0^*) \cdot d\bar{s} = \oint_S \bar{E} \times \bar{H}_0^* \cdot d\bar{s},$$

$$= \oint_{S_0} \bar{E} \times \bar{H}_0^* \cdot d\bar{s} - \oint_{\Delta S} \bar{E} \times \bar{H}_0^* \cdot d\bar{s} = -\oint_{\Delta S} \bar{E} \times \bar{H}_0^* \cdot d\bar{s}, \tag{3.31}$$

where $\hat{n} \times \bar{E} = 0$ on S and $\hat{n} \times \bar{E}_0 = 0$ on S_0. Using this results we have,

$$\omega - \omega_0 = \frac{-j\oint_{\Delta S} \bar{E}_0^* \times \bar{H} \cdot d\bar{s}}{\int_{V_0}(\epsilon\bar{E} \cdot \bar{E}_0^* + \mu\bar{H} \cdot \bar{H}_0^*)d\nu}, \tag{3.32}$$

as we don't have the value of $\bar{E}$ and $\bar{H}$, this equation won't be a useful equation to relate the resonant frequency to the shape perturbations. But, by making an assumption that ΔS is small, we can approximate the perturbed fields $\bar{E}$, $\bar{H}$ by the original fields $\bar{E}_0$, $\bar{H}_0$,and ω in the denominator by ω_0, to give the fractional change in resonant frequency as

$$\frac{\omega - \omega_0}{\omega} \approx \frac{-\int_{\Delta V}(\mu|\bar{H}_0|^2 - \epsilon|\bar{E}_0|^2)d\nu}{\int_{V_0}(\epsilon|\bar{E}_0|^2 + \mu|\bar{H}_0|^2)d\nu} = \frac{\Delta U_m - \delta U_e}{U_m + U_e}, \tag{3.33}$$

where U_m and U_e are the stored magnetic energy and electric energy, respectively and ΔU_m and ΔU_e are their changes due to the shape perturbation. According to the equation above increasing or decreasing the volume of the cavity causes increase or decrease of the resonant frequency.

3.1 Perturbation from irises

There is a theoretical model which states that the aperture is equivalent to an electric or/and magnetic dipole moments [8]. These dipole moments are respectively proportional to the normal electric and tangential magnetic field of the incident wave. The assumption we are going to use is that the hole is small compared with the wavelength. There is no

magnetic dipole moment for an array of identical TM_{010}-mode cavities with iris-loaded and electric-dipole moment is equal $P = -2a^3\epsilon_0 E_0/3$, where "a" is the aperture radius, and E_0 is the unperturbed electric field. This electric dipole moment causes a perturbation and the result of this perturbation is the shift of the resonant frequency according to Eq. (3.33) due to the interaction energy of the dipoles which change the stored energy of the cavities. The difference between the energy before and after the creation of the iris is [4],

$$\Delta U_e = -a^3\epsilon_0 E_0^2(1 - e^{-\alpha h}cos\psi)/6, \tag{3.34}$$

where $\alpha \approx 2.405/a$ is the attenuation per unit length of the field for the TM_{01} waveguide mode through a hole in a wall of thickness h, and ψ is the phase advance per cavity of the traveling wave. Substituting $\omega_0 = 2.405c/b$ where b is the cavity radius, ΔU_e and stored energy for TM_{010} mode into the Eq. (3.33) , and some manipulation we have,

$$\omega = \omega_0[1 + G(1 - cos(\psi)e^{-\alpha h})], \tag{3.35}$$

where $G = \frac{2a^3}{3\pi J_1^2(2.405)b^2\ell}$. $\psi = k_z\ell$ is the phase advance per cavity and b, ℓ are the cavity radius and axial length of the cavity, respectively. Considering the definition of group velocity we have,

$$v_g = \frac{d\omega}{dk_z} = \frac{2(2.405)c}{3\pi J_1^2(2.405)}(\frac{a}{b})^3 sin(\psi)e^{-\alpha h}, \tag{3.36}$$

where we can replace $\lambda = 2.61b$ in case of TM_{010} and obtain,

$$\frac{\nu_g}{c} = \frac{4(2.61)^2}{3J_1^2(2.405)}(\frac{a}{\lambda})^3 sin(\psi)e^{-\alpha h}. \tag{3.37}$$

Replacing $\alpha \approx \frac{2.405}{a}$ into the above equations and writing the Taylor series of the exponential function and considering $h = 0.08\lambda$ for a practical periodic accelerating structure, and substituting into the Eq.s (3.36) and (3.37), they can be written as,

$$\frac{\nu_g}{c} = \frac{4(2.61)^2}{3J_1^2(2.405)} sin(\psi)[(\frac{a}{\lambda})^3 - 0.19(\frac{a}{\lambda})^2 + 0.0185(\frac{a}{\lambda}) - 0.0012 + 0.000057(\frac{\lambda}{a})]. \tag{3.38}$$

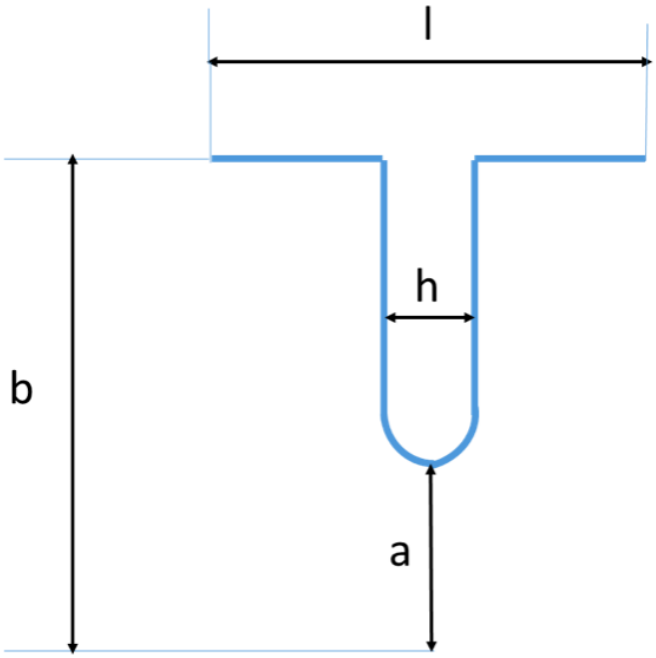

Figure 3.2: TW cavity shape for the $2\pi/3$ mode. b, a, h and l are cavity radius, iris aperture radius, iris thickness and 1/3 of the cell length, respectively.

$$\frac{\nu_g}{c} = \frac{2(2.405)}{3\pi J_1^2(2.405)} sin(\psi)[(\frac{a}{b})^3 - 0.496(\frac{a}{b})^2 + 0.126(\frac{a}{b}) - 0.0213 + 0.0026(\frac{b}{a})]. \quad (3.39)$$

where the equations above are group velocity as a function of a/λ and a/b, respectively.

3.2 Simulation results

In this section we obtain the group velocity by "HFSS code" in ANSYS [15]. HFSS (High Frequency Structures Simulator) is a user-friendly software package, initially released by ANSOFT that allows to evaluate the 3D electromagnetic field distribution inside a structure. In order to do this, it solves the Maxwell's equations in the frequency domain. The numerical method employed is the FEM (Finite Element Method). HFSS divides the 3D model into a relatively large number of small domains, that represent the mesh. The RF power is fed to the periodic structure flowing along the structure while electromagnetic mode excited with 120° phase advance per cell is similar to the TM_{010} in a circular

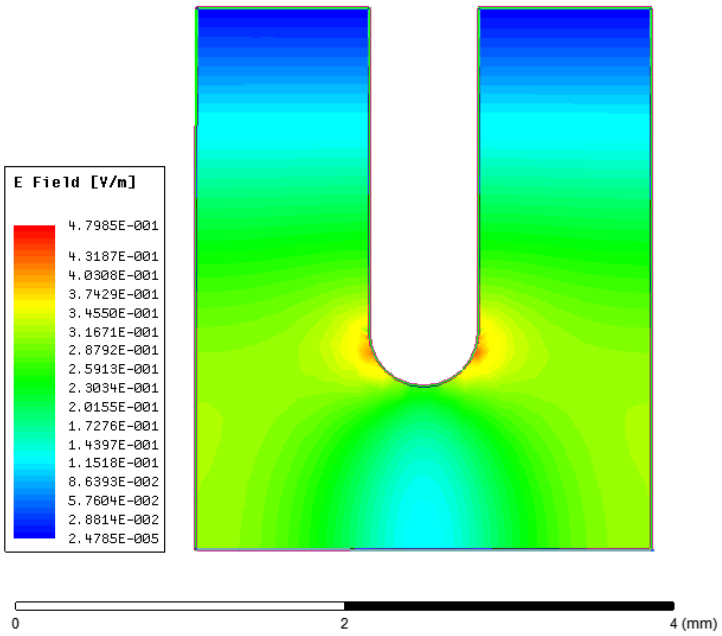

Figure 3.3: Electric field magnitude for the TM_{010} mode of the high accelerating periodic structure. As we expected minimum value of the field is near the outer surface of the cavity.

waveguide. By applying proper boundary conditions it's not necessary to simulate all structure because the code HFSS allows to simulate periodic structures by only using one period, as shown in Fig.(3.2).

The condition "Master/Slave" enables to impose a phase shift, 120° for the multi-cell structures, between two faces of the single cell. Then, a simulation with the eigenmode solver finds the frequency at which the electromagnetic field satisfies the phase shift desired. Exploiting the symmetry in the field, only a fraction of the full cell is used for simulations and a condition of perfect magnetic boundary, called "perfect H", is applied. Electric and Magnetic field magnitudes have plotted in Fig.s (3.3) and (3.4) for the TM_{010} mode of the high accelerating periodic structure. As we can observe minimum value of the electric field and maximum value of the magnetic field are near the outer surface of the cavity as they were expected for the TM_{010} mode.

After finding the frequency shift per phase shift we put it in the following equation to calculate the group velocity,

$$\frac{\nu_g}{c} = \frac{2\pi h}{c}\ tg\ \alpha, \tag{3.40}$$

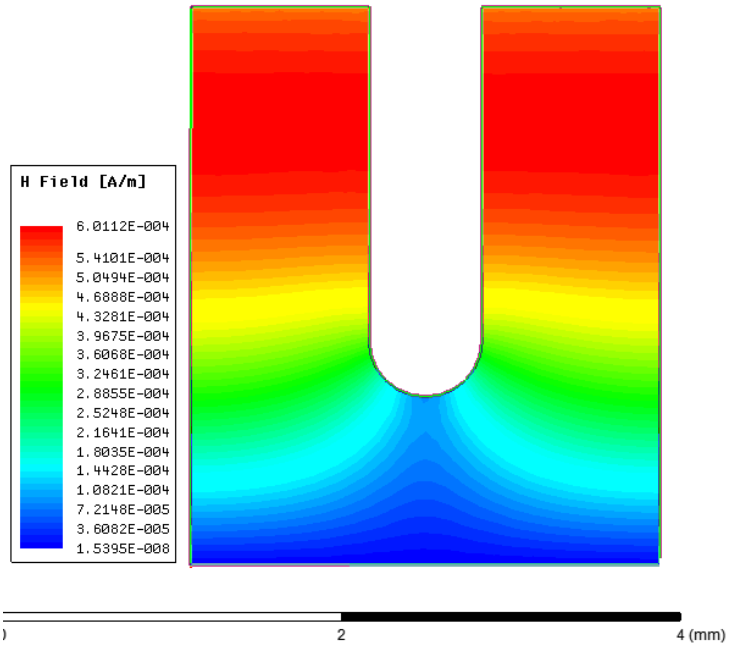

Figure 3.4: Magnetic field magnitude for the TM_{010} mode of the high accelerating periodic structure. As it can be observed maximum value of the field is near the outer surface of the cavity.

where

$$tg\ \alpha = \frac{df}{d\phi}. \tag{3.41}$$

From Eq. (3.40) it is possible to plot dispersion curve obtaining the frequency mode as a function of the phase advance of the TW structure. The iris radius, iris thickness, cavity radius are 2 mm, 1mm, 5.15 mm and 1.333 mm, 0.667, 3.43 mm for 23.988 GHz and 35.982 GHz respectively. The results have plotted in Figs. (3.5.a) and (3.5.b) and also have shown in the following tables.

a[mm]	b	ν_g [23.988 GHz]	$\frac{a}{b}$ [Hfss]
1.0000	4.8616	0.0027c	0.206
1.5000	4.9764	0.0120 c	0.301
2.0000	5.1530	0.0365 c	0.388
2.5000	5.3854	0.0727 c	0.464
3.0000	5.6637	0.1190 c	0.530

(a)

a[mm]	b	ν_g [35.982 GHz]	$\frac{a}{b}$ [Hfss]
0.6667	3.2398	0.0027c	0.206
1.0000	3.3161	0.0120 c	0.301
1.3333	3.4345	0.0365 c	0.388
1.6667	3.5899	0.0727 c	0.464
2.0000	3.7759	0.1190 c	0.530

(b)

Iris radius[mm]	ν_g [23.988 GHz]	$\frac{a}{\lambda}$ [Hfss]
1.0000	0.0027c	0.080
1.5000	0.0120 c	0.120
2.0000	0.0365 c	0.160
2.5000	0.0727 c	0.20
3.0000	0.1190 c	0.240

(c)

Iris radius[mm]	ν_g [35.982 GHz]	$\frac{a}{\lambda}$ [Hfss]
0.6667	0.0027c	0.080
1.0000	0.0120 c	0.120
1.3333	0.0365 c	0.160
1.6667	0.0727 c	0.200
2.0000	0.1190 c	0.240

(d)

Table 3.1: Simulation results of the Group Velocity for high accelerating periodic structure. (a) Group velocity as a function of a/b at frequency 23.988 GHz . a and b are iris radius and cavity radius, respectively. (b) Group velocity as a function of a/b at frequency 35.982 GHz. (c) Group velocity as function of a/λ at frequency 23.988 GHz. (d) Group velocity as a function of a/λ at frequency 35.982 GHz.

Deg	Rad	[F=23.988GHz]	Frequency[35.882GHz]
0	0.0000	23249148601	34881627818
30	0.5236	23316457686	34971979664
60	1.0472	23498798208	35244918474
90	1.5708	23745362614	35613864890
120	2.0944	23988849524	35980658987
150	2.6180	24163140378	36249545345
180	3.1416	24233428460	36349213280

Table 3.2: Simulation results of the frequency mode as a function of the phase advance of the TW structure . The iris radius, cavity radius, ν_g/c are 2 mm, 5.15 mm, 0.0365 and 1.333 mm, 3.43 mm, 0.0365 for 23.988 GHz and 35.982 GHz respectively.

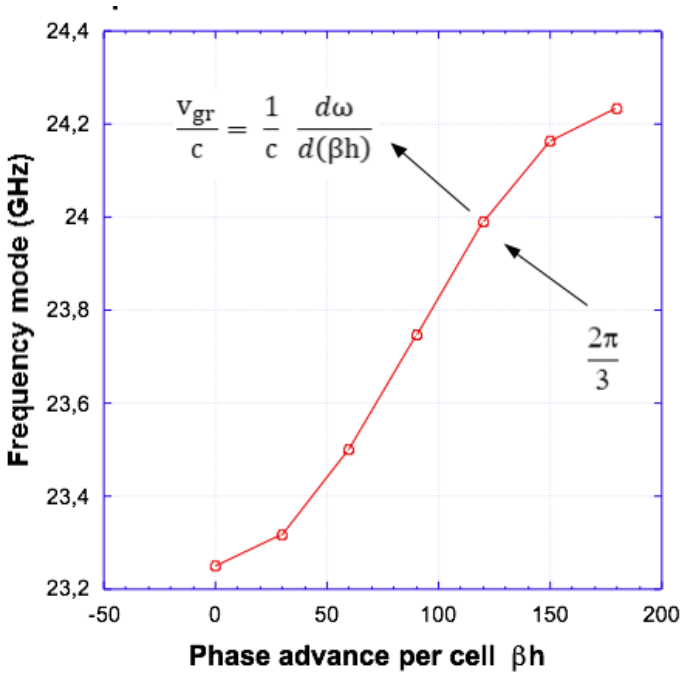

(a)

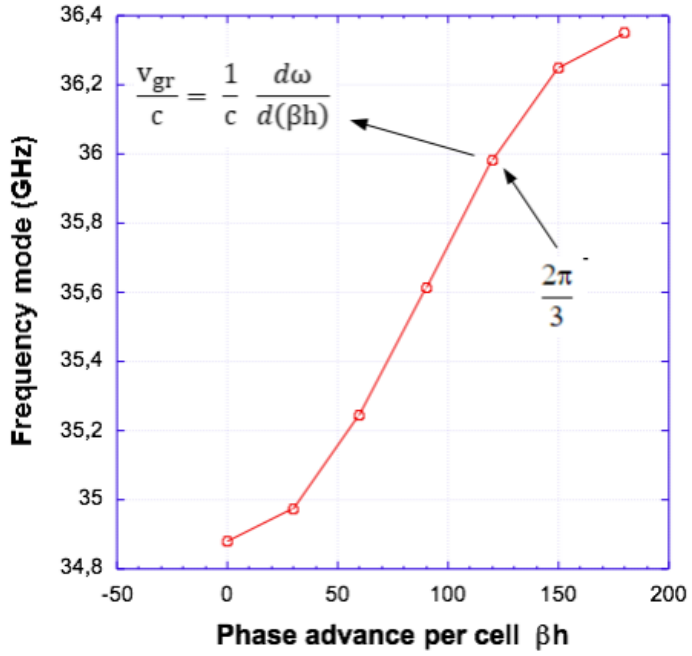

(b)

Figure 3.5: Frequency mode as a function of the phase advance of the TW structure for (a) 23.988 GHz, the iris radius, iris thickness, cavity radius, are 2 mm, 1mm and 5.1530 mm, respectively. (b) 35.982 GHz, the iris radius, iris thickness, cavity radius are 1.3333 mm, 0.6667 and 3.4345 mm, respectively.

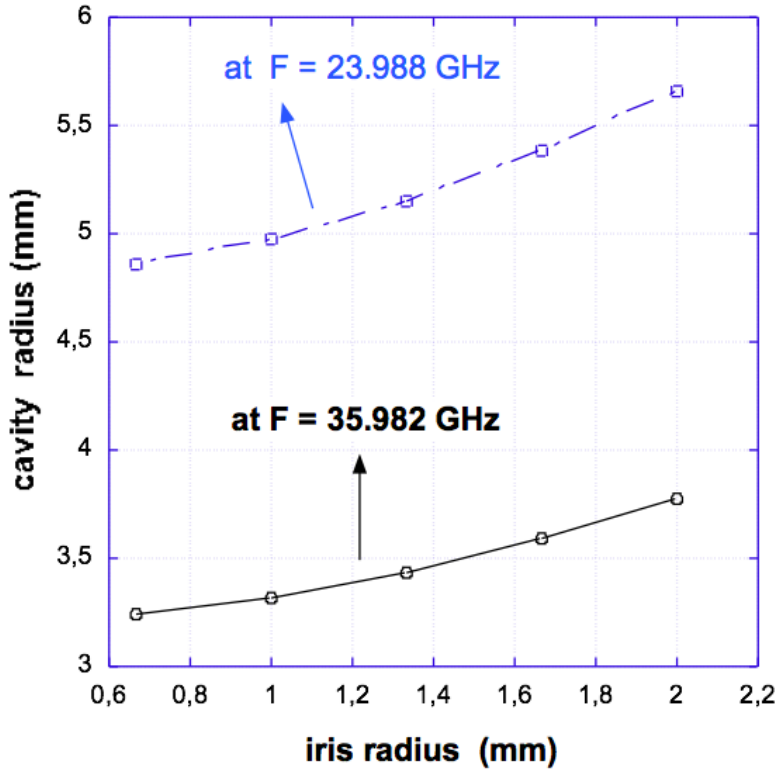

Figure 3.6: Cavity radius as a function of the iris radius at 23.988 GHz and 35.982 GHz

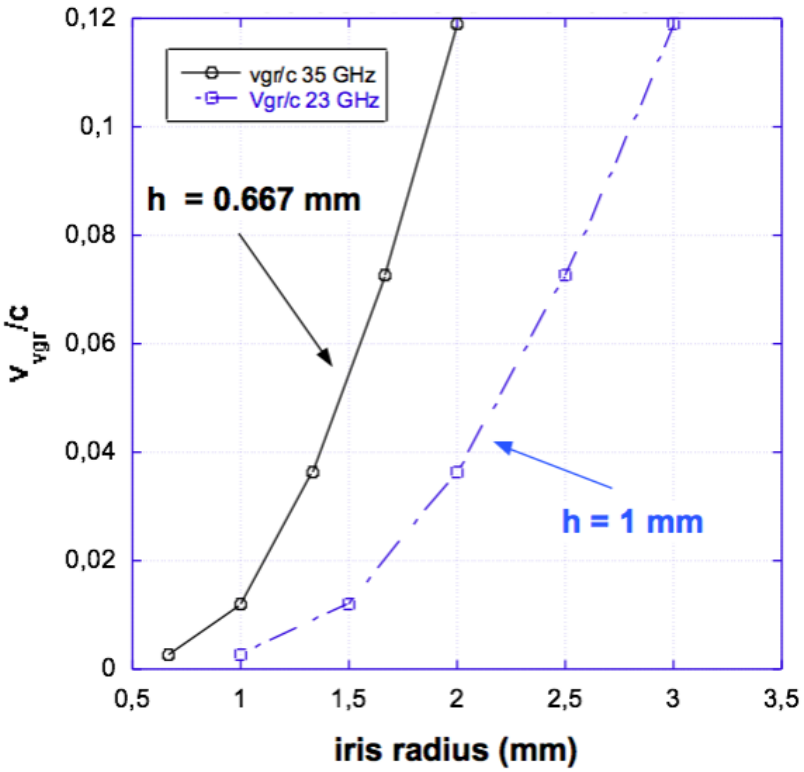

Figure 3.7: Group velocity (v_g/c) as a function of the iris radius at 23.988 GHz and 35.982 GHz

ν_g/c	$\Delta(a/b)[\nu_g/c = f(a/b)]$	$\Delta(a/\lambda)[\nu_g/c = f(a/\lambda)]$
0.0027	0.014 (6.8 %)	0.005 (6.3 %)
0.0120	0.017 (5.6 %)	0.008 (6.7 %)
0.0365	0.020 (5.2 %)	0.004 (2.5 %)
0.0727	0.025 (5.4 %)	0.013 (6.5 %)
0.1190	0.030 (5.6 %)	0.027 (11.2 %)

Table 3.3: Table of Errors for a/b and a/λ as a function of Group Velocity. a, b, λ are iris radius, cavity radius and RF wavelength, respectively. The percentage of errors between analytical and numerical results for a/b as a function of ν_g/c is almost constant (5%) but we have a variation of percentage of errors for a/λ as function of ν_g/c.The biggest error relates to the biggest iris radius (Group Velocity) and it would be 11.2 %.

3.3 Comparison Between HFSS Simulation and Analytical Results

In this work we obtained the group velocity for different value of iris radius. Related cavity radius for different group velocity have shown in Fig. (3.6). As we could expected by increasing the iris radius, cavity radii should be increased. The reason is as the iris radius is changing, the resonant frequency will be changed and we should increase the cavity radius to put the cavity in a resonant mode.

In Fig (3.7) we plotted the variation of group velocity respect to the iris radius. As we observe the group velocity has been increased with a steep slope for higher frequency and this is coincident with Eq. (3.37). In other words, keeping the same iris radius and varying the frequency, group velocity is bigger for the higher frequency. As an example, group velocities for the cavities with the iris radius a=2 mm operating at 23.988 GHz and 35.982 GHz are 0.0365 c and 0.119 c, respectively. In order to have a relation in which the group velocity be independent from the frequency operation we plotted Eq.s (3.38) and (3.39). Fig.s (3.8) , (3.9) are a/λ and a/b as function of the v_g/c. v_g denotes for group velocity and c is speed of light. Increasing group velocity, a/λ and a/b increase, both analytically and numerically. As we can see in Table (3.3) and Figs. (3.10), (3.11), the percentage of errors between analytical and numerical results for a/b as function of ν_g/c is almost constant (5% of the simulation results). The reason is because by increasing

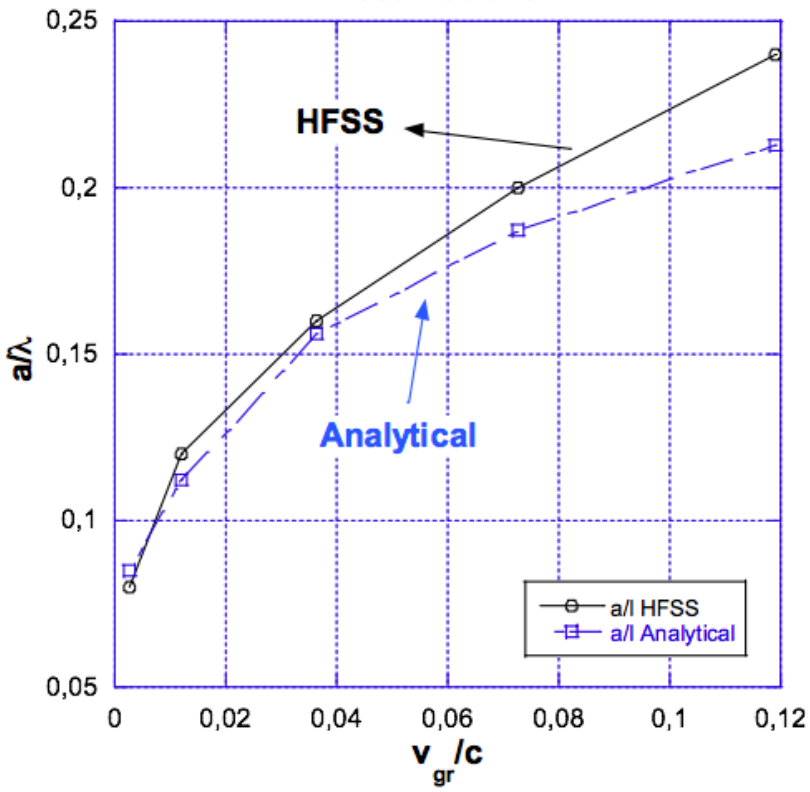

Figure 3.8: a/λ as a function of the group velocity v_g/c. Comparison between the HFSS and Analytical estimations. a is iris radius and λ will be RF wavelength.

the iris radius we should increase cavity radius and a/b increase simultaneously with a constant ratio as the group velocity increases. On the other hand we have a variation of percentage of errors for a/λ as function of ν_g/c because we should fix RF wavelength constant. Considering a constant value for λ and increasing the cavity radius, a/λ should be increased with different ratio because numerically this ratio increases with a higher value respect to the analytical value.

As an additional information, if we are going to explain these errors quantitatively not percentage of the errors, we can say that for small group velocities errors between HFSS and analytical are small compare with large group velocities. It should be noted that according to Fig (3.7) small group velocities relate with small iris radii. Increasing the iris radii, the errors between analytical and HFSS are increasing. One physical reason is that because in EQ. (3.38) we use an electric polarization coefficient for electric moment which is $\alpha = -2/3a^3$. This is the coefficient polarization obtained by Bethe [8]. As Bethe has obtained the coefficient for small holes compare to the wavelength, he mentioned in his article that it is possible to extend to the holes comparable in size with the wavelength

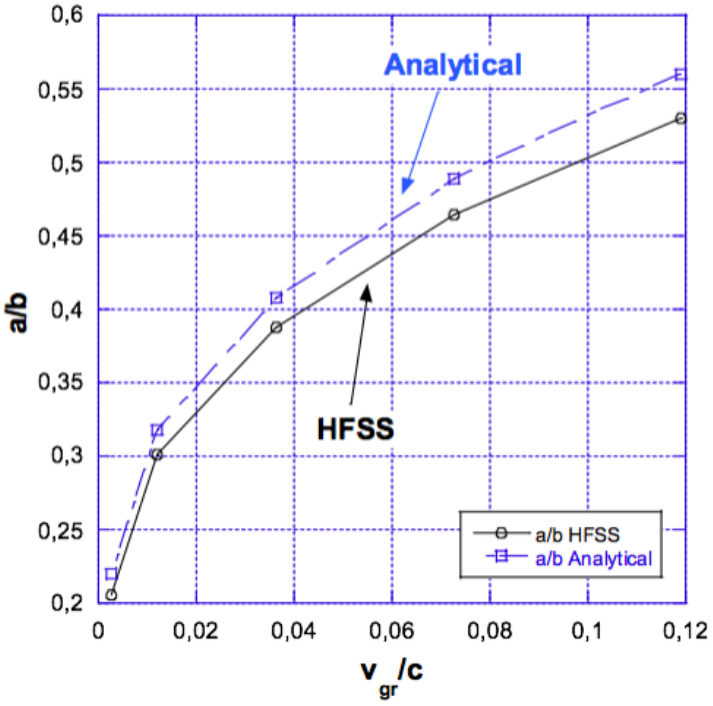

Figure 3.9: a/b as a function of the group velocity v_g/c. Comparison between the HFSS and Analytical estimations. a and b are iris radius and cavity radius, respectively.

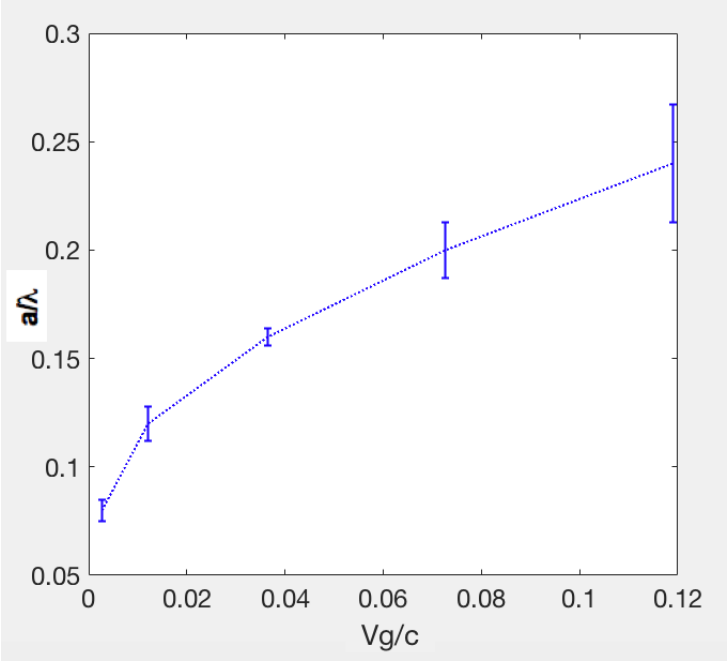

Figure 3.10: Error between analytical and numerical solutions for a/λ as a function of Group Velocity. a is iris radius and λ is RF wavelength. The biggest error relates to the biggest iris radius (Group Velocity) and it would be 11.2 %

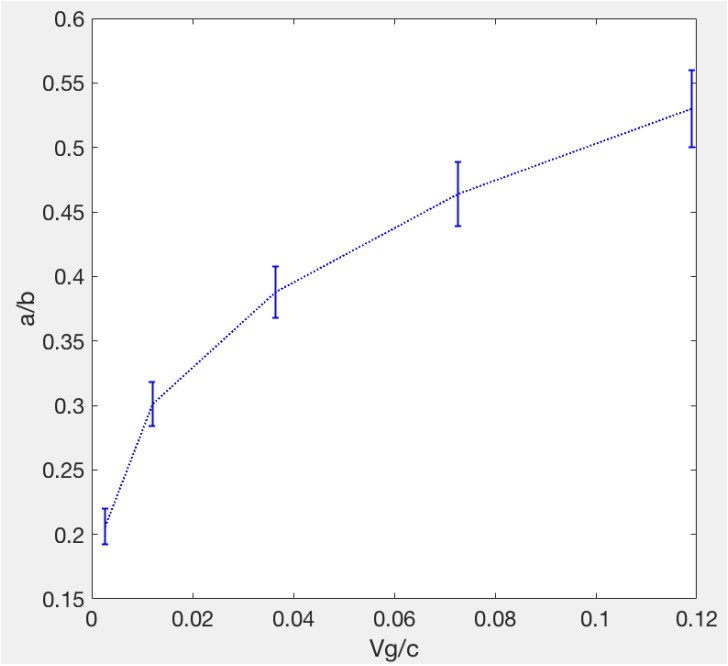

Figure 3.11: Error between analytical and numerical solutions for a/b as a function of Group Velocity. The error increases by increasing the iris radii or relative group velocity but the percentage of errors remain constant. a, b are iris and cavity radius, respectively.The percentage of errors between analytical and numerical results for a/b as a function of ν_g/c is almost constant (5%).

considering the E_0, normal electric field, contain factors of the type e^{ikr} in which the variation in the Green's function must be considered and he said that the correction for the holes comparable to the wavelength will be of relative order $(ka)^2$ rather than ka where k is the wavenumber and r is the aperture radius. Eggimann [16] solved the problem of diffraction of arbitrary electromagnetic field by a circular perfectly conducting disk using a series representation in powers of $k = 2\pi/\lambda$ and he obtained an expression for electric and magnetic moments using the results of generalized Babinet's principle [17] and considering that the disk problem and the aperture problem are equivalent if some consideration would be taken, the final results were the following expressions for the induced electric dipole moment:

$$P_z = \frac{4}{3}a^3\epsilon_0(E_z^0 - \frac{1}{10}(ka)^2[3E_z^0 + \frac{1}{k^2}\frac{\partial^2 E_z^0 l}{\partial z^2}] + j\frac{4}{9\pi}(ka)^3 E_z^0) \tag{3.42}$$

in which taking first and second term of the equation we have a term that is proportional to $(ka)^2$ as Bethe was mentioned about the hole size comparable with the wavelength.

Considering the electric moment according to Eggimann, but taking two terms instead of the whole equation we have: $P_z = \frac{4}{3}a^3\epsilon_0 E_z^0(1 - \frac{3}{10}(ka)^2)$. The change in the stored energy in this case would be less than that obtained from electric-dipole moment based on Bethe's theory. The consequence of the minor energy change due to the irises will be the less perturbations, and the less perturbations lead to the less shift frequency from the resonant frequency and as this means the less frequency slope respect to the phase shift which is nothing other than minor group velocity and it yields a better agreement with numerical solutions.

Chapter 4

TM Modes for Standing Waves in Pill-box Cavity

The design of an RF linac is a complex task and more generally consists in two step. Cavity design is the first step in which the knowledge about the field pattern inside the cavity lead to the minimizing ohmic losses of the cavity. The second step is beam dynamics in which synchronicity keeps good beam quality into the whole structure. Normally the design starts from determining the desired performance of the cavity and the constraints which limit the possibilities of implementation. The next issue which is important to be considered would be the side effects the cavity will have due to the impedance it presents to the beam at the spurious higher order mode frequencies. Finally optimizing the overall design and the main parameters such as shape dimensions of the cavity should be chosen. In this chapter we calculate analytically the shunt impedance, quality factor (Geometric factor) and R/Q independent of the frequency for TM modes for a single cylindrical "pill-box" cavity as these modes in a chain of cylindrical "pill-box" cavities provide accurate model for the accelerating fields in more realistic accelerating structures and the properties of a single cylindrical resonator were simple to treat analytically, and it was as a starting point for accelerating structures.

4.1 From waveguide to cavity resonator

All modern accelerators use powerful radio frequency systems to produce the requisite strong electric fields, with frequencies ranging from a few MHz to several GHz. The

longitudinal electric field is necessary to accelerate (increase the energy) of charged particles. In such systems waveguides are preferred as resonators and to conduct the beam, since they have low losses and can deliver very high power.

Maxwell's equations predict the propagation of electromagnetic energy away from time-varying sources (current and charge) in the form of waves. Consider a linear, homogeneous, isotropic media in a source-free region. We start with the source-free, instantaneous Maxwell's equations written in terms of E and H only,

$$\nabla \ . \ E = 0, \tag{4.1}$$

$$\nabla \ . \ B = 0, \tag{4.2}$$

$$\nabla \times \ E \ + \frac{\partial B}{\partial t} = 0, \tag{4.3}$$

$$\nabla \times \ B \ - \ \frac{1}{c^2} \ \frac{\partial E}{\partial t} = 0. \tag{4.4}$$

Applying the curl operator ($\nabla\times$) to the third equation we have,

$$\nabla \times \nabla \times E + \nabla \times \frac{\partial B}{\partial t} = 0. \tag{4.5}$$

The time derivative of the Eq. (4.4) yields,

$$\nabla \times \frac{\partial B}{\partial t} = \frac{1}{c^2} \frac{\partial^2 E}{\partial t^2}, \tag{4.6}$$

substituting the equation above inside the Eq. (4.5) using the vector identity $\nabla \times \nabla \times A = \nabla \ . \ \nabla \ . \ A - \nabla^2 A$, the Laplace equation results:

$$\nabla^2 E \ - \frac{1}{c^2} \frac{\partial^2 E}{\partial t^2} = 0, \tag{4.7}$$

which is nothing other than a general wave equation for the propagation of an electromagnetic wave in a waveguide. The complete solution of the equation above can be found in appendix A.

4.1.1 Rectangular Waveguide

There is a homogeneous plane wave solution at a fixed frequency for the Eq. (4.7) as it can be written,

$$E = E_{0y}cos(\omega t - k.r), \tag{4.8}$$

where the following notes can be summarized:

- the vector k: is the wave number in free space ($k = \omega/c$), in the direction of the propagation of the wave,
- the wave propagate in the xz-plane in a direction α,
- the wavelength along the z -axis is bigger than the free space wavelength as $\lambda/cos\alpha > \lambda$,
- linear polarization of the electric field has been chosen in the y-direction,
- The phase velocity in the z -direction is $\frac{c}{\sqrt{1-(\frac{\omega_c}{\omega})^2}} > c$, where ω_c is related to the cut-off frequency.
- $k \; . \; r = \frac{\omega}{c}(zcos\alpha + xsin\alpha)$ where α is an angle of plane wave propagating direction respect to the horizontal z-axis.

Since the electric field is polarized in the y-axis, perfectly conducting planes can be inserted in the y-axis perpendicular to this polarization without perturbing the field distribution. Figure (4.1) shows the superposition of two homogeneous plane waves with equal amplitudes and propagating at angles α and $-\alpha$ creating a rectangular waveguide with the amplitude [18],

$$E_y = 2cos(\frac{\omega}{c}sin\alpha x)cos(\omega t - \frac{\omega}{c}cos\alpha z) = 2cos(k_\perp x)cos(\omega t - k_\perp z). \tag{4.9}$$

This mode has no field dependence on y-axis and it has just x- dependence on field. This special case is called TE_{10} mode, where TE refers to transverse electric. It should be noted that there is no electric field component on the z axis. In the index of TE_{10}, 1 refers to the x axis and 0 to y axis. The cutoff frequency of an electromagnetic waveguide is the lowest frequency for which a mode will propagate in it. Likewise, the cutoff wavelength

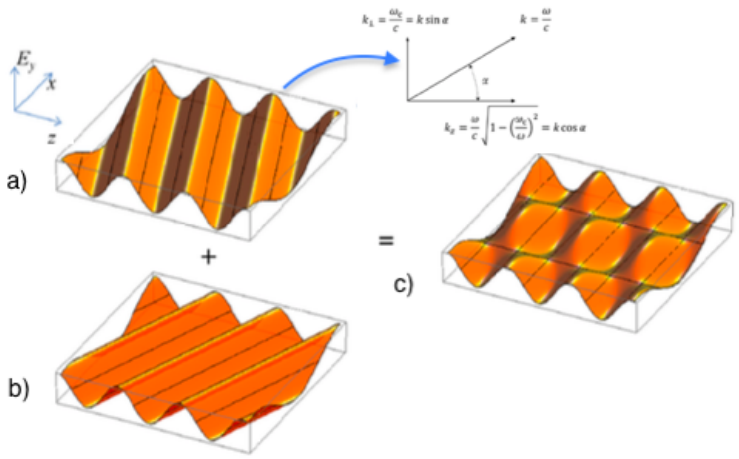

Figure 4.1: The superposition of two homogeneous plane waves forms a waveguide mode a) plane wave propagating at an angle α with respect to the horizontal z-axis b) plane wave propagating at an angle $-\alpha$ with respect to the horizontal z -axis c) a waveguide mode has been constructed from two homogenous plan wave by the superposition principle [18].

is defined as the maximum wavelength that will propagate into the waveguide. The cut-off wavelength can be found with the characteristic equation of the Helmholtz equation (Appendix A) , which is derived from the electromagnetic wave equation ((Eq. (4.7))) by setting the longitudinal wave number equal to zero and solving for the wavelength. Thus, any exciting frequency of the corresponding wavelength lower than the cutoff frequency will attenuate, rather than propagate. Therefore, the cut-off wavelength for the rectangular waveguides would be:

$$\lambda_c = \frac{2}{\sqrt{(\frac{m}{a})^2 + (\frac{n}{b})^2}}, \tag{4.10}$$

where m and n are integers and define the various mode in excited waveguide. Practical application have modes with m, n between 0 and 2. Table (4.1) summarizes the results for wave propagation in rectangular waveguide [19].

4.1.2 Cylindrical Waveguides

It is possible to construct the modes in round waveguides by the superposition of homogeneous plane waves, the same we have performed in the case of rectangular waveguides. Transforming Eq. (4.9) to the cylindrical coordinates, one obtain an expression for the resulting field E_y for the circular TM_{01} mode as [32],

Quantity	TE_{mn} Mode	TM_{mn} Mode
k	$\omega\sqrt{\mu\epsilon}$	$\omega\sqrt{\mu\epsilon}$
k_c	$\sqrt{(\frac{m\pi}{a})^2+(\frac{n\pi}{b})^2}$	$\sqrt{(\frac{m\pi}{a})^2+(\frac{n\pi}{b})^2}$
β	$\sqrt{k^2-k_c^2}$	$\sqrt{k^2-k_c^2}$
λ_c	$\frac{2\pi}{k_c}$	$\frac{2\pi}{k_c}$
λ_g	$\frac{2\pi}{\beta}$	$\frac{2\pi}{\beta}$
ν_p	$\frac{\omega}{\beta}$	$\frac{\omega}{\beta}$
ν_g	$\frac{d\omega}{d\beta}$	$\frac{d\omega}{d\beta}$
α_d	$\frac{k^2 tan\delta}{2\beta}$	$\frac{k^2 tan\delta}{2\beta}$
E_z	0	$B_{mn} sin\frac{m\pi x}{a}\ sin\frac{n\pi y}{b} e^{-j\beta z}$
H_z	$A_{mn} cos\frac{m\pi x}{a}\ cos\frac{n\pi y}{b} e^{-j\beta z}$	0
E_x	$\frac{j\omega\mu n\pi}{k_c^2 b}\ A_{mn} cos\frac{m\pi x}{a}\ sin\frac{n\pi y}{b} e^{-j\beta z}$	$\frac{-j\beta m\pi}{k_c^2 a}\ B_{mn} cos\frac{m\pi x}{a}\ sin\frac{n\pi y}{b} e^{-j\beta z}$
E_y	$\frac{-j\omega\mu m\pi}{k_c^2 a}\ A_{mn} sin\frac{m\pi x}{a}\ cos\frac{n\pi y}{b} e^{-j\beta z}$	$\frac{-j\beta n\pi}{k_c^2 b}\ B_{mn} sin\frac{m\pi x}{a}\ cos\frac{n\pi y}{b} e^{-j\beta z}$
H_x	$\frac{j\omega m\pi}{k_c^2 a}\ A_{mn} sin\frac{m\pi x}{a}\ cos\frac{n\pi y}{b} e^{-j\beta z}$	$\frac{-j\omega\epsilon n\pi}{k_c^2 b}\ B_{mn} sin\frac{m\pi x}{a}\ cos\frac{n\pi y}{b} e^{-j\beta z}$
H_y	$\frac{j\omega n\pi}{k_c^2 b}\ A_{mn} cos\frac{m\pi x}{a}\ sin\frac{n\pi y}{b} e^{-j\beta z}$	$\frac{-j\omega\epsilon m\pi}{k_c^2 a}\ B_{mn} cos\frac{m\pi x}{a}\ sin\frac{n\pi y}{b} e^{-j\beta z}$
Z	$Z_{TE} = \frac{k\eta}{\beta}$	$Z_{TM} = \frac{\beta\eta}{k}$

Table 4.1: Summary of Results for Rectangular Waveguide

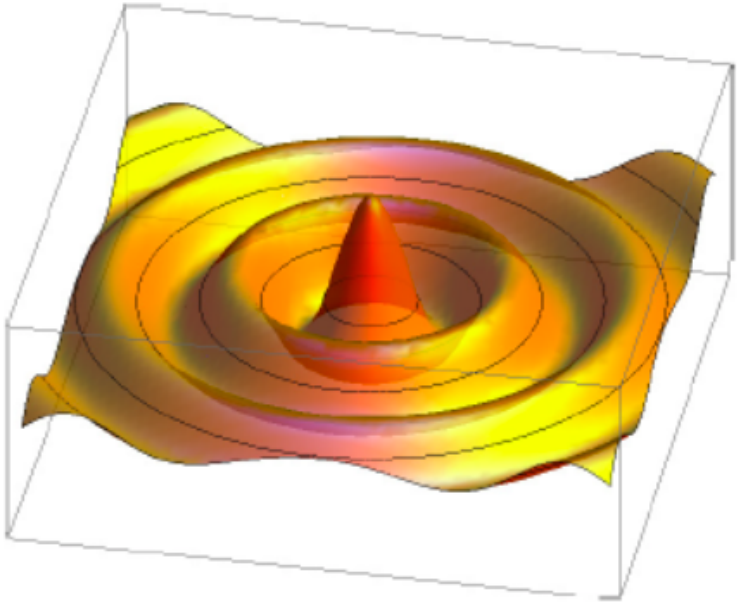

Figure 4.2: Superposition of the homogeneous plane waves can be constructed a Bessel function $J_0(k\rho)$ in which the metallic walls may be inserted where $J_0(k\rho) = 0$ (black lines) and it means at these points the electric field is always zero [32].

$$E_y = \frac{1}{2\pi}\int_0^{2\pi} cos(k\rho(cos(\alpha-\theta))) + d(\alpha-\theta) = J_0(k\rho),$$

which is the integral representation of the Bessel function J_0 as it shows in Fig. (4.2). As we observe in the figure, the superposition of the homogeneous plane waves construct a Bessel function $J_0(k\rho)$ in which the metallic walls may be inserted where $J_0(k\rho) = 0$ and it means at these points the electric field is always zero so that without perturbing this field distribution we construct a circular waveguide at these points. It should be noted that as this field is a radial standing-wave pattern, at these radii we have perfectly conducting boundary conditions.

The cutoff frequencies of TM and TE modes in a round waveguide of radius "b" are given respectively as,

$$\frac{\omega_c}{c} = \frac{\chi_{m,n}}{b}, \tag{4.11}$$

$$\frac{\omega_c}{c} = \frac{\chi'_{m,n}}{b}, \tag{4.12}$$

Quantity	TE_{nm} Mode	TM_{nm} Mode
k	$\omega\sqrt{\mu\epsilon}$	$\omega\sqrt{\mu\epsilon}$
k_c	$\frac{p'_{nm}}{a}$	$\frac{p'_{nm}}{a}$
β	$\sqrt{k^2-k_c^2}$	$\sqrt{k^2-k_c^2}$
λ_c	$\frac{2\pi}{k_c}$	$\frac{2\pi}{k_c}$
λ_g	$\frac{2\pi}{\beta}$	$\frac{2\pi}{\beta}$
ν_p	$\frac{\omega}{\beta}$	$\frac{\omega}{\beta}$
ν_g	$\frac{d\omega}{d\beta}$	$\frac{d\omega}{d\beta}$
α_d	$\frac{k^2 tan\delta}{2\beta}$	$\frac{k^2 tan\delta}{2\beta}$
E_z	0	$(Asinn\phi + Bcosn\phi)\ J_n(k_c\rho)\ e^{-j\beta z}$
H_z	$(Asinn\phi + Bcosn\phi)\ J_n(k_c\rho)\ e^{-j\beta z}$	0
E_ρ	$\frac{-j\omega\mu n}{k_c^2\rho}\ (Asinn\phi - Bcosn\phi)\ J_n(k_c\rho)\ e^{-j\beta z}$	$\frac{-j\beta}{k_c}\ (Asinn\phi + Bcosn\phi)\ J'_n(k_c\rho)\ e^{-j\beta z}$
E_ϕ	$\frac{j\omega\mu}{k_c}\ (Asinn\phi + Bcosn\phi)\ J_n(k_c\rho)\ e^{-j\beta z}$	$\frac{-j\beta n}{k_c^2\rho}\ (Asinn\phi - Bcosn\phi)\ J'_n(k_c\rho)\ e^{-j\beta z}$
H_ρ	$\frac{-j\beta}{k_c}\ (Asinn\phi + Bcosn\phi)\ J_n(k_c\rho)\ e^{-j\beta z}$	$\frac{-j\omega\epsilon n}{k_c^2\rho}\ (Asinn\phi - Bcosn\phi)\ J'_n(k_c\rho)\ e^{-j\beta z}$
H_ϕ	$\frac{-j\beta n}{k_c^2\rho}\ (Asinn\phi - Bcosn\phi)\ J_n(k_c\rho)\ e^{-j\beta z}$	$\frac{-j\omega\epsilon}{k_c}\ (Asinn\phi + Bcosn\phi)\ J'_n(k_c\rho)\ e^{-j\beta z}$
Z	$Z_{TE} = \frac{k\eta}{\beta}$	$Z_{TM} = \frac{\beta\eta}{k}$

Table 4.2: Summary of Results for Circular Waveguide [19].

where $\chi_{m,n}$ denotes the nth zero of the Bessel function J_m and $\chi'_{m,n}$ is the derivative of the Bessel function. The lowest TM mode is the TM_{01} mode with $\chi_{01} \approx 2.405$. On the other side the lowest TE mode for a circular waveguide is TE_{11} with $\chi'_{11} \approx 1.84$. Table (4.2) summarizes the results for wave propagation in circular waveguide.

In the Fig. (4.3) we show the transverse electric and magnetic field distributions of different modes in the rectangular and round waveguides and the general equations for these field distributions will be written in the following sections.

4.1.3 Standing waves in the pillbox cavity

A general solution of wave equation is given,

$$U(r,t) = Ae^{i(\omega t + k.r)} + Be^{i(\omega t - k.r)}, \tag{4.13}$$

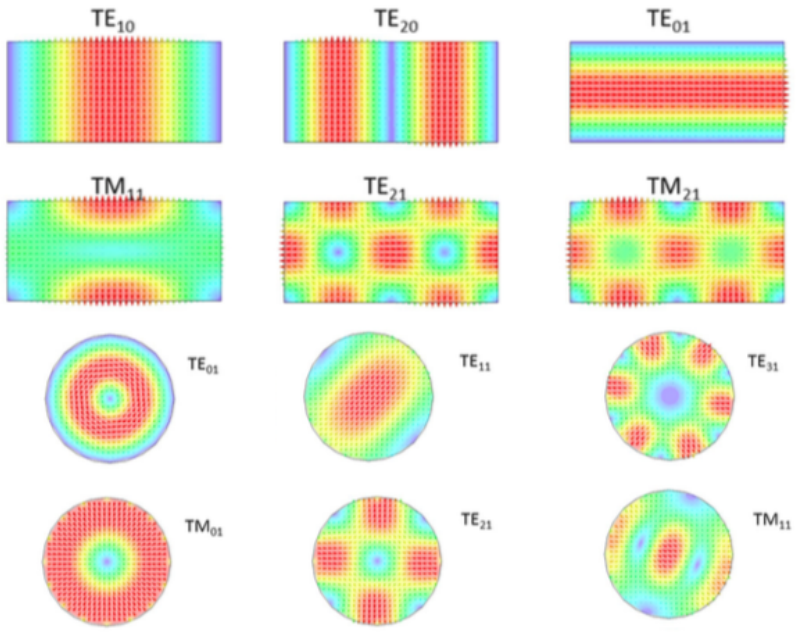

Figure 4.3: Transverse electric and magnetic field distributions of different modes in the rectangular and round waveguides

two waves moving in opposite directions with arbitrary amplitudes A and B. The superposition of a forward and backwards traveling wave has static amplitude $2Acos(kr)$ (standing wave) when $A = B$ as,

$$U(r,t) = Ae^{i\omega t}(e^{ik.r} + e^{-ik.r}) = 2Acos(k.r)e^{i\omega t}. \tag{4.14}$$

The amplitude of the superposition of both waves is zero if: $kr = (n + \frac{1}{2})\pi$, where n=$\pm 1, \pm 2, \pm$ 3, ..., . Introduction of metal walls at this positions will not change the configuration of the field. If the entrance and exit of a waveguide is closed by two perpendicular conducting sheets apart a distance "ℓ", then a stable standing wave is formed if the following condition is satisfied:

$$\ell = q\frac{\lambda_z}{2}, \tag{4.15}$$

with $q = 0, 1, 2, ...$

Only certain well defined wavelengths λ_r (Resonant wavelengths) are present in the cavity:

$$\frac{1}{\lambda^2} = \frac{1}{\lambda_c^2} + \frac{1}{\lambda_z^2}, \tag{4.16}$$

where λ_c is the cut-off wavelength. Putting $\ell = q\frac{\lambda_z}{2}$ into the equation above we get,

$$\frac{1}{\lambda^2} = \frac{1}{\lambda_r^2} = \frac{1}{\lambda_c^2} + \frac{1}{4}(\frac{q}{\ell})^2. \tag{4.17}$$

Near to the resonance wavelength, λ_r, the quality factor ,"Q", of the resonance cavity is high and losses are low. These advantages are used in accelerators to generate high accelerating voltages.

The cut-off wavelength for the rectangular waveguides as resonant cavities is $\lambda_c = \frac{2}{\sqrt{(\frac{m}{a})^2+(\frac{n}{b})^2}}$, therefore the resonant wavelength would be:

$$\lambda_r = \frac{2}{\sqrt{(\frac{m}{a})^2 + (\frac{n}{b})^2 + (\frac{q}{\ell})^2}}, \tag{4.18}$$

or in terms of discrete eigenfrequencies as,

$$\frac{\omega_{m,n,p}}{c} = \sqrt{(\frac{m\pi}{a})^2 + (\frac{n\pi}{b})^2 + (\frac{p\pi}{\ell})^2}. \tag{4.19}$$

where m, n, q are integers and define the various mode in the resonant cavity. Practical application have modes with m, n, q between 0 and 2.

Another type of resonance cavities which are the preferred design for producing accelerating voltages are cylindrical resonant cavities. Let's consider the TM_{01} mode. The resonant wavelength can be obtained by inserting the expression of the cut-off wavelength into the general resonance condition,

$$\lambda_c = \frac{2\pi b}{x_1}, \tag{4.20}$$

where x_1 is the first zero of the Bessel function ($x_1 = 2.40483$) and b is the radius of the cavity:

$$\frac{1}{\lambda^2} = \frac{1}{\lambda_c^2} + \frac{1}{4}(\frac{q}{\ell})^2, \tag{4.21}$$

$$\frac{1}{\lambda^2} = (\frac{x_1}{2\pi b}) + \frac{1}{4}(\frac{q}{\ell})^2, \tag{4.22}$$

then the resonance condition for a cylindrical resonant cavity,

$$\lambda_r = \frac{1}{\sqrt{(\frac{x_1}{2\pi b}) + \frac{1}{4}(\frac{q}{\ell})^2}}, \tag{4.23}$$

or

$$\frac{\omega_{m,n,p}}{c} = \sqrt{(\frac{\chi_{m,n}}{b})^2 + (\frac{p\pi}{\ell})^2}. \tag{4.24}$$

with $q = 0, 1, 2, ...; x1 = 2.405$ is the first zero of the Bessel function. In cylindrical accelerators the mode with $q = 0$ (TM_{010}) is used. Then the resonance wavelength is:

$$\lambda_r = \frac{2\pi b}{x_1}. \tag{4.25}$$

It should be noted that for this mode TM_{010} ,"l" does not affect the resonant wavelength. The fundamental mode of a pillbox cavity (TM_{010} mode) is given,

$$\frac{\omega_{0,pillbox}}{c} \approx \frac{2.405}{b}. \tag{4.26}$$

The fields of the TM_{010} mode (pillbox) are given by

$$E_z = E_0 \; J_0(kr) \; cos(\omega t), \tag{4.27}$$

$$H_\phi = -\frac{E_0}{\eta_0} \; J_1(kr) \; sin(\omega t), \tag{4.28}$$

where m=p=0, n =1. p=0 indicates that there is no axial field dependence and consequently the eigenfrequency is the cutoff frequency of the TM_{01} mode of the round waveguide. In the following section we will discuss on the fields of TM modes in a general way.

4.2 TM_{mnp}

TM modes in a chain of cylindrical "pill-box" cavities provide accurate model for the accelerating fields in more realistic accelerating structures. The properties of a single cylindrical resonator are simple to treat analytically, and will be as a starting point for a discussion of standing-wave accelerating structures. TM solution to the wave equation in cylindrical coordinates has the form [4], with the sinusoidal time dependence removed:

$$E_z = J_m(k_{mn}r) \; cos(m\theta) \; cos(k_z z), \tag{4.29}$$

$$E_r = p \; J'_m(k_{mn}r) \; cos(m\theta) \; sin(k_z z), \tag{4.30}$$

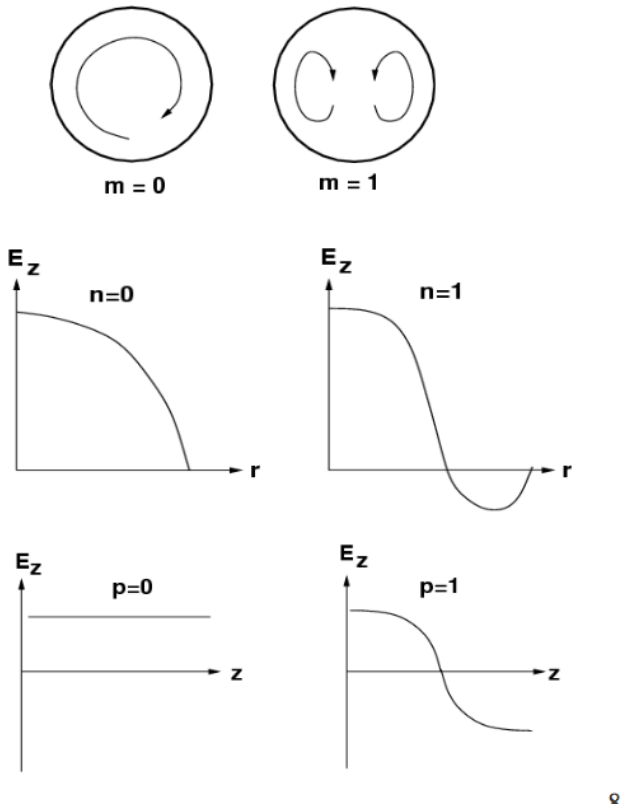

Figure 4.4: The variation of the three indices m,n and p in TM_{mnp} modes

$$E_\theta = \frac{p}{r}\ J_m(k_{mn}r)\ sin(m\theta)\ sin(k_z z), \tag{4.31}$$

$$B_z = 0, \tag{4.32}$$

$$B_r = -\frac{i}{r}\ J_m(k_{mn}r)\ sin(m\theta)\ cos(k_z z), \tag{4.33}$$

$$B_\theta = -i\ J'_m(k_{mn}r)\ cos(m\theta)\ cos(k_z z), \tag{4.34}$$

where m, n, p are integers that describe the mode of the solution. The J_m are Bessel functions of the first kind. J'_m is the derivative of the Bessel function. $k_z = \frac{\pi p}{L_{Cavity}}$, $\frac{\omega^2}{c^2} = k_{mn}^2 + k_z^2$ and the "i" in the equations for B is $\sqrt{-1}$ and indicates that the E and B fields are 90° offset from each other in RF phase. The integers in the TM Mode are indicated as,

- "m" is the number of variation of field of the azimuthal variable ϕ, m = 0, 1, 2, ...

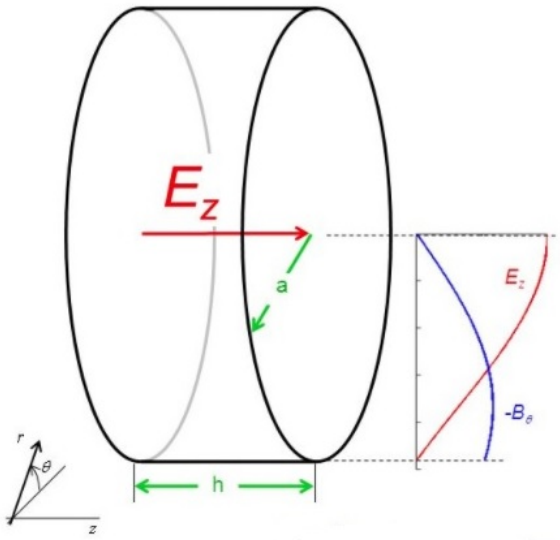

Figure 4.5: Fields in a pillbox cavity for the TM_{010} mode

- "n" is the number of nulls in E_z along the radial direction, n = 1, 2, 3, ...
- "p" is the number of nodes of E_z along the z-axis, p = 0, 1, 2, ...

The variation of the three indices have been shown in Figure (4.4).

4.3 TM_{010}

Consider a pill-box cavity with radius b and axial length ℓ. The axial electric and azimuthal magnetic field components for the lowest order accelerating mode TM_{010} mode are (see Fig.s (4.5) and (4.6)),

$$E_z = E_0 \; J_0(k_c r) \; cos(\omega t), \tag{4.35}$$

$$H_\phi = -\frac{E_0}{\eta_0} \; J_1(k_c r) \; sin(\omega t), \tag{4.36}$$

where $\eta_0 = 377$ is the impedance of free space and it's a physical constant relating the magnitudes of the electric and magnetic fields of electromagnetic radiation traveling through free space and it has the exact value $\eta_0 = 376.73$ Ohms, k_c is cutoff wavenumber and it has a definition $k_c = \frac{2\pi}{\lambda_c} = \chi_{01}/b$ and $\chi_{01} = 2.405$ is the first root of J_0.
The stored energy in pill-box cavity is given by:

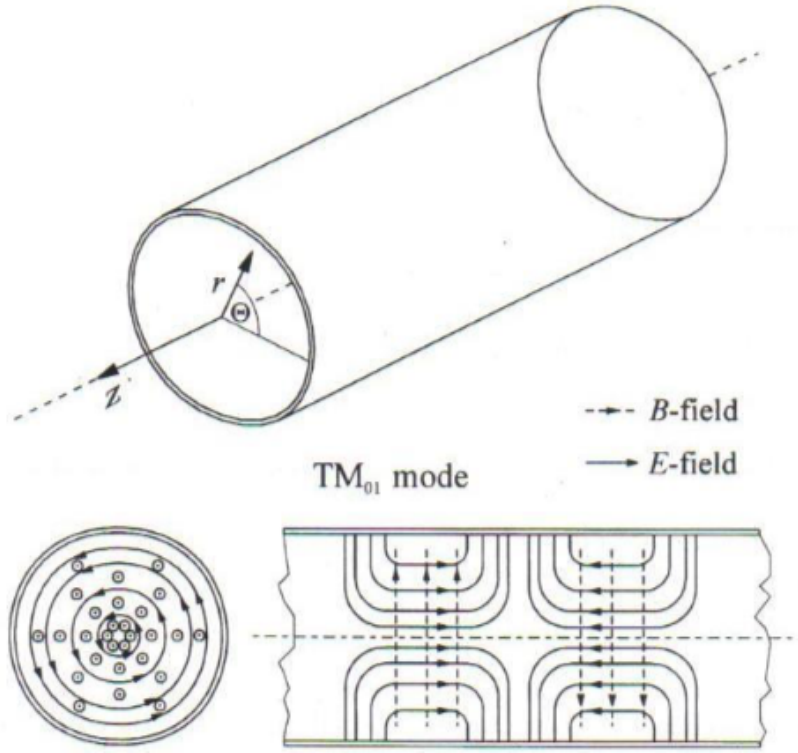

Figure 4.6: TM_{010} Mode

$$U = \frac{\epsilon_0}{2} \int_V E_z^2 dV, \tag{4.37}$$

where ϵ_0 is vacuum permittivity, sometimes called the electric constant and has a value of approximately $8.85 \times 10^{-12} F/m$. E_z is the longitudinal electric field as given in Eq. (4.35) and the integral should be taken over the volume of the cavity.

$$U = \frac{\epsilon_0}{2} \int_0^b \int_0^{2\pi} \int_0^\ell E_0^2 J_0^2(k_c r)\ cos^2\phi\ r\ dz\ d\phi\ dr, \tag{4.38}$$

where $\phi = \omega t$ and $J_0(k_c r)$ is the Bessel function of the first kind. integrating over the internal surface of the cavity we have,

$$U = \frac{\epsilon_0}{2}\ E_0^2 \ell\pi \int_0^b r\ J_0^2(k_c r)\ dr, \tag{4.39}$$

$$= \frac{\epsilon_0}{4}\ \pi\ \ell\ E_0^2\ b^2(J_0^2(k_c b)\ +\ J_1^2(k_c b)),$$

$$= \frac{\epsilon_0}{4}\ \pi\ \ell\ E_0^2\ b^2(J_0^2(\chi_{01})\ +\ J_1^2(\chi_{01})),$$

considering that $J_0^2(\chi 01) \approx 0$ we have,

$$U = \frac{\pi\epsilon_0}{4}\ b^2\ \ell\ E_0^2\ J_1^2(k_c b). \tag{4.40}$$

or

$$U = \frac{\pi\epsilon_0}{4}\ b^2\ \ell\ E_0^2\ J_1^2(\chi_{01}). \tag{4.41}$$

If dA is the area element on the cavity walls, the average power dissipation per cycle is

$$P = \frac{R_s}{2}\ \int_A H_\phi^2 dA, \tag{4.42}$$

where R_s is defined as RF surface resistance and is given by

$$R_s = \frac{1}{\sigma\delta}, \tag{4.43}$$

σ is conductivity of the material and δ is define as skin depth. Copper, with a room-temperature resistivity of $\rho = 1/\sigma = 1.7\times10^{-8}$ ohm/m, is the most commonly used metal for accelerator applications. For a good but not perfect conductor, fields and currents are not exactly zero inside the conductor, but are confined to within a small finite layer at the surface, called the skin depth. In a real conductor, the electric and magnetic fields, and the current decay exponentially with distance from the surface of the conductor, a phenomenon known as the skin effect. The skin depth is given by

$$\delta = \sqrt{\frac{2}{\sigma\mu_0\omega}}. \tag{4.44}$$

Because of the skin effect, the ac and dc resistances are not equal. Physically, the skin effect is explained by the fact that RF electric and magnetic fields applied at the surface of a conductor induce a current, which shields the interior of the conductor from those fields. Using Eq. (4.43) we find $R_s = \sqrt{\frac{\mu_0\omega}{2\sigma}}$, which shows that the ac or RF surface resistance is proportional to the square root of the frequency. Let's return to calculate average power dissipation. "A" is the inner surface of a closed cavity and the dissipation can be calculated in two parts, one the power dissipated of the cavity walls and the other, the losses in the end caps of the cavity. The total dissipation is obtained from the summation of the power losses in both the wall and the end caps.

$$P_L = P_{LW} + P_{LE}, \tag{4.45}$$

P_{LW} is power losses in the walls and it can be written after some calculation as $P_{LW} = \frac{\pi R_s a\ell}{2}(\frac{E_0}{\eta_0})^2\ J_1^2(\chi_{01})$ where R_s is surface resistance, a and ℓ are radius and length of the cavity, respectively. $\eta_0 = 377$ ohms and $\chi_{01} = 2.405$ is the first root of J_0. P_{LE} is the losses in the end caps of the cavity and it can be obtained from the procedure below

$$P_{LE} = \frac{R_s}{2}\int_0^b\int_0^{2\pi}\ (-\frac{E_0}{\eta_0}\ J_1(kr)\ sin(\omega t))^2 r dr,$$

$$= \pi R_s(\frac{E_0}{\eta_0})^2\int_0^b\ rJ_1^2(kr)dr. \tag{4.46}$$

To calculate the integration of the Eq.(4.46) we use equation below, integrating over the cavity radius,

$$\int_0^b rJ_1^2(k_c r)dr = \frac{b}{2}[bJ_0^2(k_c b)\ + bJ_1(k_c b) - \frac{2}{k}J_0(k_c b)\ .\ J_1(k_c r)], \tag{4.47}$$

considering that $J_0^2(\chi_{01}) \approx 0$ and putting the integration result into the Eq. (4.46) we get,

$$P_{LE} = \frac{\pi R_s b^2}{2}(\frac{E_0}{\eta_0})^2\ J_1^2(k_c b) = \frac{\pi R_s b^2}{2}(\frac{E_0}{\eta_0})^2\ J_1^2(\chi_{01}). \tag{4.48}$$

Finally we obtained en equation for total power dissipated of the cavity for the fundamental mode of the resonance cavity, TM_{010},

$$P = \frac{R_s}{2}\int_A H_\phi^2\ dA = \frac{\pi b R_s E_0^2}{2\eta_0^2}\ (b+\ell)J_1^2(\chi_{01}). \tag{4.49}$$

Quality factor:

Quality factor , Q, is the ratio of the stored energy (U) to the power lost on the wall (P) in one RF cycle. It is one of the main cavity parameters and it is given by,

$$Q = \frac{U}{P/2\pi f} = \omega\frac{U}{P}, \tag{4.50}$$

substituting stored energy and power dissipated from Eq.s (4.41) and (4.49) to the equation above we have,

$$Q = \frac{\pi f\epsilon_0\eta_0^2}{R_s}\ \frac{b\ell}{b+\ell}, \tag{4.51}$$

where the η_0 is impedance in free space and is equal to $\eta_0^2 = \frac{\mu_0}{\epsilon_0}$, putting this equation into the Eq.(4.51) we have,

$$Q = \frac{\pi c \mu_0}{\lambda R_s} \frac{b\ell}{b+\ell}, \tag{4.52}$$

λ denotes the wavelength of the TM_{010} and it can be written as,

$$\lambda_{TMnmp} = \frac{2}{\sqrt{(\frac{p}{\ell})^2 + (\frac{\chi_{nm}}{\pi b})^2}} = \frac{2}{\sqrt{(\frac{\chi_{01}}{\pi b})^2}} = 2.61b, \tag{4.53}$$

considering the relation $c\mu_0 = \frac{1}{\sqrt{\epsilon_0 \mu_0}}\mu_0 = \sqrt{\frac{\mu_0}{\epsilon_0}} = \eta_0 = 377$ and $\lambda_{TM010} = 2.61b$ for pill-box cavity and putting into the Eq.(4.52) we get,

$$Q = \frac{1}{R_s} \frac{453}{1+\frac{b}{\ell}}. \tag{4.54}$$

The equation above has been plotted as we shows in figure (4.7). Horizontal axis is unitless parameter and it is the ratio of cavity length to the cavity radius, b/ℓ. Figure shows the quality factor versus b/ℓ $(radius/gap)$ for a pill-box in the resonance frequency 11.424 GHz. As we observe the quality factor decreases as the ratio (b/ℓ) increases with a scale of $f^{-\frac{1}{2}}$. Another quantity is used practically only for cavities and its called geometric factor and it is independent of the losses in the cavity walls and only depends on the geometry of the cavity. Geometric factor versus b/ℓ $(radius/gap)$ for a pill-box has shown in the figure (4.8), it is independent of the losses and the frequencies of the cavity and only depends on the geometry of the cavity,

$$G = QR_s = \frac{453}{1+\frac{b}{\ell}}. \tag{4.55}$$

Shunt Impedance upon Quality factor(R/Q):

R/Q should be considered as a fundamental quantity (even if its notation suggests a derived quantity); it is independent of the cavity losses and depends only on the cavity geometry as it will be demonstrated later. It is given as $\frac{R}{Q} = \frac{V^2}{\omega U}$. To calculate the R/Q we need to obtain the voltage of acceleration,

$$V_{acc} = \int_{-\ell/2}^{+\ell/2} E_0 \, . \, e^{jkz} \, dz = \frac{E_0 \ell sin(\frac{\pi\ell}{\lambda})}{(\frac{\pi\ell}{\lambda})}, \tag{4.56}$$

where E_0 is the average longitudinal electric field of the cavity. Substituting the Eq. (4.56) into the equation $\frac{R}{Q} = \frac{V^2}{\omega U}$ we get,

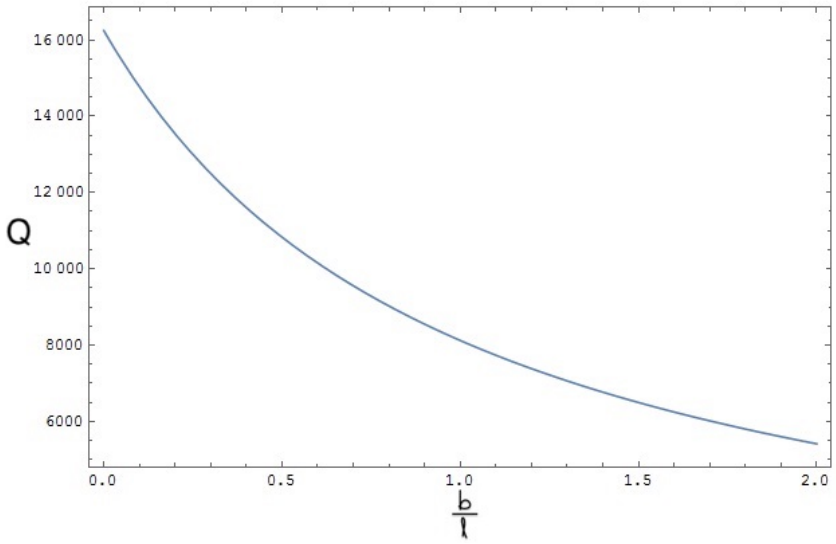

Figure 4.7: Figure (5.8). Quality factor versus b/ℓ ($radius/gap$) for a pill-box for the resonance frequency 11.424 GHz. As it can be seen the quality factor decreases as the ratio (b/ℓ) increases with a scale of $f^{-\frac{1}{2}}$.

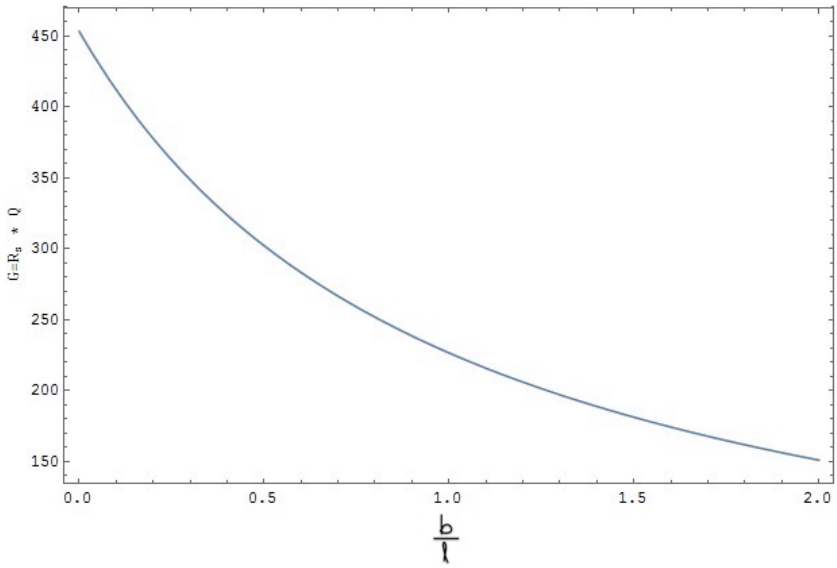

Figure 4.8: Geometric factor versus b/ℓ ($radius/gap$) for a pill-box, it is independent of the losses and the frequencies of the cavity and only depends on the geometry of the cavity.

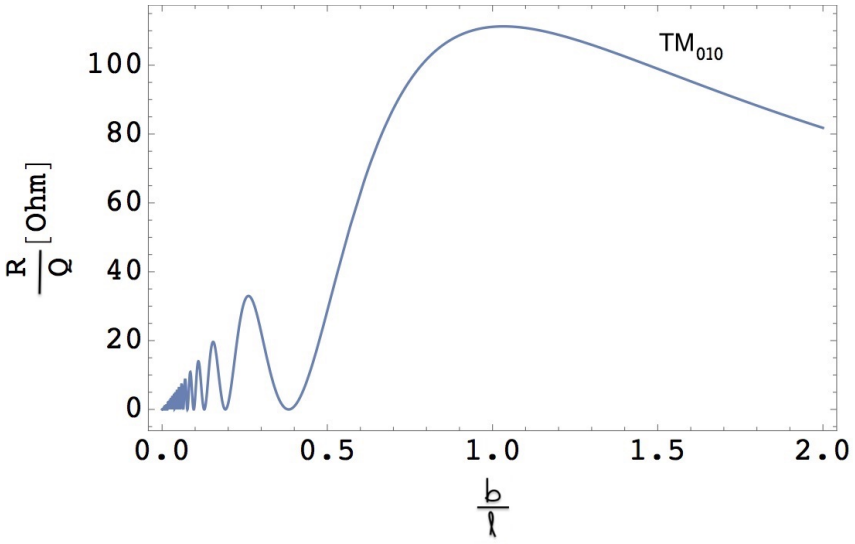

Figure 4.9: R/Q(Ohm) Vs. b/ℓ (radius/gap) in a pill-box

$$\frac{R}{Q} = \frac{2\eta_0}{\chi_{01}^2 J_1^2(\chi_{01})}[\frac{sin(\frac{\pi}{2.61x})}{(\frac{\pi}{2.61x})}]^2 \frac{1}{2.61x}, \tag{4.57}$$

since $\frac{2\eta_0}{\chi_{01}^2 J_1^2(\chi_{01})} \approx 483.75$ then,

$$\frac{R}{Q} = 483.75[\frac{sin(\frac{\pi}{2.61x})}{(\frac{\pi}{2.61x})}]^2 \frac{1}{2.61x}. \tag{4.58}$$

As it has shown in the figure (4.9), this parameter (R/Q) has a maximum value when $\frac{b}{\ell}$ (radius/gap) is 1. In other word when radius of the cavity is equal to the length of the cavity this figure of merit is maximum.

Another cavity parameter is shunt impedance. It can be obtained multiplying the R/Q per Q.

$$R = \frac{K}{R_s}[\frac{sin(\frac{\pi}{2.61x})}{(\frac{\pi}{2.61x})}]^2 \frac{453}{1+x} \frac{1}{2.61x}, \tag{4.59}$$

where K$\approx$ 484.

Shunt impedance is one of the key parameter for the optimization of the accelerating voltage when we are dealing with an available power. The maximum the shunt impedance means the optimum the accelerating voltage. Although shunt impedance is a quantity that is to be optimized from traditional point of view but it may not be the quantity to optimize if the beam current is substantial and the voltage has to be excited by the same beam current in the same impedance [18]. As we shows in Fig. (4.10) at $b/\ell \approx 1$ shunt impedance is maximum. One maybe interested to know these parameters for one meter,

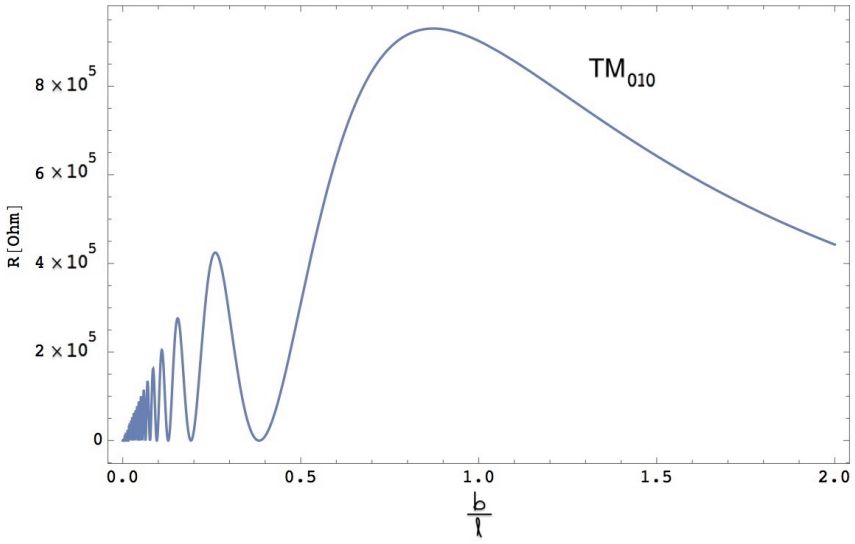

Figure 4.10: R(Ohm) Vs. b/ℓ (radius/gap) for f=11.424 GHz in a pill-box

$$\frac{R}{Q/L} = \frac{Kf}{c}[\frac{sin(\frac{\pi}{2.61x})}{(\frac{\pi}{2.61x})}]^2. \tag{4.60}$$

$$\frac{R}{L} = \frac{Kf}{cR_s}[\frac{sin(\frac{\pi}{2.61x})}{(\frac{\pi}{2.61x})}]^2\frac{453}{1+x}, \tag{4.61}$$

where K$\approx$ 484.

One of the most important parameters to choose when designing a linac is the operating frequency. To make this choice, it is important to know how the cavity parameters vary with the frequency. The accelerator parameters of interest which we have calculated have a frequency scaling factor as follows,

$$Q \propto f^{-\frac{1}{2}}. \tag{4.62}$$

$$\frac{R}{Q} \propto f. \tag{4.63}$$

$$R \propto f^{\frac{1}{2}}. \tag{4.64}$$

4.4 TM_{110}

Considering the same cavity as we have seen in the case of the lowest TM mode with radius b and axial length ℓ. The axial electric and azimuthal and radial magnetic fields

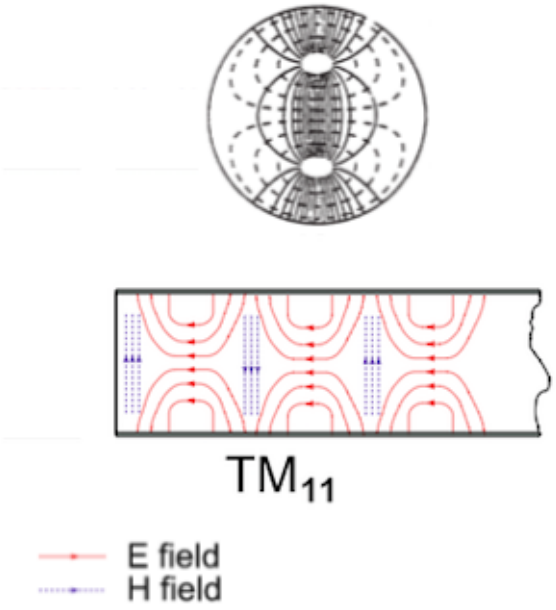

Figure 4.11: Fields distribution in a pillbox cavity for TM_{110} Mode

components for the high order accelerating mode (TM_{110}) are (see Fig. (4.11)),

$$E_z = E_0 \; J_1(k_c r) \; sin\phi, \tag{4.65}$$

$$H_\phi = -j\frac{E_0}{\eta_0} \; J_1'(k_c r) \; sin\phi, \tag{4.66}$$

$$H_r = j\frac{E_0}{\eta_0}\frac{J_1'(kr)}{k_c r} \; cos\phi, \tag{4.67}$$

where E_z is longitudinal electric field, E_0 is average axial electric field, $J_1(kr)$ is bessel function of the first kind, ϕ is the azimuthal angle, H_ϕ and H_r are the azimuthal and radial magnetic fields, respectively. $\eta = 377$ Ohms, $k = \frac{2\pi}{\lambda} = \chi_{11}/b$ and $\chi_{11} = 3.83$ is the first root of J_1. The stored energy is given as follows,

$$U = \frac{\pi\epsilon_0}{4} \; b^2 \; \ell \; E_0^2 \; J_0^2(\chi_{11}). \tag{4.68}$$

The losses in the cylindrical wall for the TM_{110} mode can be written,

$$P = \frac{R_s}{2} \int_A H_\phi^2 dA \tag{4.69}$$

$$= \frac{R_s}{2}\int_A (-\frac{E_0}{\eta_0} \; J_1'(k_c r) \; sin(\phi))^2 dA, \tag{4.70}$$

where R_s is defined as RF surface resistance and has shown in Eq. (4.43). The total dissipation as we have mentioned in the section of TM_{010}, is obtained from the summation of the power losses in both the walls and the end caps. Replacing azimuthal magnetic field, H_ϕ from Eq. (4.66), taking the integral over internal cavity walls in cylindrical coordinate and putting derivative of the first kind of Bessel function, $J_1'(\chi_{11}) = \frac{1}{2}[J_0(\chi_{11}) - J_2(\chi_{11})] = J_0(\chi_{11})$ into the equation, the power dissipation of the walls can be written as,

$$P_{LW} = \frac{\pi R_s b\ell}{2}(\frac{E_0}{\eta_0})^2 \ J_0^2(\chi_{11}). \tag{4.71}$$

Similarly, for the losses in the end caps we take the integral over end caps, substituing $J_1'(kr) = -\frac{J_1(kr)}{kr} + J_0(kr)$ and $kr = \chi_{11}$ in the Eq. (4.70) we obtain,

$$P_{LE} = \pi R_s(\frac{E_0}{\eta_0})^2 \ \int_0^b [\frac{J_0^2(k_c r)}{(k_c r)^2} - \frac{2J_0(k_c r)\ J_1(k_c r)}{k_c r} + J_0^2(k_c r)]\ r\ dr, \tag{4.72}$$

$$= \frac{\pi R_s b^2}{2}(\frac{E_0}{\eta_0})^2 \ J_0^2(\chi_{11}).$$

Total dissipation of TM_{110} mode is obtained from the summation of the power losses in both the wall and the end caps such that

$$P_L = P_{LW} + P_{LE}, \tag{4.73}$$

$$= \frac{\pi R_s}{2}(\frac{E_0}{\eta_0})^2 \ J_1^2(\chi_{11})[b^2 + bh].$$

Having stored energy and power dissipated from previous equations, the quality factor can be written,

$$Q = \frac{\pi c \mu_0}{\lambda R_s}\ \frac{b\ell}{b+\ell}. \tag{4.74}$$

To simplify the Eq.(4.74) we begin to write the relation between the wavelength and the size of the cavity,

$$\lambda_{TMnmp} = \frac{2}{\sqrt{(\frac{p}{\ell})^2 + (\frac{\chi_{nm}}{\pi b})^2}}, \tag{4.75}$$

For the TM_{110} we have,

$$\lambda_{TM110} = \frac{2}{\sqrt{(\frac{\chi_{11}}{\pi b})^2}}, \tag{4.76}$$

$$\lambda_{TM110} = 1.64b, \tag{4.77}$$

considering this relation $c\mu_0 = \frac{1}{\sqrt{\epsilon_0\mu_0}}\mu_0 = \sqrt{\frac{m u_0}{\epsilon_0}} = \mu_0 = 377$ and $\lambda = 1.64b$ for pill-box cavity and putting into the Eq.(4.74) for quality factor we obtain,

$$Q = \frac{\pi\eta_0}{1.64bR_s}\frac{b\ell}{b+\ell}, \tag{4.78}$$

$$= \frac{722}{R_s}\frac{\ell}{b+\ell},$$

and at the end replacing $x = b/\ell$ into the equation,

$$Q = \frac{1}{R_s}\frac{722}{1+\frac{b}{\ell}}. \tag{4.79}$$

The geometric factor which is independent of the losses in the cavity and just depend on the geometry of the cavity can be written,

$$G = QR_s = \frac{722}{1+\frac{b}{\ell}}. \tag{4.80}$$

We perform the same procedure for TM_{110} that has been accomplished to calculate the shunt Impedance upon quality factor(R/Q) and shunt impedance (R) for the lowest mode TM_{010} and we obtain ,

$$\frac{R}{Q} = K\ [\frac{sin(\frac{\pi}{1.64x})}{(\frac{\pi}{1.64x})}]^2\frac{1}{1.64x}, \tag{4.81}$$

$$R = K\ [\frac{sin(\frac{\pi}{1.64x})}{(\frac{\pi}{1.64x})}]^2\frac{722}{1+x}\frac{1}{1.64x}, \tag{4.82}$$

where $K = \frac{2\eta_0}{\chi_{01}^2 J_1^2(\chi_{01})} \approx 317$. As it shows in figure (4.12), (R/Q) has a maximum value at b/ℓ=1.5 for the TM_{110} mode and maximum value for shunt impedance is at a value a little less than 1.5 as we can observe in figure (4.13).

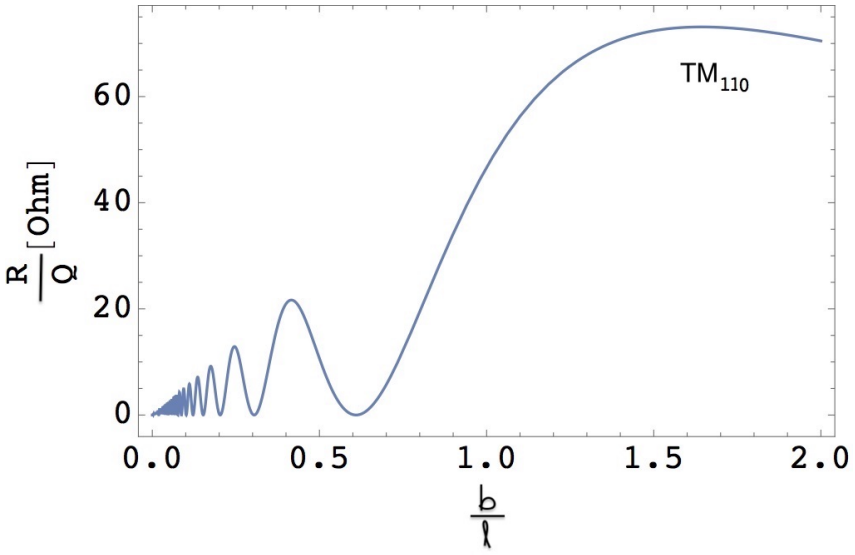

Figure 4.12: R/Q (Ohm) Vs. b/ℓ (radius/gap) in a pill-box

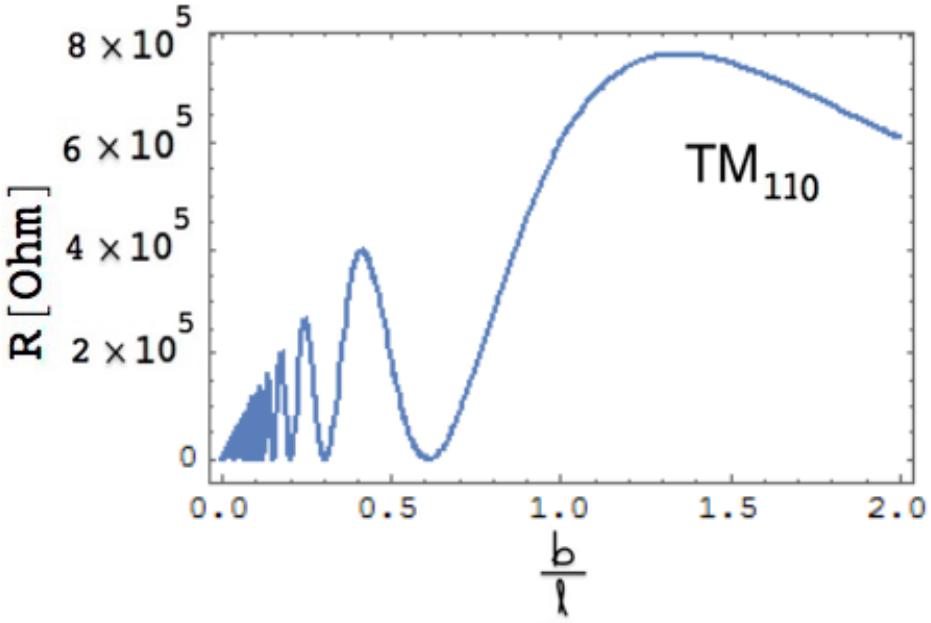

Figure 4.13: R(Ohm) Vs. b/ℓ (radius/gap) for f=11.424 GHz in a pill-box

4.5 TM_{011}

Considering the same pillbox cavity as we have calculated the characteristic parameters for TM_{010} and TM_{110} but this time we would be interested to calculated those parameters for another high order mode (TM_{011}). The axial and radial electric and azimuthal magnetic fields components for this mode are,

$$E_z = E_0 \ J_0(\frac{\chi_{01}\rho}{b}) \ cos(\omega t), \tag{4.83}$$

$$E_\rho = \frac{\lambda}{2\ell} E_0 \ J_1(\frac{\chi_{01}\rho}{b}) \ sin(\omega t), \tag{4.84}$$

$$H_\phi = -j\frac{E_0}{\eta_0} J_1(\frac{\chi_{01}\rho}{b}) \ cos(\omega t), \tag{4.85}$$

where $\eta_0 = 377$ ohms, $k = \frac{2\pi}{\lambda} = \chi_{01}/b$ and $\chi_{01} = 2.405$ is the first root of J_0. The stored energy and power dissipation are the same as TM_{010} because the longitudinal electric and azimuthal magnetic fields for TM_{010} and TM_{011} are the same and they can be written,

$$U = \frac{\pi\epsilon_0}{4} \ \ell \ E_0^2 \ J_1^2(\chi_{01}). \tag{4.86}$$

$$P = \frac{R_s}{2} \ \int_A H_\phi^2 dA = \frac{\pi b R_s E_0^2}{2\eta_0^2}(b+\ell) \ J_1^2(\chi_{01}). \tag{4.87}$$

The quality factor is the ratio of the stored energy (U) to the power lost on the wall (P) in one RF cycle and it would be,

$$Q = \frac{\pi f \epsilon_0 \eta_0^2}{R_s} \ \frac{b\ell}{b+\ell}, \tag{4.88}$$

substitution of $\eta_0^2 = \frac{\mu_0}{\epsilon_0}$ into the Eq.(4.88),

$$Q = \frac{\pi c \mu_0}{\lambda R_s} \ \frac{b\ell}{b+\ell}, \tag{4.89}$$

as we know the relation between λ, b and ℓ for TM_{011} mode is $\lambda = \frac{2}{\sqrt{(\frac{1}{\ell})^2+(\frac{\chi_{01}}{\pi b})^2}}$ where a and ℓ are radius and length of the cavity respectively. Putting in the Eq.(4.89) we get,

$$Q = \frac{188.5\pi}{R_s} \ \sqrt{1+(\frac{\chi_{01}}{\pi b})^2}\frac{1}{1+x}, \tag{4.90}$$

where x is the ratio of cavity radius to the length of the cavity ($x = \frac{b}{\ell}$) and by multiplication of R_s with quality factor, Geometry factor is obtained, which depends only in size of the cavity, $G = QR_s = 188.5\pi\ \sqrt{1 + (\frac{\chi_{01}}{\pi b})^2}\frac{1}{1+x}$. To calculate the R/Q for this mode we need to obtain the voltage of acceleration,

$$V_{acc} = E_0 J_0(\frac{\chi_{01}\rho}{b})\frac{2\pi\ell cos(\frac{k\ell}{2})}{\pi^2 - k^2\ell^2}. \tag{4.91}$$

We can simplify $\pi^2 - k^2\ell^2$ by substitution of k and ℓ with the Eq.(4.92) and Eq.(4.93):

$$k = \frac{2\pi}{\lambda}, \tag{4.92}$$

$$\ell = \frac{\lambda}{2}\sqrt{1 + (\frac{\chi_{01}}{\pi b})^2}. \tag{4.93}$$

To obtain the Eq.(4.93) for the length of the cavity we performed the following procedure, starting from the relation between wavelength and the size of the cavity for TM_{011},

$$\lambda = \frac{2}{\sqrt{\frac{1}{\ell^2} + (\frac{\chi_{01}}{\pi b})^2}}, \tag{4.94}$$

with some simplification and substituting x = b/ℓ into the equation we have,

$$\ell^2 = \frac{\lambda^2}{4}[1 + (\frac{\chi_{01}}{\pi x})^2], \tag{4.95}$$

and finally we have obtained the formula for the length of the cavity: $\ell = \frac{\lambda}{2}\sqrt{1 + (\frac{\chi_{01}}{\pi x})^2}$. We return to our calculation to obtain the voltage of acceleration,

$$V_{acc} = |E_0 J_0(\frac{\chi_{01}\rho}{b})\frac{2\pi\ell cos(\frac{k\ell}{2})}{\pi^2 - k^2\ell^2}|. \tag{4.96}$$

Just to remind the process it should be noted that we are trying to simplify $\pi^2 - k^2\ell^2$ by substitution of k and L from Eqs.(4.92) and (4.93) in the equation,

$$\pi^2 - k^2\ell^2 = -(\frac{\chi_{01}}{x})^2. \tag{4.97}$$

By substituting the Eq.(4.97) into the Eq.(4.96) for voltage of accelerating we can simplify as:

$$V_{acc} = |E_0 J_0(\frac{\chi_{01}\rho}{b})\frac{2\pi\ell cos(\frac{k\ell}{2})}{-(\frac{\chi_{01}}{x})^2}|. \tag{4.98}$$

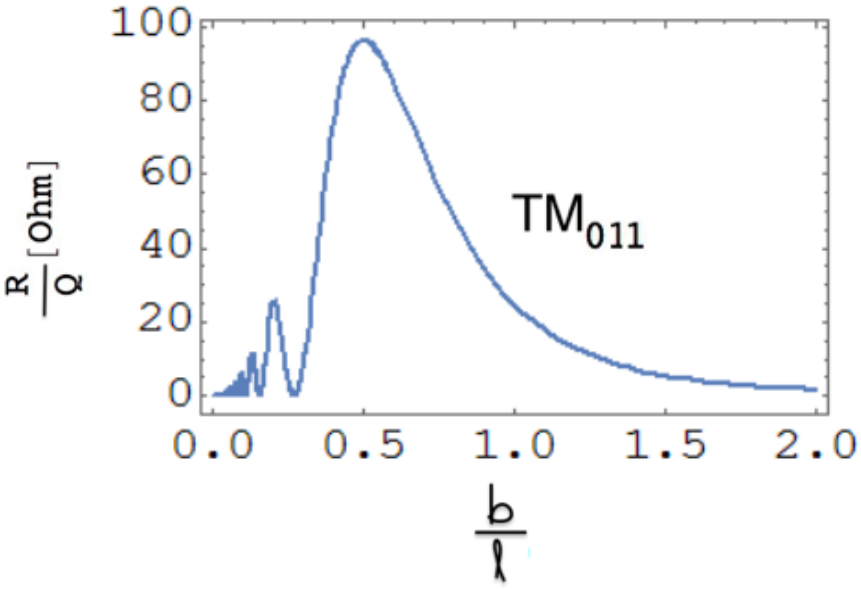

Figure 4.14: R/Q (Ohm) Vs. b/ℓ (radius/gap) in a pill-box

And now we are able to calculate R/Q and R as follows,

$$\frac{R}{Q} = \frac{7.52\pi}{c\ \epsilon\ J_1^2(\chi_{01})}\ \frac{x^3}{\chi_{01}^4}\ \frac{cos^2(\sqrt{(\frac{\pi}{2})^2 + (\frac{\chi_{01}}{2x})^2})}{\sqrt{\pi^2 x^2 + \chi_{01}^2}}. \tag{4.99}$$

$$R = \frac{7.52}{c\ \epsilon\ J_1^2(\chi_{01})}\ \frac{x^2}{\chi_{01}^4}\ \frac{188.5\pi}{R_s}\ \frac{x}{1+x}\ cos^2(\sqrt{(\frac{\pi}{2})^2 + (\frac{\chi_{01}}{2x})^2}). \tag{4.100}$$

As we can observe in Fig.s (4.14) and (4.15), (R/Q) and shunt impedance have their maximum value at b/ℓ=0.5 for the TM_{011} mode.

We can divide the length of the cavity in the formula for R/Q and obtain the shunt impedance over quality factor per meter,

$$\frac{R}{Q/L} = \frac{15\pi^2 f}{c^2\ \epsilon\ J_1^2(\chi_{01})}\ \frac{x^4}{\chi_{01}^4}\ \frac{cos^2(\sqrt{(\frac{\pi}{2})^2 + (\frac{\chi_{01}}{2x})^2})}{\pi^2 x^2 + \chi_{01}^2}. \tag{4.101}$$

4.6 Summary

We have obtained the general expressions of the Quality factor, Shunt impedance upon quality factor for TM_{mnl} as follows,

$$Q(m,n,p,b,\ell) = \sqrt{\frac{c\mu\sigma}{2}}\ \frac{\sqrt{b}\ \chi_{mn}}{p + \frac{b}{\ell}} \qquad p = 0, \tag{4.102}$$

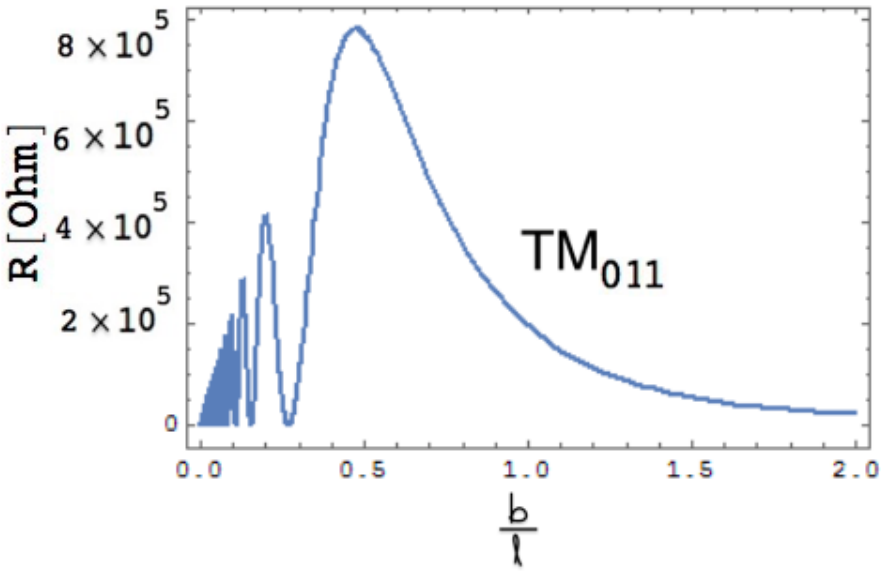

Figure 4.15: R(Ohm) Vs. b/ℓ (radius/gap) for f=11.424 GHz in a pill-box

$$Q(m,n,p,b,\ell) = \sqrt{\frac{c\mu\sigma}{2}} \quad \sqrt[4]{\chi_{mn}^2 + (\pi p \frac{b}{\ell})^2} \frac{\sqrt{b}}{p + \frac{2b}{\ell}} \quad p > 0, \tag{4.103}$$

$$R/Q(m,n,p,x=b/\ell) = \frac{8}{(2^m m!)^2} \; \frac{1}{\pi\epsilon c} \; \frac{x \; \chi_{mn}^{2(m-1)}}{(\sqrt{\chi_{mn} + (\pi p x)^2})^{2m+1}}$$
$$\times [\frac{sin(\frac{\sqrt{(\pi p)^2 + (\frac{\chi_{mn}}{x})^2} - \pi p}{2})}{J_{m+1}(\chi_{mn})}]^2 \; \times \frac{1 \;\; p = 0 \; and \; 2 \;\; p > 0}{2 \;\; m = 0 \; and \; 1 \;\; m > 0}, \tag{4.104}$$

where m, n, p are integers that describe the mode of the solution. The J_m are Bessel functions of the first kind. TM Modes are described by three indices, m, n, p ,

m is the number of variation of field of the azimuthal variable ϕ: m = 0, 1, 2, ...,

n is the number of nulls in E_z along the radial direction n = 1, 2, 3, ...,

p is the number of nodes of E_z along the z-axis. p = 0, 1, 2, ...

Chapter 5

RF Design and Optimization of standing-wave three cell cavities structure

5.1 RF Design

The necessity of the new devices with highest accelerating gradients in order to fabricate compact accelerators at X-band for scientific and industrial applications requires a high advance technology. To determine a reliable ultra high gradient accelerators an extensive experimental and theoretical program are required and many laboratories are working on this issue as they will be the future linear accelerators. In particular, systematic studies on new materials and associated microwave technology for X-band accelerator structures are in progress to achieve accelerating gradients well above 120 MeV/m.

In this framework, we designed and optimized a new accelerating structures working at 11.424 GHz. The structure is a standing wave linear structures with three cells and two circular waveguides located at the beginning and the end of the structure. It has designed in a manner that field gradient at the central cell be twice in order to maximize the RF (radio- frequency) performance and consequently the effective shunt impedance at that cell. Since the breakdown phenomenon is a challenging open problem, we decided to optimize the structure as it shows in Fig. (5.1) to solve the breakdown problem. Indeed, in order to improve the accelerating gradient or generally speaking the higher power performance of X-band structures we must use materials with a high tolerance to surface

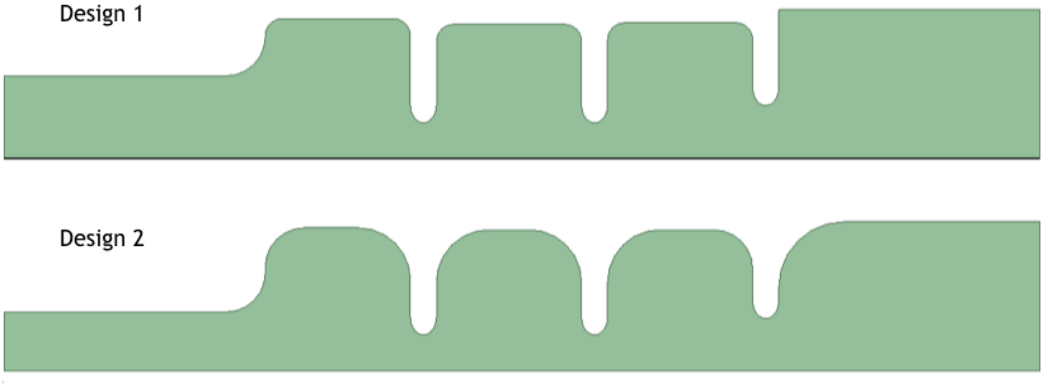

Figure 5.1: Top: standard design for cell-to-cell brazing manufacturing; bottom: high radius fillet are manufactured as for open structures. The optimized cavity has been proposed by SLAC (V. Dolgachev)

fatigue because of avoiding the damage due to the pulsed heating effects, e.g., materials with a higher fusion point, and to avoid the fabrication of soft metal devices as occurs using conventional brazing techniques [22, 23, 25, 26, 27].

In order to characterize a normal conducting high accelerating structure with maximum gradients operating at X-band with extremely low probability of RF breakdown, an electroformed SW structures has been fabricated and characterized by SLAC and INFN with collaboration of other institute around the world at 11.424 GHz, coated with Au-Ni and with different surface roughness [11].

In this chapter we first introduce the procedure of designing RF High gradient structure and then we will optimize the structure to improve characteristics of the model. The numerical code employed for electromagnetic simulations is HFSS [15] (High Frequency Structures Simulator). The geometric 3D model of the structure is given in Fig. (5.2). All geometric parameters needed for the RF design are also shown. HFSS is a software package, initially released by ANSOFT that allows to evaluate the 3D electromagnetic field distribution inside a structure. In order to do this, it solves the Maxwell equations in the frequency domain. The numerical method employed is the FEM (Finite Element Method). HFSS divides the 3D model into a relatively large number of small domains, that represent the mesh. The RF power is fed to the periodic structure flowing along the structure while electromagnetic mode excited with 180° phase advance per cell is similar to the TM_{010} in a circular waveguide. By applying proper boundary conditions

it's not necessary to simulate all structure because the code HFSS allows to simulate periodic structures by only using some percentage of the structure. Then, a simulation with the eigenmode solver finds the frequency at which the electromagnetic field satisfies the phase shift desired. Exploiting the symmetry in the field, only a fraction of the full cell is used for simulations and a condition of perfect magnetic boundary, called "perfect H", is applied. Electric and Magnetic field magnitudes have plotted in Fig.s (5.13) and (5.15) for the TM_{010} mode of the high accelerating periodic structure. As we can observe minimum value of the electric field and maximum value of the magnetic field are near the outer surface of the cavity as it should have been for the TM_{010} mode. This SW High gradient structure is a multi-cell standing-wave structure. The device is contain three cells fed by a circular waveguide. As the central cell has a gradient twice higher than the adjacent ones, it is used to match the RF power from the input circular waveguide. The mode excited to design and test the structure is the π-mode. With this layout, breakdowns occur predominantly in the central cell with the highest gradient cell while the two side cells show surface conditions less perturbed due to lower RF power absorbed per breakdowns [22, 23].

Usually, all cells have the same radius in the first place but when we are going to design the structure in order to get two times longitudinal electric field at its maximum value in the second (center) cell we should change the radius of the cells in a small amount and finally the radius of the cells have a small different in one another. It has been possible to exploit the symmetry of the structure so that, for simulation purposes, only some percentage of the full device is considered. By doing so, computational time turned out to be faster than the full geometry case. The material chosen for the surfaces of structure is normal-conductivity and a boundary condition of "perfect H" is imposed.

5.2 Design Procedure

High accelerating periodic structure design analytically is a difficult task and it requires field solver codes like HFSS that via this code we are able to solve numerically Maxwell's equations for the specified boundary conditions. The procedure for optimization of the structure depends on the constrains of the problem. For example for maximizing the effective shunt impedance of a single cavity ($R_{eff} = R \times T^2$, R is shunt impedance and T

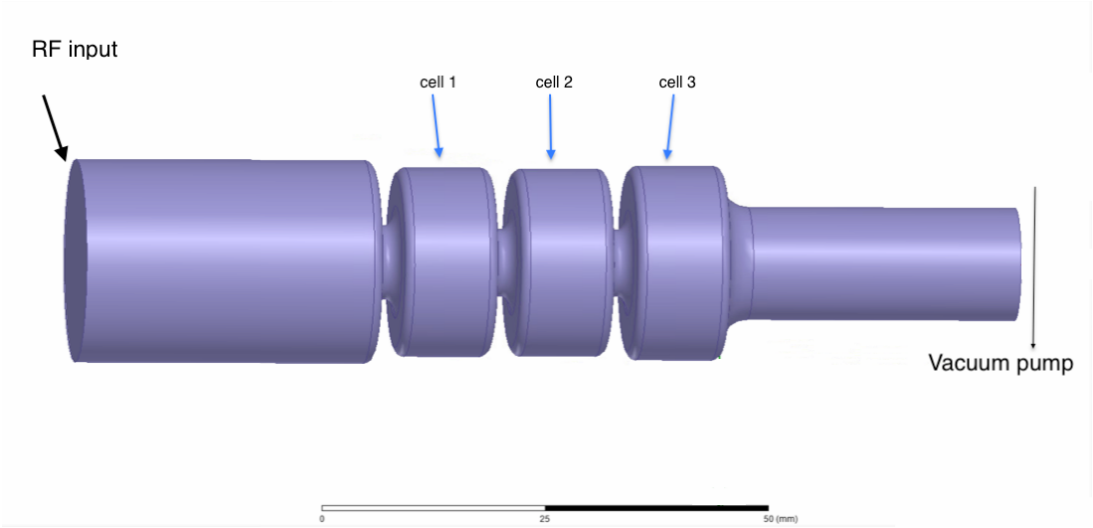

Figure 5.2: The 3D model of a three cell cavities connected to the two circular waveguides located at the beginning and the end of the structure. Two ports have been introduced in the model.

is transit-time factor) transit-time factor should be increased by reducing the gap and for this reason cavity shape may have a nose cone. If the gap is too small then the voltage gain becomes small. With this example we were going to demonstrate that for an optimization of a structure a plan is needed for designers and this plan follows some rules. The design of the high accelerating structure in our case mainly follows three steps:

- choice of geometric dimensions in order to set the cavity resonant frequency at $f_\pi = 11.424\ GHz$, in the π-mode operation,
- achievement of a field flatness condition, that is two times of the field amplitude in the second cell,
- achievement a good reflection coefficient (S11) for the structure.

The algorithm used for the achievement of the specifications listed above employs a linear system of partial differential equations, solved iteratively as follows:

$$\frac{\partial f}{\partial b_1}\Delta b_1 + \frac{\partial f}{\partial b_2}\Delta b_2 + \frac{\partial f}{\partial b_3}\Delta b_3 + \frac{\partial f}{\partial a}\Delta a = \Delta f, \tag{5.1}$$

$$\frac{\partial f f_1}{\partial b_1}\Delta b_1 + \frac{\partial f f_1}{\partial b_2}\Delta b_2 + \frac{\partial f f_1}{\partial b_3}\Delta b_3 + \frac{\partial f f_1}{\partial a}\Delta a = \Delta f f_1, \tag{5.2}$$

$$\frac{\partial ff_2}{\partial b_1}\Delta b_1 + \frac{\partial ff_2}{\partial b_2}\Delta b_2 + \frac{\partial ff_2}{\partial b_3}\Delta b_3 + \frac{\partial ff_2}{\partial a}\Delta a = \Delta ff_2, \tag{5.3}$$

$$\frac{\partial \Gamma}{\partial b_1}\Delta b_1 + \frac{\partial \Gamma}{\partial b_2}\Delta b_2 + \frac{\partial \Gamma}{\partial b_3}\Delta b_3 + \frac{\partial \Gamma}{\partial a}\Delta a = \Delta \Gamma, \tag{5.4}$$

where the differential terms represent the sensitivity of the resonant frequency (f), field flatness (ff_1,ff_2) and reflection coefficient (Γ) with respect to the cell radii b1, b2 , b3 and iris radius "a" . These radii are considered the only geometric variables in order to speed the solution of the system, thus they are the unknown parameters of the system. The Δf, Δff_1, Δff_2, and $\Delta\Gamma$ are the differences between the values obtained at each iteration and the required ones:

$$\Delta f = f_{iteration} - f_{optimum}, \tag{5.5}$$

$$\Delta ff_1 = ff_{1iteration} - ff_{1optimum}, \tag{5.6}$$

$$\Delta ff_2 = ff_{2iteration} - ff_{2optimum}, \tag{5.7}$$

$$\Delta\Gamma = \Gamma_{iteration} - \Gamma_{optimum}, \tag{5.8}$$

where we assume $f_{optimum} = 11.424\,GHz$, $ff_{1optimum} = ff_{2optimum} = 2$, and $20log_{10}\Gamma_{optimum} = -45dB$.

The linear partial differential equations above are the instrument that we can employ to achieve fast optimized and required objective with the help of HFSS. For example if our goal is to find a desired field flatness at a certain frequency we can use three equation of that system as follows,

$$\begin{bmatrix} \frac{\partial f}{\partial b_1} & \frac{\partial f}{\partial b_2} & \frac{\partial f}{\partial b_3} \\ \frac{\partial ff_1}{\partial b_1} & \frac{\partial ff_1}{\partial b_2} & \frac{\partial ff_1}{\partial b_3} \\ \frac{\partial ff_2}{\partial b_1} & \frac{\partial ff_2}{\partial b_2} & \frac{\partial ff_2}{\partial b_3} \end{bmatrix} \begin{bmatrix} \Delta b_1 \\ \Delta b_2 \\ \Delta b_3 \end{bmatrix} = \begin{bmatrix} \Delta f \\ \Delta ff_1 \\ \Delta ff_2 \end{bmatrix} \tag{5.9}$$

It should be noticed that we removed the effect of aperture radius on field flatness because as we will show later this effect is small and it can be negligible while it has a strong contribution when we are going to achieve a minimum reflection coefficient.

First matrix in the linear partial differential equations is called sensitivity matrix that we recall it from the equation above as,

$$\begin{bmatrix} \frac{\partial f}{\partial b_1} & \frac{\partial f}{\partial b_2} & \frac{\partial f}{\partial b_3} \\ \frac{\partial f f_1}{\partial b_1} & \frac{\partial f f_1}{\partial b_2} & \frac{\partial f f_1}{\partial b_3} \\ \frac{\partial f f_2}{\partial b_1} & \frac{\partial f f_2}{\partial b_2} & \frac{\partial f f_2}{\partial b_3} \end{bmatrix} \tag{5.10}$$

By the sensitivity matrix or mathematically speaking the Jacobian matrix we are able to find an interval in which we choose three optimized parameter for the cell radii (b1, b2, b3) after few iterations. The procedure to find an optimized cell and iris radii will be brought later.

As an example we are going to find how much the cavity radii should be changed to get an optimized frequency and field flatness when we are in a condition that for $b_1 = 10.634$, $b_2 = 10.551$, $b_3 = 10.927$ with the corresponding frequencies 11.4257, 11.4284 and 11.4261, respectively. Field flatness also are $ff_1 = 0.5028, 0.3897, 0.4530$ and $ff_2 = 0.5266, 0.5280, 0.5746$, respectively for b_1, b_2 and b_3. Substituting the preceding results we can find the sensitivity matrix. Replacing all these values into the Eq. (5.9) and with the help of Jacobian matrix and running some simulation we obtain the following results: $b_1 = 10.633$ mm, $b_2 = 10.550mm$ and $b_1 = 10.926$. The resonant frequency is at 11.424 GHz and the phase shift between the cells assures the build-up of the π mode.

For a pill-box or periodic structures with array of pill-boxes operating at a given resonant frequency, frequency varies inversely with the cavity radius. As it has shown in Fig.(5.3) the resonant frequency vary inversely with the cell radii.

The peak surface electric field and magnetic field are two important constraints for the cavity designers. In normal-conducting cavities, a typical ratio of peak surface electric field E_s to average axial field E_0 is 6, otherwise the value more than that can result in electric breakdown [4]. To avoid the electric breakdown we choose three cells. The central cell has a gradient twice higher than the adjacent ones. With this layout, breakdowns occur predominantly in the central cell with the highest gradient cell while the two side cells show surface conditions less perturbed due to lower RF power absorbed. The quantity normalized field flatness, that we'll refer to as "ff" further on, can be defined as $ff = \frac{E_m}{E_M} \times 100\%$, where E_m and E_M are the minimum and maximum value of the amplitude of the axial electric field. We will define two field flatness, one is the ratio between the amplitude of the axial electric fields of central cell to the first cell which we denoted

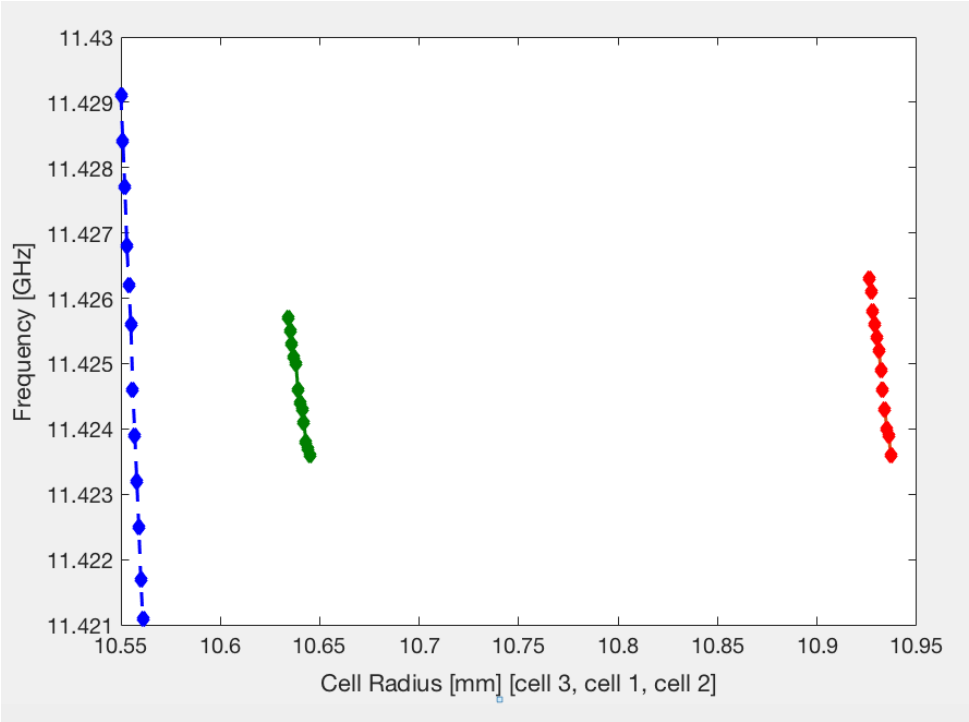

Figure 5.3: Frequency mode as function of the cell radii of the SW structure for 11.424 GHz. Green, red and blue points are the frequency mode of the first, second and third cells, respectively.

as "ff_1" and the other field flatness would be "ff_2" which is nothing other than the ratio between amplitude of the central field to the field of the third cell. To achieve $ff_1 = ff_2 = 2$ for our purpose we have to change the radius of the cells in a small amount and finally the radius of the cells have a small different in one another. The variation of field flatness with the cell radii has shown in Fig. (5.4). As it can be observed, ff_1 and ff_2 have a small fluctuation by changing the radius of the first cell. In some points we do not have a variation in field flatness. It should be noticed that reducing a field flatness in a cell radius for example when the first cell has a radius equal 10.638 mm, the corresponding field flatness is increasing to fix the axial electric field constant at a certain iris (aperture) radius.

After achieving the highest gradient cell at the central cell with the ratio two times respect to the other cells as it could be seen in Fig (5.5), it is time to decrease the reflection coefficient at the entrance of the cells in the waveguide to raise the amplitude of the axial electric fields inside the cells. The aperture radius is usually a key parameter to satisfy the beam dynamics requirement for high transmission coefficient. Changing the iris radius coupled between the waveguide and first cell is a convenient key and only way to

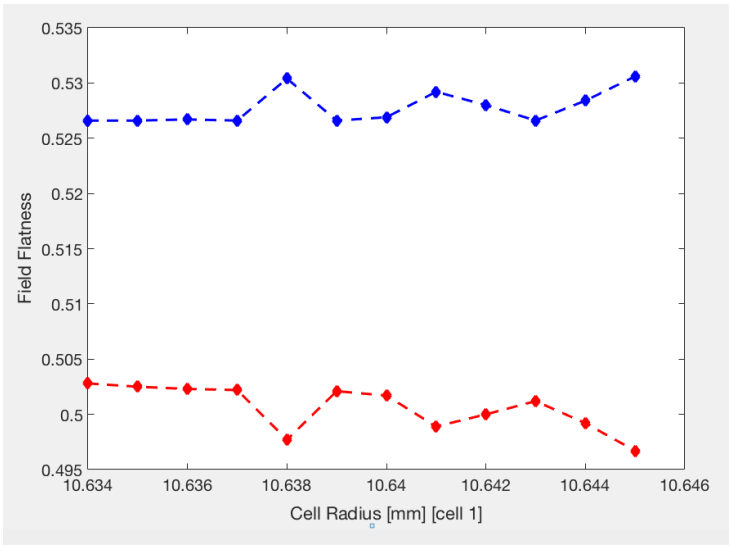

(a)

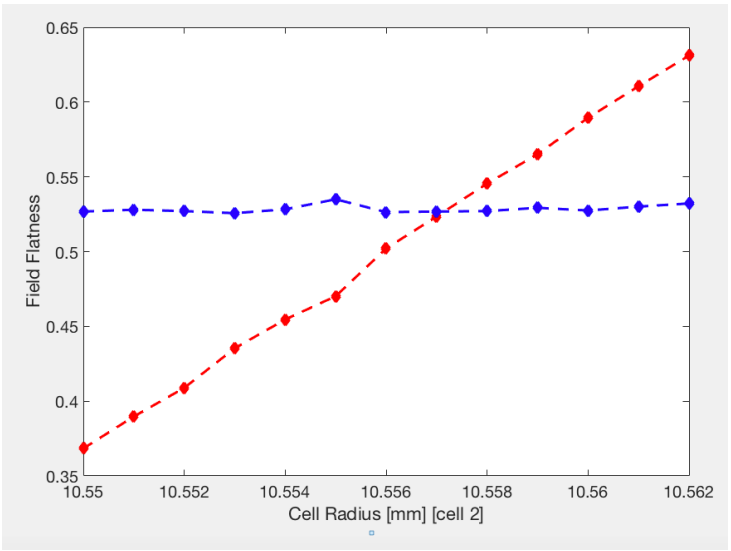

(b)

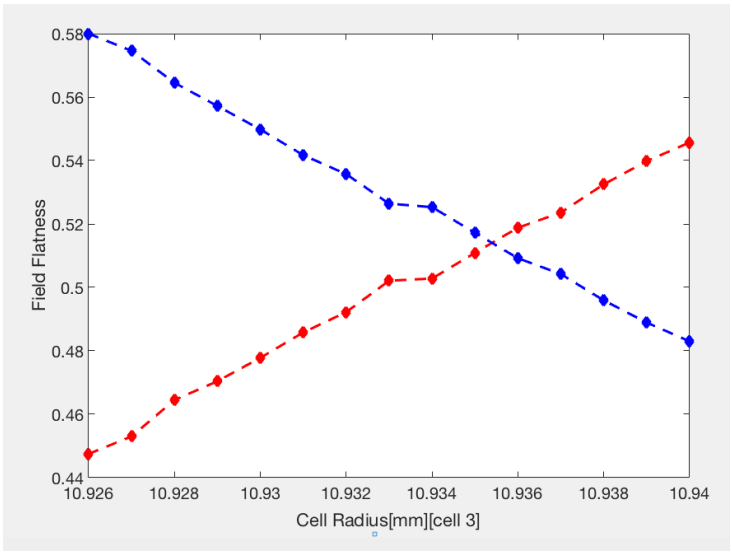

(c)

Figure 5.4: Field flatness as function of the cell radii of the SW structure for 11.424 GHz. (a), (b) and (c) are the field flatness as function of the first, second and third cell radius , respectively. Red and blue points are ff_1 and ff_2, respectively.

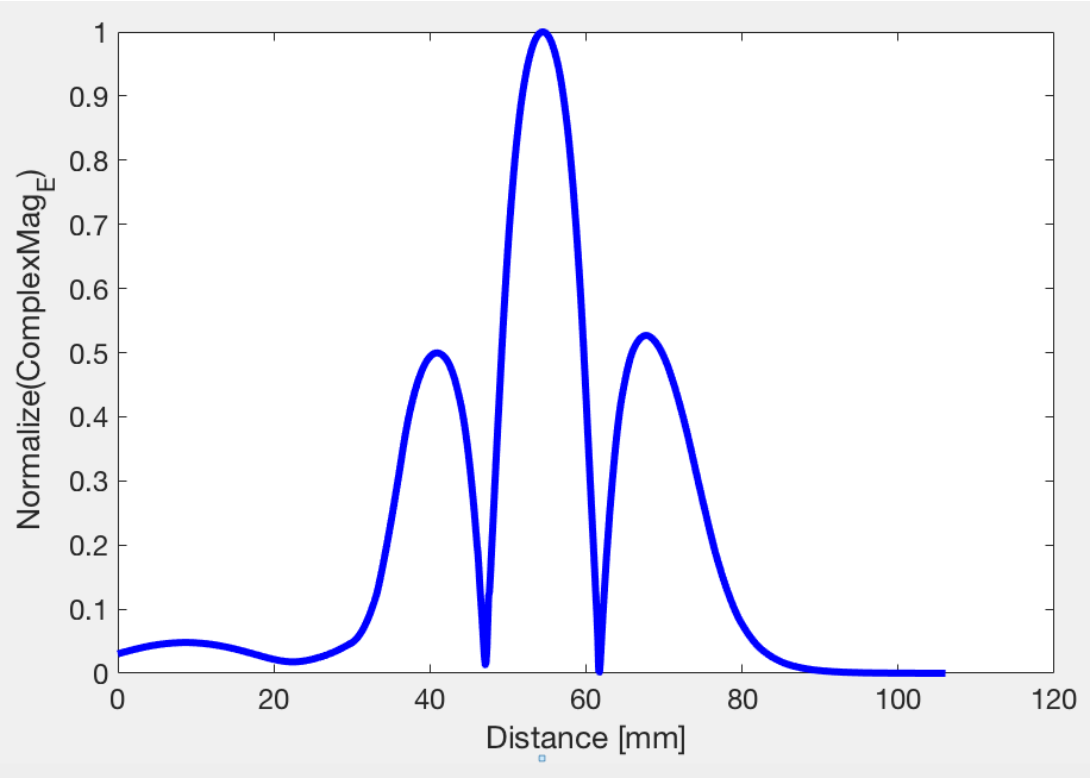

Figure 5.5: Amplitude of the axial electric field Ez [V/m] at the resonance frequency f_π = 11.4228 GHz

achieve a minimum reflection coefficient (Γ) or on the other word a maximum transmission coefficient (T). In practice, the most commonly quoted parameter for reflection coefficient is s_{11}. S_{11} represents how much power is reflected from the waveguide, and hence is known as the reflection coefficient . It is common to express ratios in physics and engineering in decibels which calculates as 10 times the logarithm (base 10) of some base power ratio. The same thing can be done for s_{11} but as s_{11} is the ratio of voltages, so power is based on the square of the voltage and converting a voltage ratio to decibels we can write $s_{11} = 20\ log_{10}\Gamma$. If s_{11}=0 dB, then all the power is reflected from the waveguide nothing is passed to the cell cavities. If s_{11}=-10 dB, this implies that almost 0.3 of the incident waves will be reflected. s_{11}=-40 dB means 0.01 of the waves are reflected and majority of the waves will be delivered to the cavities.

Fig. (5.6) implies that at the frequency 11.4247 GHz, where s_{11} ≈-30 dB we have the minimum reflection from the iris coupled between the waveguide and the first cell and consequently the transmission from that aperture would be at its maximum value at that frequency. The accelerator bandwidth can also be determined from the figure. The bandwidth can be obtained either from s_{11} or s_{21} in the case of under coupling where

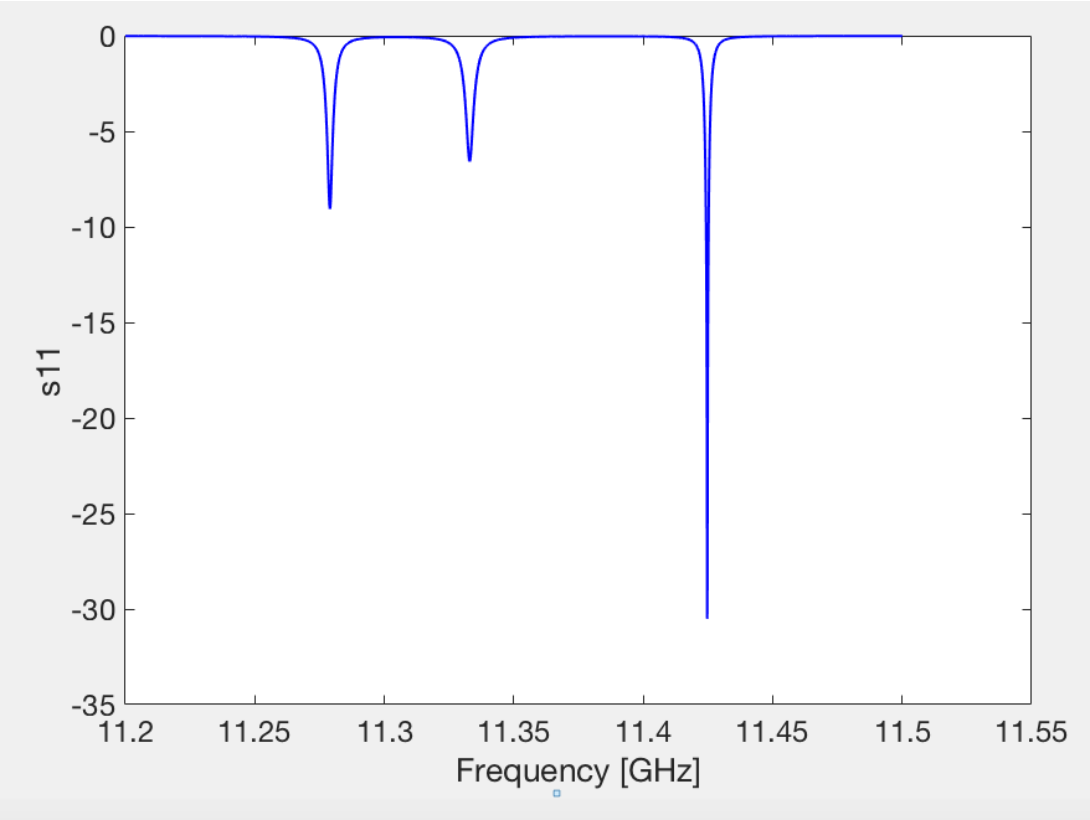

Figure 5.6: Amplitude of Reflection coefficient, s_{11} as a function of the frequency simulated by HFSS.

coupling coefficient (β) is less than 1. In the case of over coupling it is measured from s_{21}. In our case we can measure it with both of them. If the bandwidth is defined as the frequency range where s_{11} is to be less than -3 dB, then the bandwidth would be roughly 3 MHz, with 11.4263 GHz the high end and 10.4233 GHz the low end of the frequency band. Fig (5.7) shows the same result as we discussed for s_{11} but we have maximum transmission coefficient at the frequency operation, 11.4247 GHz.

Fig (5.8) shows the phase shift of the on-axis electric field inside the SW section. As we can observe the phase shift between each cells is π. Fig (5.9) shows the dependence of s_{11} to the aperture radius. As it can be observed from the figure increasing the iris radius, the reflection coefficient decrease until to the certain radius which has the minimum reflection from the waveguide and maximum transmission to the structure. On the other hand after that point by increasing the iris radius, reflection coefficient will be increased and we are in a condition of low transmission. This point is called critical coupling and the structure for the iris radius less than that point is under coupling condition and for the iris radius bigger than that point is over coupling. For our convenient of interpretation

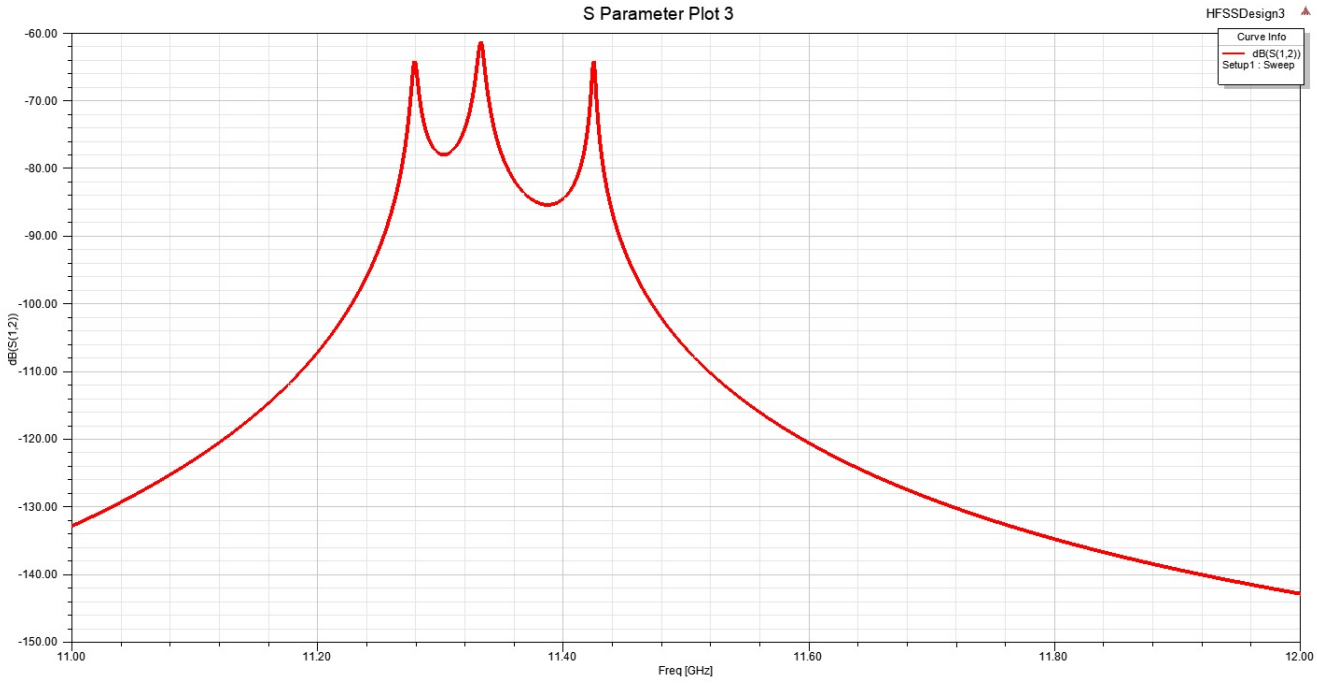

Figure 5.7: Amplitude of Transmission coefficient, s_{21} as a function of the frequency

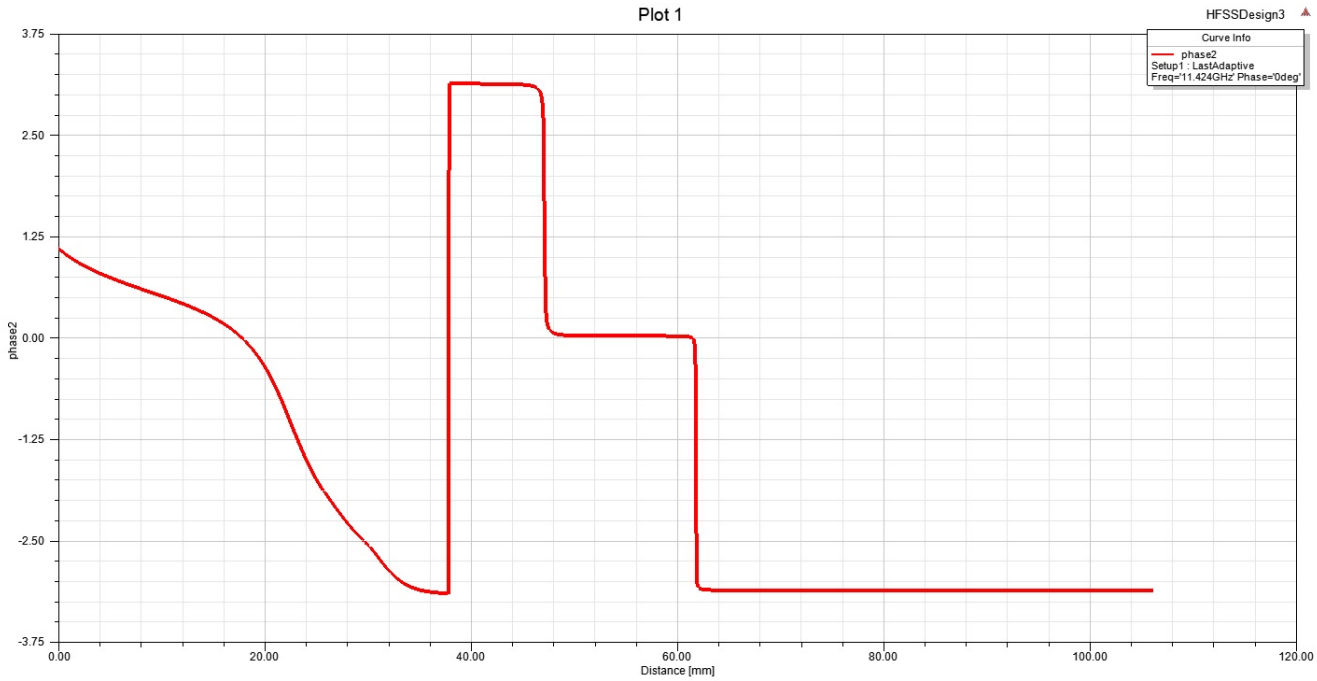

Figure 5.8: Phase of the on-axis electric field inside the SW section.

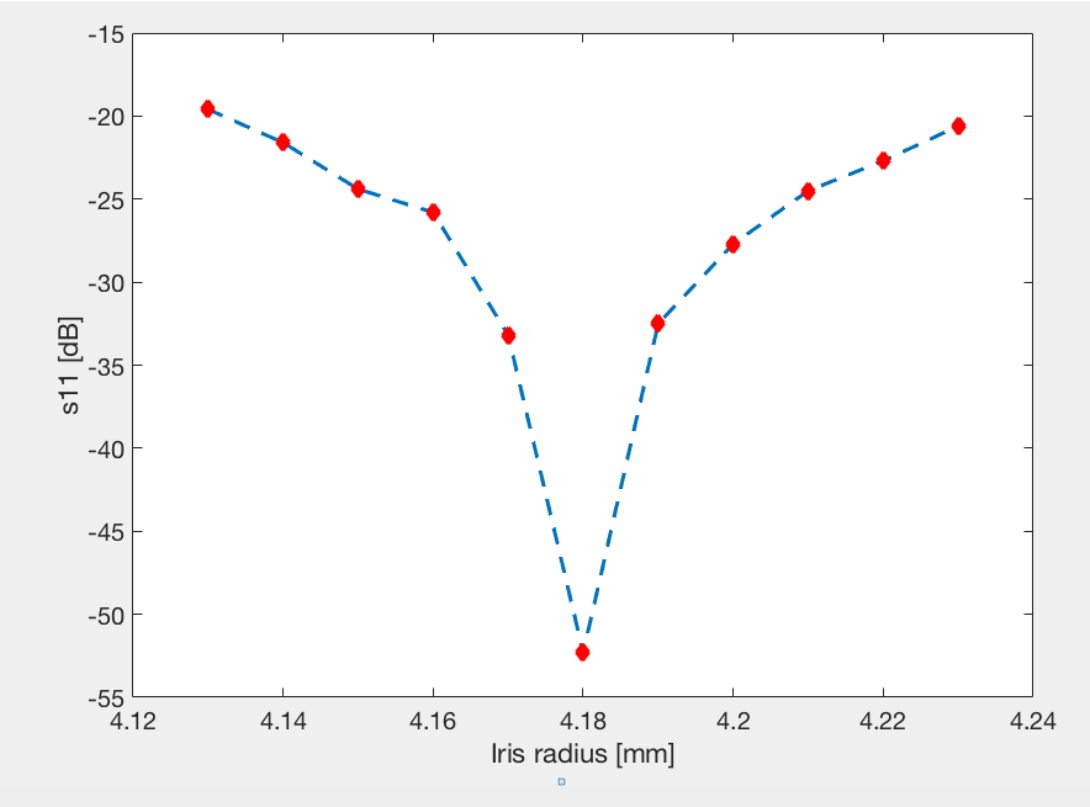

Figure 5.9: Reflection coefficient as a function of iris radius.

of the matching problem we can use Smith chart. The Smith chart as we can observe in Fig. (5.10) is a polar plot of complex reflection coefficient. A Smith chart is developed by examining the load where the impedance must be matched. Instead of considering the impedance we express its reflection coefficient which is more useful when we dealing with RF frequencies. As we can observe from the Fig. (5.10) our structure at the $\Gamma \approx -30$ will be at the critical coupling.

5.2.1 Choice of iris thickness and radius

The irises with a radius "a" are the holes through which the TM_{01} , of an equivalent circular waveguide, propagates. After taking into account characteristic results on the SW structure like minimum reflection coefficient from the waveguide and desired field flatness at the desired frequency which is nothing other than the resonant frequency we chose:

- Iris radius= 4.18 mm
- Iris thickness= 2.6 mm

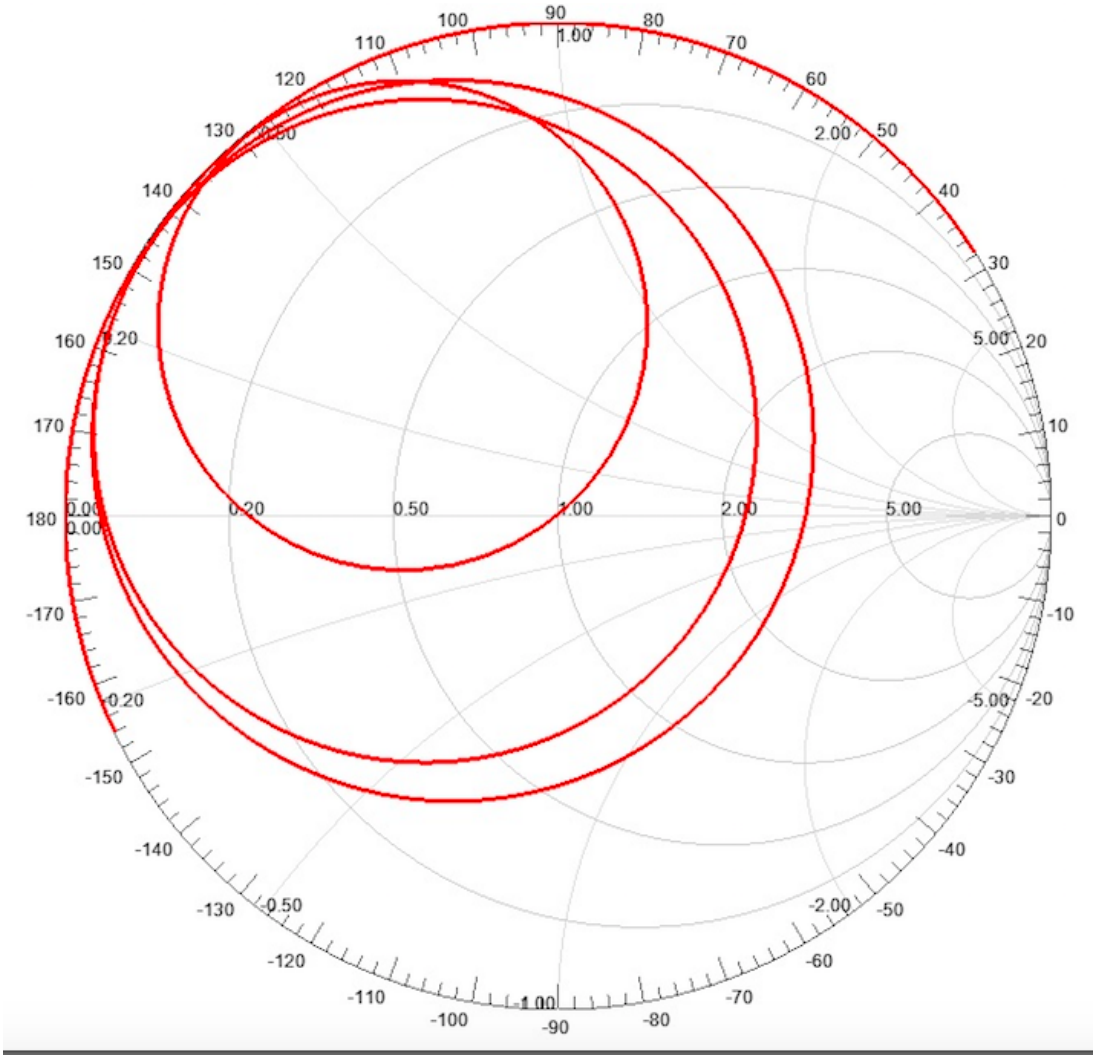

Figure 5.10: Smith chart

5.2.2 Geometric dimensions of the input waveguide

An X-band standard rectangular waveguide is used to fed the RF power into the structure through the coupler cell. The geometric dimensions are:

- a= 10.16 mm
- b= 22.86 mm

All of the other dimensions are given in the following sections, since derived from optimization methods achieved by using numerical codes like HFSS.

5.3 Tuning of the structure

- Frequency Tuning
- Field-Faltness Tuning
- S_{11} Tuning

A very small antenna (SMA antenna) is used as a probe inside the structure and is positioned in the cathode plate in a location such that it is able to excite the electromagnetic field inside the cavity but, at the same time, not to alter the field distribution.
In the simulations carried out with HFSS with the "driven solution" solver, two ports have been defined, as shown in Fig. (5.2). Once the RF power from the input waveguide excites the field inside the structure, the easiest way to know the frequency is measuring the reflection coefficient between port 1 and port 2. This coefficient is known as the s_{11} as we have mentioned before and it is provided by HFSS, after performing a frequency sweep around the solution frequency. The reflection coefficient s_{11} is plotted in Fig. (5.6). The three peaks refer to the 0-mode with frequency f_1, $\frac{\pi}{2}$-mode with frequency f_2 and π-mode with frequency f_3 representing the three resonant modes inside the three-cell cavities. It is evident then that f_3 is the frequency which the full structure needs to be tuned at. In the next subsection, a method for achieving the frequency change is explained.

5.4 Adjustment of the structure cells radii

By changing the dimensions of the cell radius we can change the resonant frequency of the structure. All other dimensions can remain unmodified. Fig (5.3) shows the variation of the cell radii versus the frequency. The frequency decreases by increasing the cell radius and this would be an easy way to tune the frequency of interest. In our case the frequency of π mode should be tuned and as it has mentioned before f_3 is the corresponding frequency for this mode.

5.5 Adjustment of the coupling iris

In order to enhance the amplitude of the field inside the SW section or in the other word to minimize the reflection coefficient from the waveguide, the radius "a" of the coupling iris can be changed. It should be noted that increasing and decreasing the iris radius has a small effect on frequency shift and it will be a way when we need to minimize the reflection coefficient and simultaneously maintaining almost constant the frequency of the structure. The optimal iris radius in which the transmission of energy from waveguide to the cells is maximum is "a = 4.18 mm". The optimization results are the following:

- $R_1 = 10.639\ mm$
- $R_2 = 10.556\ mm$
- $R_3 = 11.932\ mm$

5.6 Final tuning of the structures

The value of the frequency f_3, obtained in the last section, is slightly higher than project specification in which f_3 it's better to be 11.424 GHz, at which the reflection coefficient s_{11} has to reach its minimum value. As discussed in previous sections, the s_{11} already shows low values around the project frequency. Thus, we proceed to tune the frequency by adjusting the SW radii. Using the value $R_2 = 10.558$ mm, we obtain a resonance at $f_3 = 11.4245$ GHz, that satisfies the specifications. Nevertheless, a change non negligible is observed in the reflection coefficient. It follows that it is not possible to achieve the

desired value for the resonance frequency and minimum of reflection coefficient at the same time by modifying only the SW section dimensions.

Fig. (5.11) shows the electric and magnetic field distribution along the structure. The electric field has its maximum value on the propagation direction near the z axis in the central cell where the field gradient is twice respect to other cells. (b) Magnetic field distribution along the structure. The magnetic field has its maximum value near the surface of the central cell and has its minimum value near the propagation axis.

Fig. (5.12) shows 2D design has been performed using SUPERFISH code. As we can observe electric field has its maximum value on axis. The characteristics results from SUPERFISH code have shown in Table (5.1).

5.7 Optimization of standing-wave three cell cavities structure

RF cavities designers or generally speaking accelerator structure designers when dealing with high frequency operating structures, they are always looking for a way to minimize breakdown probability to avoid damages due to the electrical breakdown or microcracks due to rf pulsed heating. So this phenomena (electrical breakdown) depends on many parameters. Materials used for the structure, geometry and surface processing technique are some of the parameters that affect on the breakdown and expanding our knowledge about these parameters help us to predict breakdown behavior of practical structures. As for the open structure discussed in the previous section, following the international trend, physicists and engineering are attempting to improve the performance of X-band accelerating structures in terms of manufacturing approaches alternative to brazing such as electroforming, or electron beam welding (EBW) [24, 28, 52, 55, 56, 57, 58]. INFN with the collaboration of SLAC have designed and fabricated a three cells standing wave copper structure operating at 11.424 GHz sealed with the EBW approach and they also manufactured an accelerating sections using the Tungsten Inert Gas (TIG) brazing technique which was an innovative technological process [52, 55]. we continued the studies of open-like three cells standing wave structures . In order to operate in a high gradient field this structure has been optimized. Figure (5.13) shows the electric field of an open-like 3-cells cavities. Proposed layouts between two sections for an open X-band three-cells structure

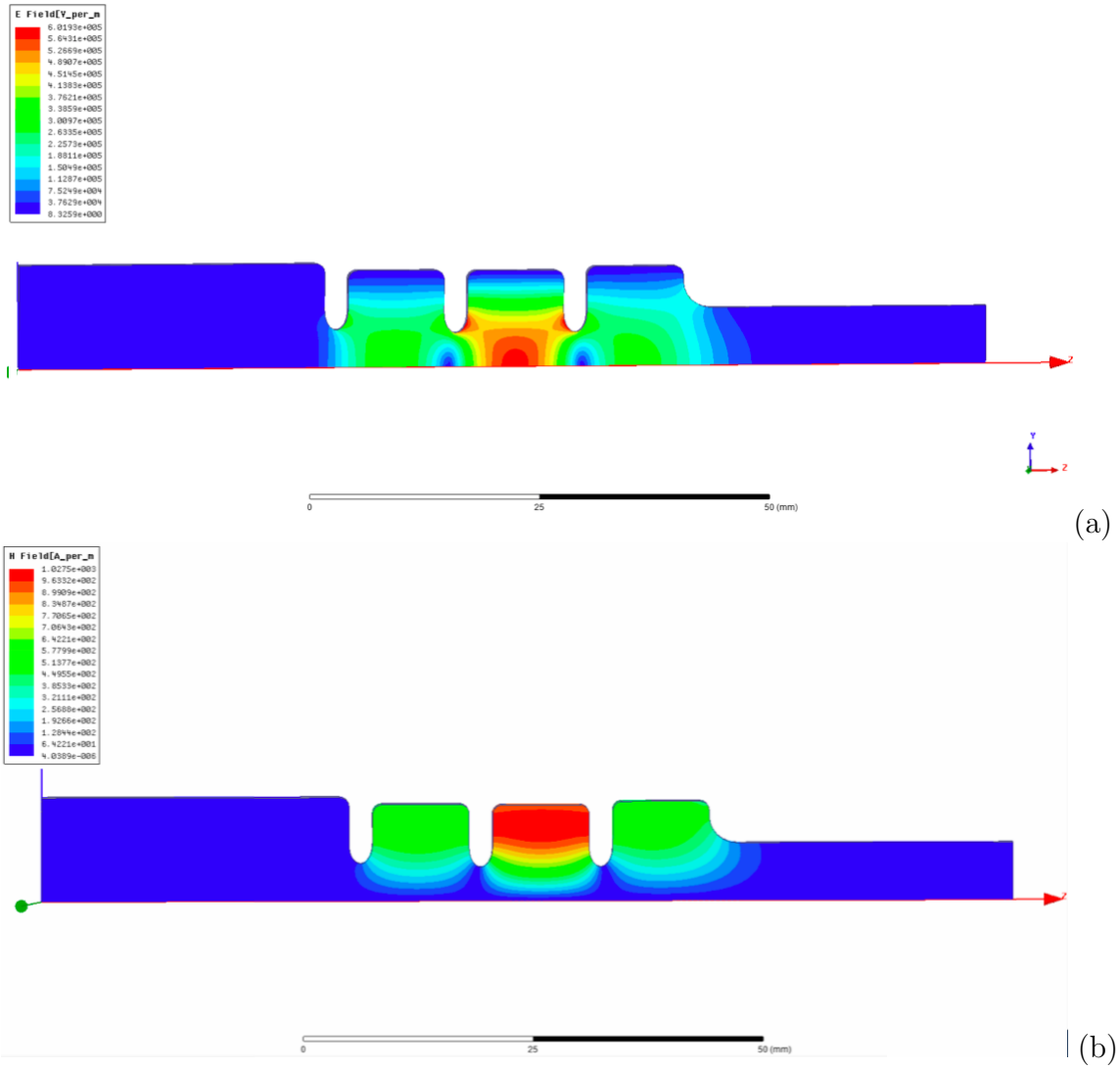

Figure 5.11: Electric and Magnetic field distribution. (a) Electric field distribution along the structure. The electric field is at its maximum value on the propagation direction near the z axis in the central cell where the field gradient is twice respect to other cells. (b) Magnetic field distribution along the structure. The Magnetic field is maximum near the outer surface of the central cell and has its minimum value near the propagation axis.

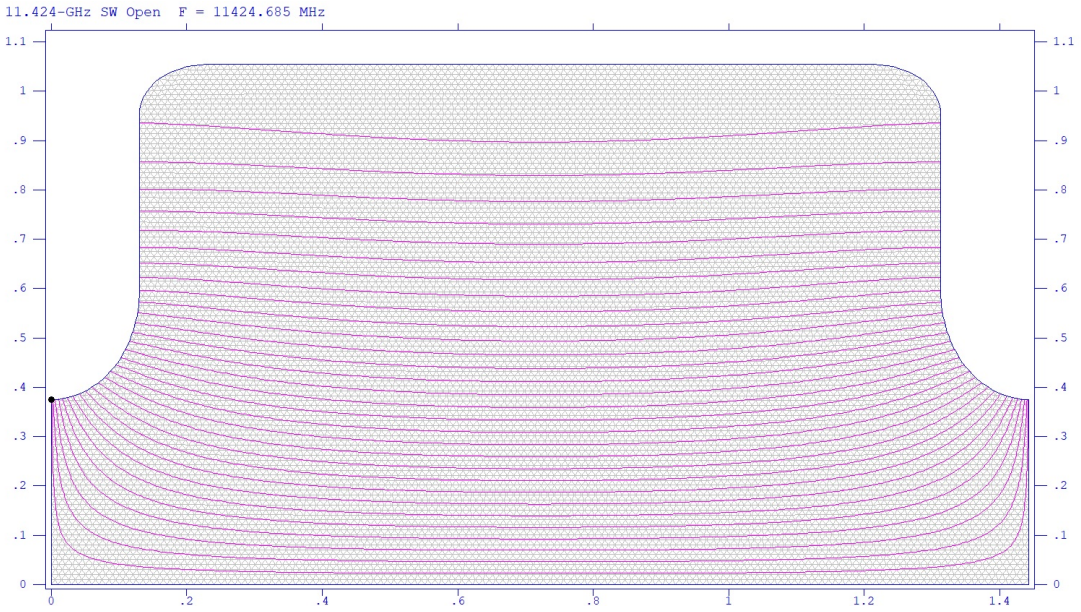

Figure 5.12: 2D design has been performed using SUPERFISH code.

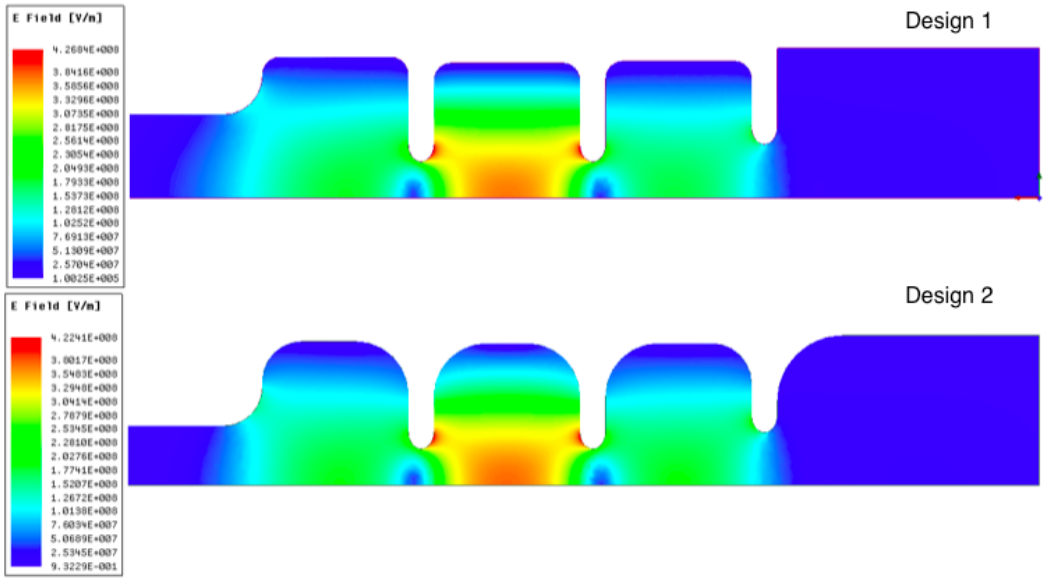

Figure 5.13: Comparison of the layouts between two sections for an open X-band three-cells structure cavity designed for X-band breakdown tests and for electroforming manufacturing. Top: standard design for cell-to-cell brazing manufacturing; bottom: high radius fillet are manufactured as for open structures. The optimized cavity has been proposed by SLAC (V. Dolgachev)

Frequency	11.424 GHz
Field Normalization (norm=1)[MV/m]	100
Normalization factor for $E_0 = 141.5MV/m$	2357
Cavity Length [mm]	13.13
Number of cells	1
Beam hole radius a [mm]	3.75
Iris Thickness h [mm]	2.6
Transit time factor T	0.707
Q-value [x1000]	9553
Stored Energy [mJ]	225.13
Shunt Impedance [MOhm/m]	170
Z*T*T[MOhm/m]	85
Shunt Impedance/Q [Ohm]	266
$E_{surf-peak}$ [MV/m] at Z, R=0.0292, 0.3806)[MV/m]	217
$H_{surf-peak}$ [MA/m] at Z, R=0.13, 0.8442)[MA/m]	0.332
Kilpatrick factor	2.49
Ratio of peak fields B_{max}/E_{max}[mT/(MV/m)]	1.9171
Peak to average ratio E_{max}/E_0	1.5389
Surface resistance[mohm]	27.8
Power dissipation [kW]	1691

Table 5.1: The characteristics results from SUPERFISH code

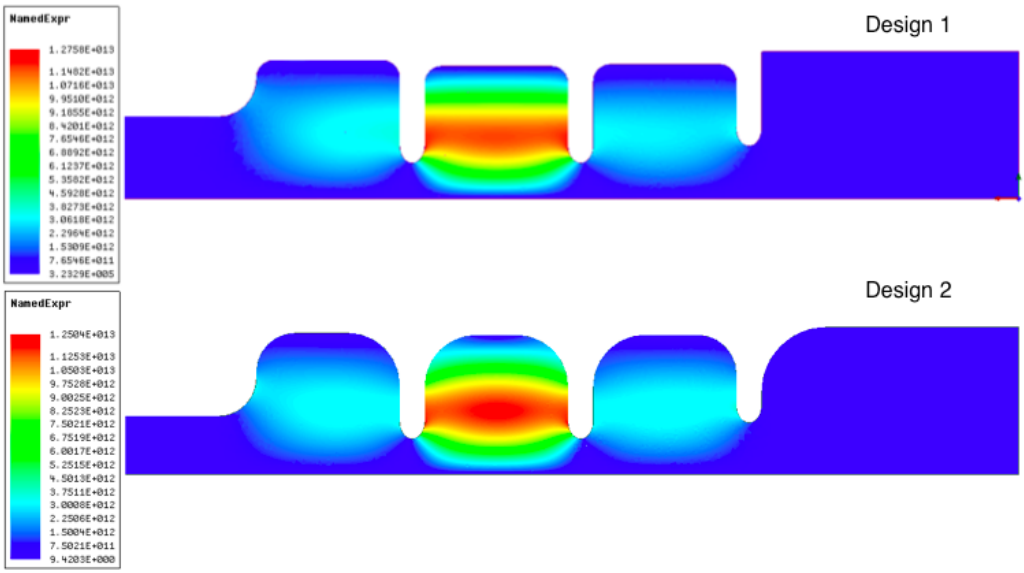

Figure 5.14: Modified pointing vector distribution

cavity designed for X-band breakdown tests and for electroforming manufacturing. The rounding between the cell and flat surface have been specifically studied to reduce the surface maximum magnetic field and, by consequence, the pulse heating in this critical region. As showed in Figure (5.1) the radius of the optimized rounding is equal to 0.5 mm. Moreover, the transverse dimension of the cavity has been optimized to reduce the maximum electric and magnetic field. Fig.s (5.14) and (5.15) show the modified pointing vector distribution and magnetic field distribution. For a ratio of 0.875 between the x dimension and the y dimension the high gradient figures of merit have been minimized. The electric maximum surface field obtained is 190 MV/m, the magnetic maximum field 0.3 MA/m and the modified Poynting vector 2.11 MW/mm2 . In Fig. (5.13) we show a three cells X-band standing wave structure designed for breakdown study at high power. This structure has a rounded profile in order to increase the quality factor Q. In table (5.2) we compare two designs for electroforming manufacturing. This approach has also been used to design a three cells W-band device at SLAC. In Table (5.2) it can be observed that in the case of rounded cavities (Design 2), the structure has the higher unloaded quality factor and higher effective shunt impedance comparing with Design 1. It should be informed that the rounded solution has also been studied while scaling for the 110 Ghz to solve the breakdown phenomena [42].

The following results have obtained,

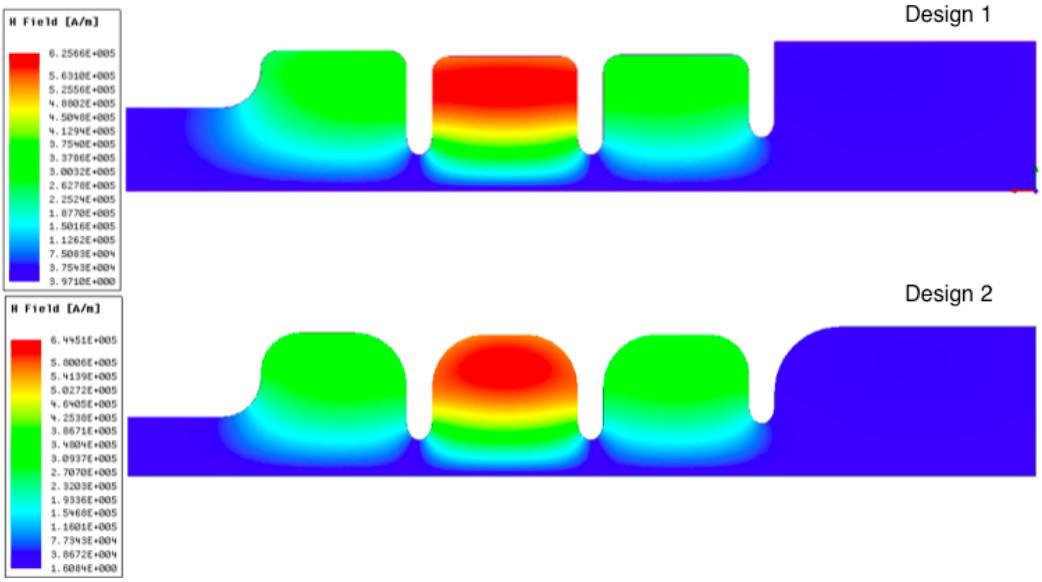

Figure 5.15: Magnetic field distribution

π mode RF parameters	Design 1	Design 2
Structure Length [mm]	79.3	79.3
Frequency [GHz]	11.4234	11.4234
P_{in} [MW]	10	10
RF pulse length [ns]	400	400
Unloaded quality factor (Q_0)	9359	9950
β coupling	1.0129	1.0145
Stored Energy [J]	1.076	1.098
$2 * R_{sh} * T^2$ [MOhm/m]	83.3	92.88
Transit time factor	0.62	0.65
$E_{peak-on-axis}$ [MV/m]	380	380
$E_{surf-peak}$ [MV/m]	427	422
$H_{surf-peak}$ [MA/m]	0.63	0.64
Pulse Heating [°C][1]	108	111
$S_c$max. $[W/\mu m^2]$[2]	12.7	12.5

Table 5.2: Comparison of two design results for electroforming manufacturing.

- the effective shunt impedance is larger for high radius fillet than standard design.
- there is a small difference for transit time factor between two cases.
- β coupling is higher in the case of high radius fillet design.
- standard design has less stored energy respect to the high radius fillet design.

[1] RF Pulsed Heating: A metal can be heated from the magnetic field on its surface due to high power pulsed RF and this causes microcracks and surface roughening when the thermal stresses induced passing from the elastic limit repeatedly. The repetition or cyclic causes fatigue which is called cyclic fatigue. To avoid the creation of microcrack and surface roughening we should limit the maximum magnetic field on the surface and this limitation lead us to a maximum achievable accelerating gradient in a normal conducting accelerator structure and this procedure can be quantified by RF Pulsed Heating process. Finally, it should be noted that RF pulsed heating causes a temperature gradient on the metal due to surface magnetic field. The peak surface magnetic field is nearly [41],

$$\Delta T = \frac{|H_{||}|^2 \sqrt{t}}{\sigma \delta \sqrt{\pi \rho C_\epsilon k}}, \tag{5.11}$$

where

t: pulse length

σ: electrical conductivity

δ: skin depth

ρ: density

C_ϵ: specific heat

k: thermal conductivity,

as ΔT should be below the upper limit of 60° to avoid the breakdown phenomena and cyclic fatigue due to the periodic thermal stress induced which are larger than the elastic limit, we should decrease the input power or RF pulse length. It should be noted that to obtain an acceptable pulsed heating we have to decrease at least 50% of the pulse length from 400 ns to 200 ns or 25% of the surface magnetic field on the metal from 0.64 MA/m to 0.48 MA/m.

[2] Modified Poynting vector estimated on the whole structure. Modified Poynting vector is a new local field quantity which gives high gradient performance limit of accelerating structures in the presence of vacuum rf breakdown and is given [59],

$$S_c = Re\{\bar{S}\} + g_c \; . \; Im\{\bar{S}\}, \tag{5.12}$$

where $Re\{\bar{S}\}$ is the real part and describes active power flow and $Im\{\bar{S}\}$ describes reactive power flow and is nothing other than the imaginary part of the Poynting vector. g_c is the weighting factor and it's equal to 1/6.

Chapter 6

Cavity Perturbation Theories, Techniques and Measurements

In practical applications small changes of the cavity's shape is a technique to modify the cavity resonator by changing the resonant frequency. The other technique which is similar to changing of the shape of the cavity is inserting of small pieces of dielectric or metallic materials. Introducing a small dielectric sample into the cavity will impose a shift in resonant frequency and by measuring this resonant frequency shift we can determine dielectric constant of the material.

Perturbation method is an approximation method which is used to calculate the effect of such a perturbations on the cavity performances which assumes that the actual fields of a cavity with a small shape or material perturbation is almost equal to those of the unperturbed cavity. Thus, this technique is similar in concept to the perturbational method for treating loss in good conductors, where one assumption we are going to use is that there is not a significant difference between the fields of a component with good conductors and one with perfect conductors. In this section we will derive expressions for the approximate change in resonant frequency when a cavity is perturbed by small changes in the material filling the cavity, or by small changes in its shape.

6.1 Material Perturbations

In cavity material perturbation method, a perturbation will impose by changing the permittivity or permeability of the material filling the cavity. By writing the Maxwell's curl

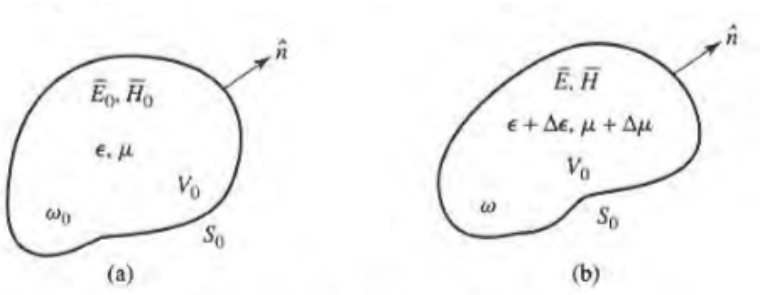

Figure 6.1: A resonant cavity perturbed by a change in the permittivity or permeability of the material in the cavity. (a) Original cavity. (b) Perturbed cavity

equations before and after the forcing perturbation and some manipulations we will obtain an equation for the resonant frequency shift relating to the field $\bar{E}_0$, $\bar{H}_0$ which are the fields of the original cavity. One assumption is that the actual fields of a cavity imposing a material perturbation are not greatly different from those of the unperturbed cavity, $\bar{E}$, $\bar{H}$. The procedure is as follows,

Maxwell's curl equations can be written as

$$\nabla \times \bar{E}_0 = -j\omega_0 \mu \bar{H}_0, \tag{6.1}$$

$$\nabla \times \bar{H}_0 = j\omega_0 \epsilon \bar{E}_0, \tag{6.2}$$

where $\bar{E}_0$, $\bar{H}_0$ and ω_0 are the fields and the resonant frequency of the original cavity. By small changing in permittivity and permeability of the material inside the cavity they can be written as

$$\nabla \times \bar{E} = -j\omega(\mu + \Delta\mu)\bar{H}, \tag{6.3}$$

$$\nabla \times \bar{H} = j\omega(\epsilon + \Delta\epsilon)\bar{E}, \tag{6.4}$$

where ω is the resonant frequency of the perturbed cavity and $\bar{E}$, $\bar{H}$ are the fields of the perturbed cavity.

Now multiply the conjugate of Eq. (6.1) by $\bar{H}$ and multiply Eq. (6.4) by $\bar{E}_0^*$ and subtracting these equations using the vector identity we have,

$$\nabla \ . \ (\bar{E}_0^* \times \bar{H}) = j\omega_0 \mu \bar{H} \ . \ \bar{H}_0^* - j\omega(\epsilon + \Delta\epsilon)\bar{E}_0^* \ . \ \bar{E}. \tag{6.5}$$

Similarly, the same procedure in the case of Eq.s (6.2) and (6.3) we have,

$$\nabla \ . \ (\bar{E} \times \bar{H}_0^*) = -j\omega(\mu + \Delta\mu)\bar{H}_0^* \ . \ \bar{H} + j\omega_0\epsilon\bar{E}_0^* \ . \ \bar{E}, \tag{6.6}$$

now adding Eq. (6.5) and Eq. (6.6), integrate over the volume ,

$$\int_{V_0} \nabla \ . \ (\bar{E}_0^* \times \bar{H} + \bar{E} \times \bar{H}_0^*) d\nu = j \int_{V_0} \{[\omega_0\epsilon - \omega(\epsilon + \Delta\epsilon)]\bar{E}_0^* \ . \ \bar{E} + [\omega_0\mu - \omega(\mu + \Delta\mu)]\bar{H}_0^* \ . \ \bar{H}\} d\nu, \tag{6.7}$$

using the divergence theorem we obtain,

$$\int_{V_0} \nabla \ . \ (\bar{E}_0^* \times \bar{H} + \bar{E} \times \bar{H}_0^*) d\nu = \oint_{S_0} (\bar{E}_0^* \times \bar{H} + \bar{E} \times \bar{H}_0^*) \ . \ d\bar{s} = 0, \tag{6.8}$$

where the surface integral is zero because $\hat{n} \times \bar{E} = 0$ on S_0, then we have,

$$j \int_{V_0} \{[\omega_0\epsilon - \omega(\epsilon + \Delta\epsilon)]\bar{E}_0^* \ . \ \bar{E} + [\omega_0\mu - \omega(\mu + \Delta\mu)]\bar{H}_0^* \ . \ \bar{H}\} d\nu = 0, \tag{6.9}$$

rewriting the equation above gives,

$$\frac{\omega - \omega_0}{\omega} = \frac{-\int_{V_0} (\Delta\epsilon \bar{E} \ . \ \bar{E}_0^* + \Delta\mu \bar{H} \ . \ \bar{H}_0^*) d\nu}{\int_{V_0} (\epsilon \bar{E} \ . \ \bar{E}_0^* + \mu \bar{H} \ . \ \bar{H}_0^*) d\nu}, \tag{6.10}$$

The assumption we are going to use for the equation above is that $\Delta\epsilon$ and $\Delta\mu$ are small because in general we do not know $\bar{E}$ and $\bar{H}$ but instead we have $\bar{E}_0$, $\bar{H}_0$. By this assumption we can approximate the perturbed fields and ω with original field of unperturbed field and resonant frequency. Then the equation above can be written as,

$$\frac{\omega - \omega_0}{\omega} \approx \frac{-\int_{V_0} (\Delta\epsilon |\bar{E}_0|^2 + \Delta\mu |\bar{H}_0|^2) d\nu}{\int_{V_0} (\epsilon |\bar{E}_0|^2 + \mu |\bar{H}_0|^2) d\nu}. \tag{6.11}$$

From the equation above we can find that decreasing ϵ or μ will increase resonant frequency. As permittivity describes the amount of charge needed to generate one unit of electric flux in a particular medium and a charge in the material with low permittivity has more electric flux than the material with high permittivity and more flux means less stored electric energy. So, the increase in resonant frequency can be related to the decrease in stored energy of the perturbed cavity. Likewise permeability is a degree of

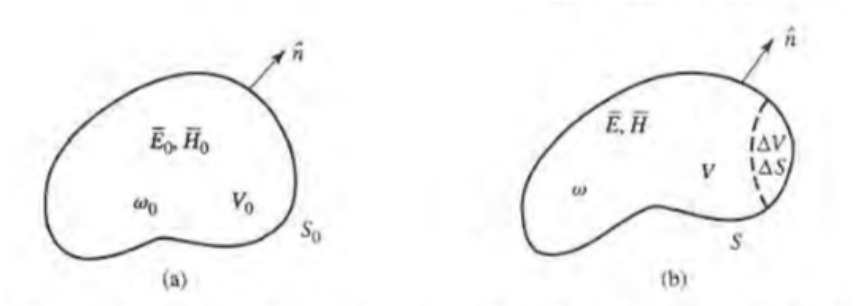

Figure 6.2: A resonant cavity perturbed by a change in shape.(a) Original cavity. (b) Perturbed cavity.

magnetization that a material obtains in response to an applied magnetic field and it can be related to the stored magnetic energy.

6.2 Shape Perturbations

In cavity shape perturbation theory, a perturbation will impose by changing the size of a cavity or inserting a tuning screw. The same assumption we have considered for the material perturbations, should be assumed in the case of shape perturbation. Maxwell's curl equations can be written for the two cases as

$$\nabla \times \bar{E}_0 = -j\omega_0 \mu \bar{H}_0, \tag{6.12}$$

$$\nabla \times \bar{H}_0 = j\omega_0 \epsilon \bar{E}_0, \tag{6.13}$$

$$\nabla \times \bar{E} = -j\omega \mu \bar{H}, \tag{6.14}$$

$$\nabla \times \bar{H} = j\omega \epsilon \bar{E}, \tag{6.15}$$

where $\bar{E}_0$, $\bar{H}_0$ and $\bar{E}$, $\bar{H}$ are the fields of the original cavity and perturbed cavity, respectively. ω_0 is the resonant frequency of the original cavity and ω is the resonant frequency of the perturbed cavity.

Now multiply the conjugate of Eq. (6.12) by $\bar{H}$ and multiply Eq. (6.15) by $\bar{E}_0^*$

$$\bar{H} \ . \ \nabla \times \bar{E}_0^* = j\omega_0 \mu \bar{H} \ . \ \bar{H}_0^*, \tag{6.16}$$

$$\bar{E}_0^* \,.\, \nabla \times \bar{H} = j\omega\epsilon \bar{E}_0^* \,.\, \bar{E}, \tag{6.17}$$

Subtracting these two equations and using the vector identity we have,

$$\nabla \,.\, (\bar{E}_0^* \times \bar{H}) = j\omega_0 \mu \bar{H} \,.\, \bar{H}_0^* - j\omega\epsilon \bar{E}_0^* \,.\, \bar{E}, \tag{6.18}$$

similarly, by multiply the conjugate of Eq. (6.13) by $\bar{E}$ and multiply Eq. (6.14) by $\bar{H}_0^*$ and subtracting the equations and using the vector identity we have,

$$\nabla \,.\, (\bar{E} \times \bar{H}_0^*) = -j\omega\mu \bar{H}_0^* \,.\, \bar{H} + j\omega_0 \epsilon \bar{E}_0^* \,.\, \bar{E}_0, \tag{6.19}$$

now adding Eq. (6.18) and Eq. (6.19) ,integrate over the volume V,

$$\int_V \nabla \,.\, (\bar{E}_0^* \times \bar{H} + \bar{E} \times \bar{H}_0^*) d\nu = -j(\omega - \omega_0) \int_V (\epsilon \bar{E} \,.\, \bar{E}_0^* + \mu \bar{H} \,.\, \bar{H}_0^*) d\nu, \tag{6.20}$$

using the divergence theorem we obtain,

$$\int_V \nabla \,.\, (\bar{E}_0^* \times \bar{H} + \bar{E} \times \bar{H}_0^*) d\nu = \oint_S (\bar{E}_0^* \times \bar{H} + \bar{E} \times \bar{H}_0^*) \,.\, d\bar{s} = \oint_S \bar{E} \times \bar{H}_0^* \,.\, d\bar{s}, \tag{6.21}$$

$$= \oint_{S_0} \bar{E} \times \bar{H}_0^* \,.\, d\bar{s} - \oint_{\Delta S} \bar{E} \times \bar{H}_0^* \,.\, d\bar{s} = -\oint_{\Delta S} \bar{E} \times \bar{H}_0^* \,.\, d\bar{s}, \tag{6.22}$$

where $\hat{n} \times \bar{E} = 0$ on S and $\hat{n} \times \bar{E}_0 = 0$ on S_0. Using this results we have,

$$\omega - \omega_0 = \frac{-j \oint_{\Delta S} \bar{E}_0^* \times \bar{H} \,.\, d\bar{s}}{\int_{V_0} (\epsilon \bar{E} \,.\, \bar{E}_0^* + \mu \bar{H} \,.\, \bar{H}_0^*) d\nu}, \tag{6.23}$$

as we don't have the value of $\bar{E}$ and $\bar{H}$, this equation won't be a useful equation to relate the resonant frequency to the shape perturbations. But, by making an assumption that ΔS is small, we can approximate the perturbed fields $\bar{E}$, $\bar{H}$ by the original fields $\bar{E}_0$, $\bar{H}_0$,and ω in the denominator by ω_0, to give the fractional change in resonant frequency as

$$\frac{\omega - \omega_0}{\omega} \approx \frac{-\int_{\Delta V} (\mu |\bar{H}_0|^2 - \epsilon |\bar{E}_0|^2) d\nu}{\int_{V_0} (\epsilon |\bar{E}_0|^2 + \mu |\bar{H}_0|^2) d\nu} = \frac{\Delta U_m - \delta U_e}{U_m + U_e}, \tag{6.24}$$

where U_m and U_e are the stored magnetic energy and electric energy, respectively and ΔU_m and ΔU_e are their changes due to the shape perturbation. According to the equation above increasing or decreasing the volume of the cavity causes increase or decrease of the

resonant frequency. The procedure for material and shape perturbation has been brought in this thesis from the author of the book with Ref. [19].

6.3 Theoretical aspects-Cavity Perturbation

By introducing a small sample of dielectric material into a resonant cavity, the resonant frequency of the cavity is changed as well as the quality factor Q of the cavity. These effects on the parameters are usually quantified and in the other word the quality factor and shift in resonant frequency can be found in the measurement of the dielectric properties of the sample. The shift in resonance frequency is considered to be mainly correlated to the dielectric constant while the change in the Q factor is associated to the dielectric loss.

6.4 Quality factor and cavity resonator

Kraszewski and Nelson in 1992 experimentally have shown that when an object is introduced in the cavity, the resonance frequency will decrease and the Q factor will be lowered, causing a broader, flatter resonance curve [29]. In the other word, the sharpness of the peak in the resonance curve can be quantified by the quality factor. Figure (6.3) shows an example of the resonant curve with and without a perturbing dielectric object in the cavity. The Q-factor of the resonator is generally defined as:

$$Q = \frac{\omega_r U_{max}}{P}, \tag{6.25}$$

where ω_r is the resonant frequency and U_{max} is energy received by the resonator and P denotes the power loss converted by the resonator. With cavity resonators, one can achieve a very high unloaded Q, with normal conducting materials up to many times 10^4. As we have shown in Table (2.1) the quality factor of the cavity resonator decreases proportionally with $f^{-1/2}$. This means that higher frequency has lower quality factor. The introduction of the dielectric in the resonator increases its resonant wavelength. The measurement is made by placing a sample completely through the centre of a waveguide that has been made into a cavity. The cavity is placed with central holes on either side. These irises give the cavity a very narrow frequency range for the transmission of the energy. Changes in the center frequency and width of this transmission characteristic,

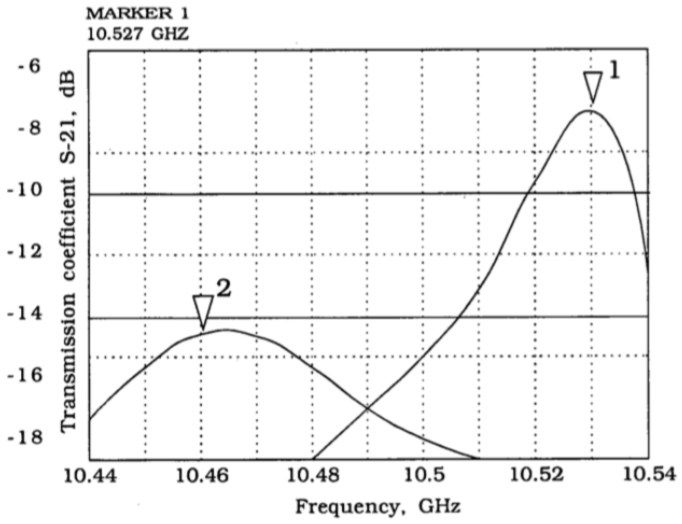

Figure 6.3: Example of a resonant curve with the perturbing dielectric object (2) and without the object (1) [29].

when a sample is inserted, provide information to calculate the dielectric constant and loss factor of the sample.

6.5 Measurements on the prototype

As it has mentioned before, an electroformed SW structure in normal conducting RF powered particle beam accelerator fabricated and characterized by SLAC and INFN to work at 11.424 GHz with maximum sustainable gradients with extremely low probability of RF breakdown, coated with Au-Ni and with different surface roughness [11]. This structure has been manufactured by Media Lario Technologies s.r.l. (Italy) and Comeb s.r.l (Italy) . The device is made due to a non-uniform gold coating in the high magnetic areas or to a diffusion of Ni inside the gold plating. Improving the quality of the gold coating, this type of structures should exhibit better performances than Cu-based structures. This mechanism has been experimentally observed looking at the autopsy of the Au-Ni electroformed structure manufactured in Frascati. In Fig. (6.4) [11] are compared photographs showing the cells of this Au-Ni electroformed structure whose RF test parameters are summarized in Table (6.1) [11].Three ports are included: the two waveguides for input/output of the RF power through the SW part, and an SMA antenna located at the cathode plate for tuning of the SW section.

Fig (6.5) shows the prototype of the High gradient accelerating structure has been ma-

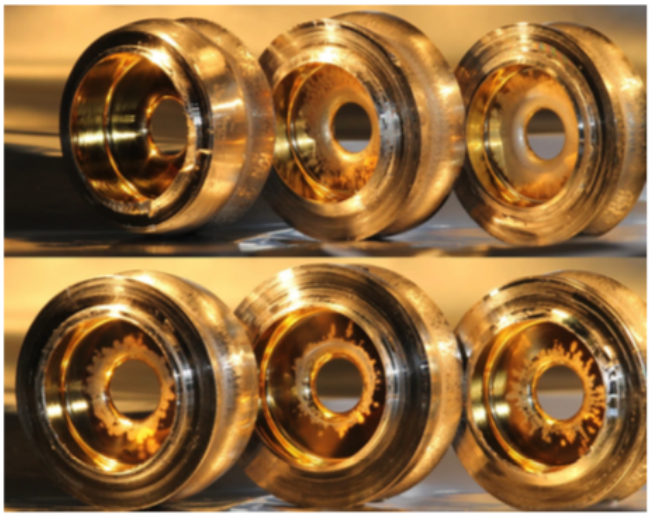

Figure 6.4: Images showing the damage of the iris of the three cells of the Au-Ni electroformed structure for RF high-power tests . The damage is consistent with the field levels [11].

chined at INFN-LNF. Measurements set up have been performed in the Department of SBAI of the University of Rome "La Sapienza". A sketch of the measurement setup is given in Fig. (6.6). By using a step-by-step motor, it is possible to pull the wire through the structure and measure the perturbations caused by the small bead. The measurement setup is referred to as "bead-pull". As explained above, we measure frequency shifts in the SW. The data obtained are stored in a PC via a GPIB (Generated Purpose Interface Bus). Nevertheless, it is possible to measure the field through the SW structure by applying Steele method which usually is used to measure a TW structure, because a standing-wave cavity can be thought as a traveling-wave linac with a cell-to-cell phase shift equal to π. Comparing the results with the results exposed from HFSS we report the features that have been quantified, showing good agreement.

Fiq. (6.7) shows an experimental measurement setup for field profile measurements. A perturbing object (1 mm in length and 1 mm in diameter) is attached to an horizontal fish lens that lays on the same direction as the axis of the structure. The bead-pull technique that we have used is based on the Slater theorem and is widely discussed elsewhere [30]. The small perturbing object inside the cavity induces a frequency shift that is related to the variation of the electric and magnetic energy stored in the cavity in the point where the object is located according to the formula:

Mode	π	$\pi/2$	0
$F(GHz)_{measured}$	11.4200	11.3241	11.27088
$F(GHz)_{calculated}$	11.42388	11.33004	11.27766
Q_0	5130	6467	5981
$Q_{0,calculated}$	9178	9388	9110
Q_{loaded}	3077	1874	1938
$Q_{extmeasured}$	7315	2351	2867
$\beta_{measured}$	0.726	2.75	2.08

Table 6.1: RF parameters of an Au-Ni electroformed structure at room temperature excited at the π-mode. The calculated parameters refer to a similar structure made in copper.

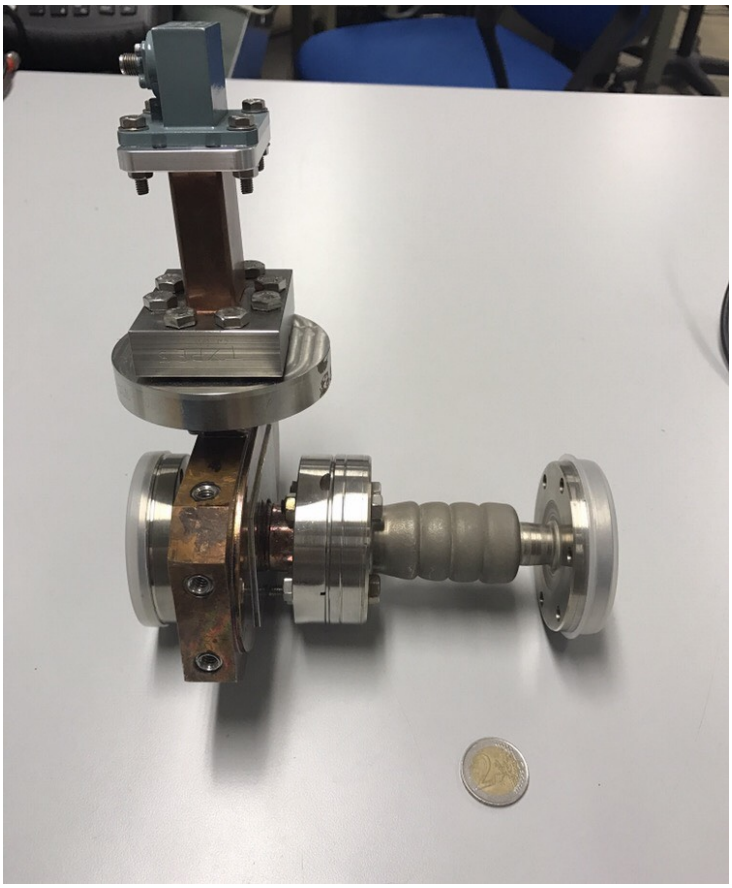

Figure 6.5: The prototype of the High gradient accelerating structure has been machined at INFN-LNF.

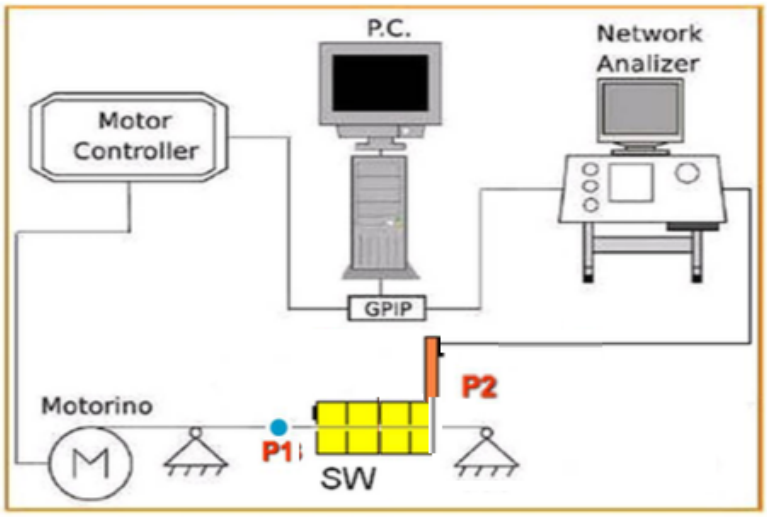

Figure 6.6: The sketch of the measurement setup

$$\frac{\omega - \omega_0}{\omega_0} = \frac{1}{4U}\int_{\Delta V}(\mu_0|\overrightarrow{H}|^2 - \epsilon_0|\overrightarrow{E}|^2)dV. \tag{6.26}$$

Considering the accelerating mode and the small transverse dimensions of the perturbing object (of the order of 0.1 mm) it is possible to find the longitudinal electric field on axis by the formula:

$$\frac{\omega_p - \omega_0}{\omega_0} = -\epsilon_0\ k_e \Delta_e \frac{E_z^2}{4U} = \frac{1}{2Q_L} tg(\phi(f_0)), \tag{6.27}$$

where k_e is the form factor of the object, ΔV is the perturbing object volume, U the total energy stored in the cavity, Q_L is the loaded quality factor of the resonance and $\phi(f_0)$ is the phase of the transmission coefficient between two ports coupled with the field in the cavity. The latest expression have been written because it is more convenient to measure the phase shift due to the resonant frequency instead of $\Delta\omega$ [31]. Moreover, for $\phi(f_0)$ reasonably small (e.g. smaller than 30°), $tg(\phi)$ is approximately equal to ϕ and this has some practical advantages.

A careful optimization of the measurement setup has been accomplished in order to minimize the systematic errors and to better understand the uncertainty of the measurements. The most important reasons of induced errors in the measurements were as they have been mentioned in other measurement set up [11].

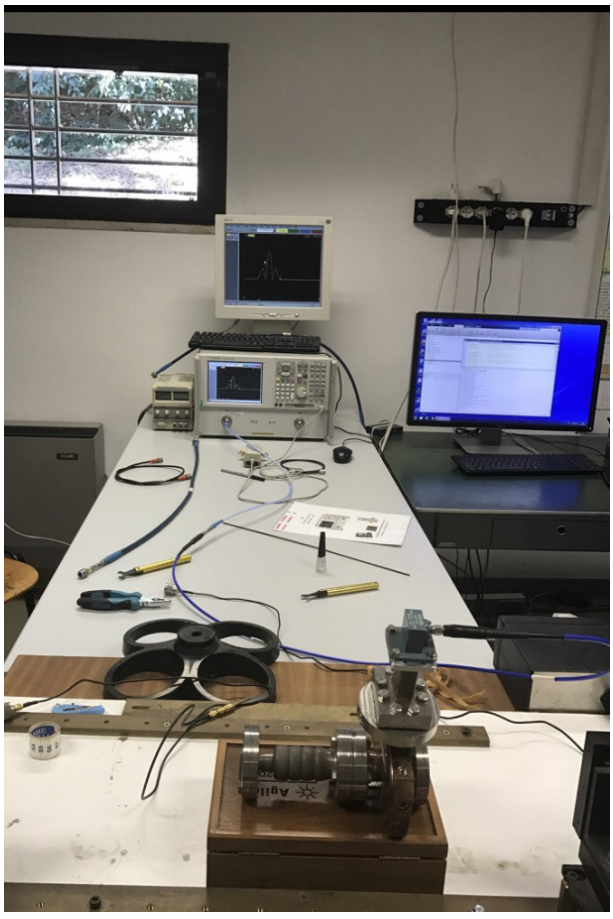

Figure 6.7: The measurement setup for Longitudinal Electric Field

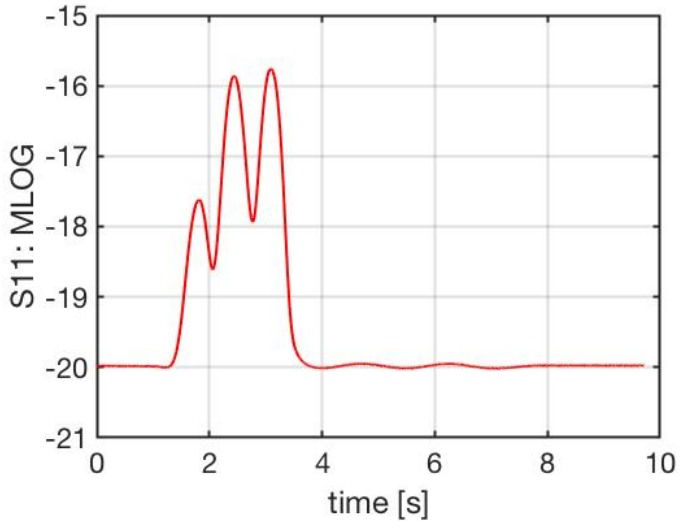

(a)

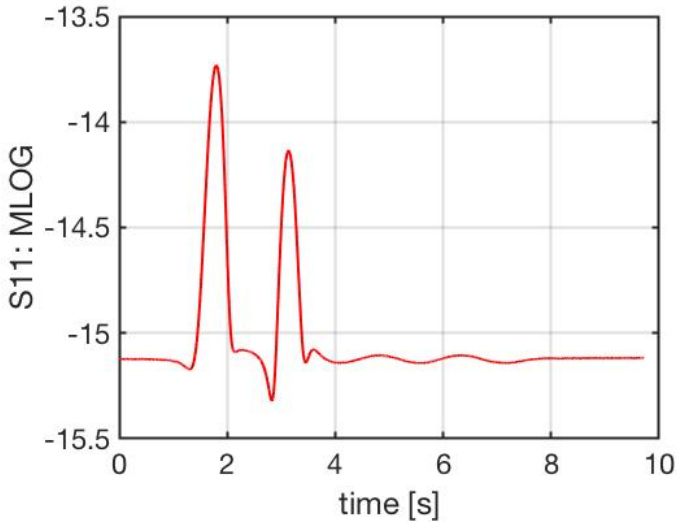

(b)

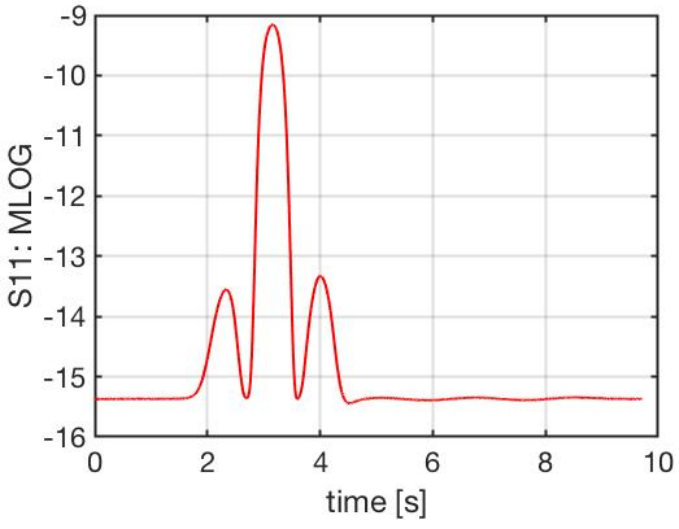

(c)

Figure 6.8: The results of the low level RF tests of the Au-Ni electroformed structure excited at the π-mode: (a) the 0-mode, on-axis field profile; (b) the $\pi/2$ mode, on-axis field profile and (c) the π mode, on-axis field profile.

- An unwanted perturbation during the frequency measurement due to the effect of wire nylon. To minimize this error we used a small wire.

- Another unwanted perturbation in the frequency measurement is the effect of the drops of glue used to fix the perturbing object. It gave a perturbation in the frequency measurement which is of the order of 10% of the total frequency variation [11]. Different measurements should be done to take into account this effect on the frequency variation.

In order to quantify the electric field inside the structure, two different methods have been employed. The Slater Method for the SW cavity and the Steele method for the TW section. The former is a resonant method that only allows to measure the amplitude of the field, the latter is a non-resonant method and it allows to calculate both amplitude and phase of the field.
Equation (6.27) shows the relationship between the amplitude $|E|$ and the frequency shift $\Delta\omega$ and equation (6.28) relates the vector E with the reflection coefficient S_{11}.

$$|E|^2 = -(\frac{4U_0}{\epsilon_0 k_{slater}})\frac{\Delta\omega}{\omega_0} = -(\frac{4U_0}{\epsilon_0 k_{slater}})\frac{\Delta\Phi_{13}}{2Q_L}, \tag{6.28}$$

$$E^2 = \frac{2P_{in}(S_{11p} - S_{11u})}{j\omega k_{steele}} = \frac{2P_{in}\Delta S_{11}}{j\omega k_{steele}}, \tag{6.29}$$

where S_{11p} and S_{11u} are perturbed and unperturbed reflection coefficient, respectively and ΔS_{11} is the difference between them which is equal to $|\Delta S_{11}|e^{j\Phi\Delta S_{11}}$.
Fiq. (6.9) shows an experimental measurement setup for the reflection coefficient and Fig. (6.10) shows S_{11} as a function of the frequency for the modes 0, $\pi/2$ and π. It should be noted that there is another mode as we can observe from Fig. (6.10), the first mode on the left, which is the dipole mode generated by mode launcher. This mode has not been cancelled and we will work analytically and numerically to compensate this mode in the future work. Typically it would be measured using a Vector Network Analyzer (VNA), which can plot s_{11}. The figure implies that at the frequency 11.4115 GHz, where $s_{11} \approx$-11dB we have the minimum reflection from the iris coupled between the waveguide and the first cell and consequently the transmission from that aperture would be its maximum value at that frequency. The accelerator bandwidth can also be determined

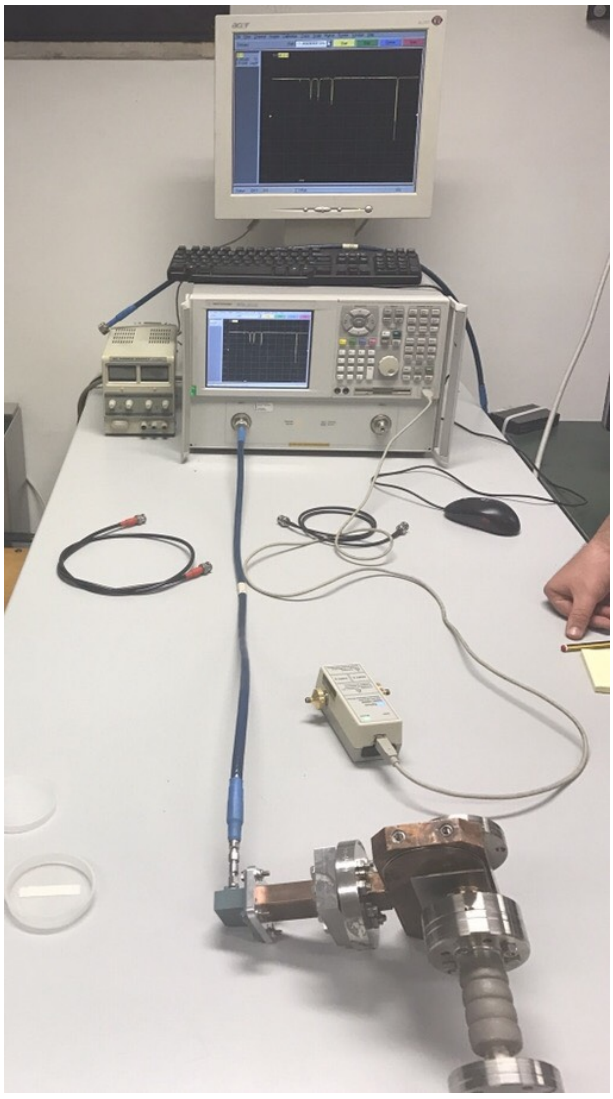

Figure 6.9: The measurement setup for s_{11}

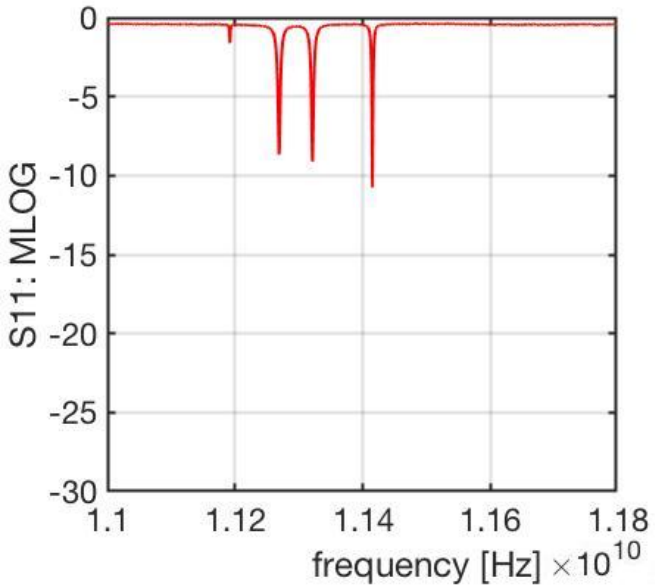

Figure 6.10: S_{11} as a function of the frequency

from the figure. If the bandwidth is defined as the frequency range where S11 is to be less than -3 dB, then the bandwidth would be roughly 0.0035 GHz, with 11.4168 GHz the high end and 10.4133 GHz the low end of the frequency band. In order to compare these results with the requirements exposed in chapter (5), we report the features that have been quantified, showing good agreement. Finally, we compare the experimental results from measurements and simulations carried out with HFSS. Figures (6.11) and (6.12) show these comparisons for the electric field amplitudes and reflection coefficient (S_{11}) and it is concluded by saying that good agreement is achieved.

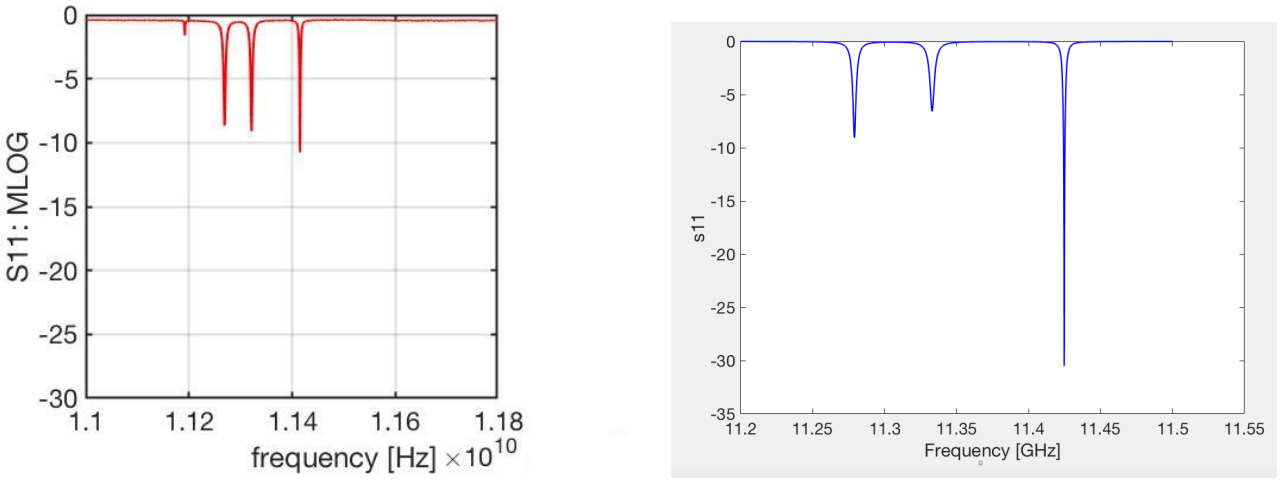

Figure 6.11: Comparison of the experimental results from measurements and simulations carried out with HFSS for reflection coefficient, S_{11} of the modes 0, $\pi/2$ and π, from left to right, respectively.

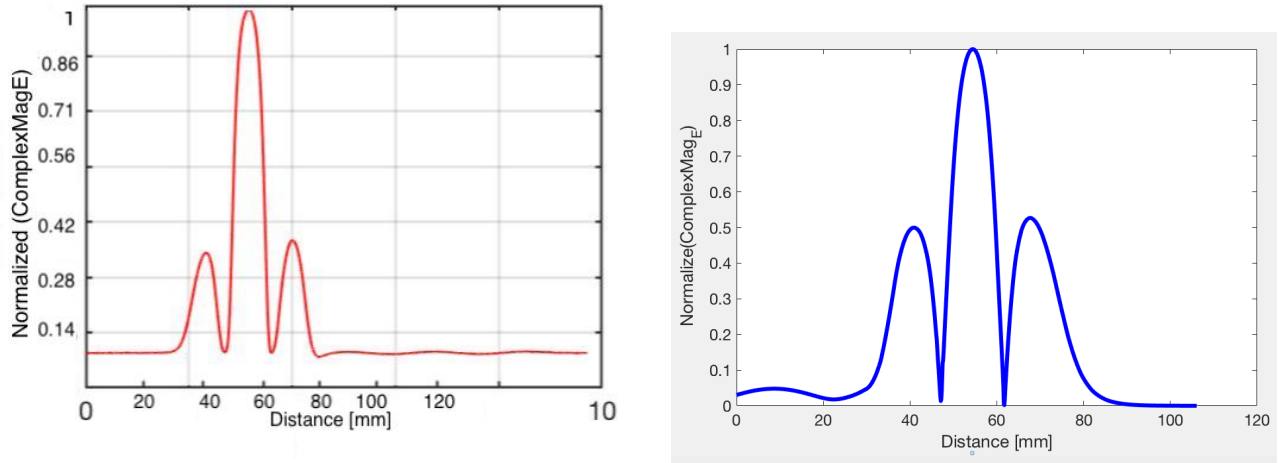

Figure 6.12: Comparison of the experimental results from measurements and simulations carried out with HFSS for electric field amplitudes of the mode π.

Chapter 7

Theoretical Approach for Reflection Coefficient Calculation OF Coupling Between Cylindrical Waveguide and Cavity

7.1 Reflection Coefficient Calculation by Circuit Theory

Resonators are the basic element of most microwave circuit and their performance strongly dependent to the quality factor. The unloaded quality factor of a cavity resonator, which signifies the sharpness in the frequency response of a resonator, is formally defined as,

$$Q_0 = \frac{\omega U}{P}, \tag{7.1}$$

or

$$Q_0 = \frac{f_0}{\Delta f}, \tag{7.2}$$

where U is average stored energy and P denotes the power dissipation. Δf refers to the frequency difference where the magnitude of reflection coefficient has the maximum value at -3 dB and the f_0 is the resonance frequency at the center of Δf. It is known as "unloaded Q" because it is not connected to an external circuit. On the other hand when the resonant cavity is connected

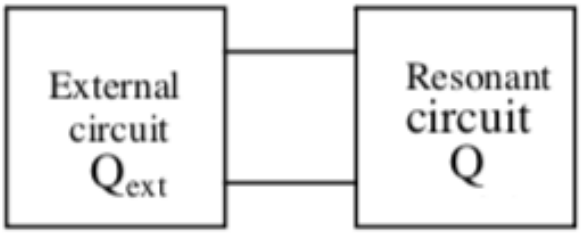

Figure 7.1: A resonant circuit loaded by an external circuit

to an external circuit, as it shows in Fig. (7.1), the Q factor is called "external Q" and denoted by Q_{ext}. The quality factor of the overall circuit is obtained as,

$$\frac{1}{Q_L} = \frac{1}{Q_0} + \frac{1}{Q_{ext}}. \tag{7.3}$$

This method to find the overall Q of a resonant circuit can be used in general to any form of resonator, may it be a waveguide resonator, a strip resonator or a lumped element resonator [4, 35, 36, 37, 38, 39]. Fig.s (7.2) shows a configuration consists of a cavity coupled to an external transmission line or waveguide usually contains the RF generator. A microwave cavity in the vicinity of resonance can be accurately represented by an RLC circuit. The external guide is assumed to be terminated with a matched load resistance Z_0 as shown in the figure. The generator is shown in the circuit on the left and the cavity coupled to the external circuit is located on the right. Equivalent circuit with all components reflected into the external circuit containing the generator is shown in Fig. (7.3). The equivalent parameters are as follows,

$$R = \frac{R_0}{n^2}, \quad L = \frac{L_0}{n^2}, \quad C = \frac{C_0}{n^2}. \tag{7.4}$$

The resonator power dissipated, the power dissipation in the external circuits and the summation of these two power dissipation which is nothing other than the total power dissipated can be written as,

$$P_c = \frac{n^2 V^2}{2R}, \tag{7.5}$$

$$P_{ext} = \frac{V^2}{2Z_0}, \tag{7.6}$$

$$P = P_c + P_{ext}. \tag{7.7}$$

The stored energy is $U = \frac{n^2 C V^2}{2}$. Using the above equations we can obtain the unloaded, loaded and external quality factors as follows,

$$Q_0 = \frac{\omega_0 U}{P_c} = \omega_0 RC, \tag{7.8}$$

$$Q_{ext} = \frac{\omega_0 U}{P} = \omega_0 n^2 Z_0 C, \tag{7.9}$$

$$Q_L = \frac{Q_0}{1+\beta}. \tag{7.10}$$

It is convenient to express the circuit model results in terms of the waveguide-to-cavity coupling parameter β, instead of the transformer turns ratio n.

$$\beta = \frac{Q_0}{Q_{ext}} = \frac{\omega_0 RC}{\omega_0 n^2 Z_0 C} = \frac{R}{n^2 Z_0}, \tag{7.11}$$

then we have,

$$n^2 = \frac{R}{\beta Z_0}. \tag{7.12}$$

Eq. (7.4) turn out to be,

$$R = \frac{R_0}{n^2} = \beta Z_0, \quad L = \frac{L_0}{n^2} = \frac{\beta Z_0 L}{R}, \quad C = \frac{C_0}{n^2} = \frac{RC}{\beta Z_0}. \tag{7.13}$$

Proceeding with the lumped-element model, Q_0 can be derived as follows[36]. The driving point admittance is

$$Y = \frac{1}{R} + j(\omega C - \frac{1}{\omega L}). \tag{7.14}$$

The susceptance vanishes at the resonant frequency $\omega = \omega_0$. Therefore, ω_0 must equal $1/\sqrt{LC}$, where L and C are the distributed inductance and capacitance of the transmission line.
The voltage across R_0 at resonance is $V(t) = R_0 I_m cos(\omega_0 t)$, then the total stored energy in the electric and magnetic fields is written as,

$$U(t) = U_e(t) + U_m(t) = \frac{C_0 R_0^2 I_m^2 cos^2(\omega_0 t)}{2} + \frac{L(\frac{1}{L}\int_0^t R_0 I_m cos(\omega_0 t) dt)^2}{2} = \frac{I_m^2 R_0^2 C_0}{2}. \tag{7.15}$$

The total energy loss is equal to the average power delivered to the circuit,

$$P = \frac{\int_0^{T_0} R_0 I_m^2 cos^2(\omega_0 t)}{T_0},$$

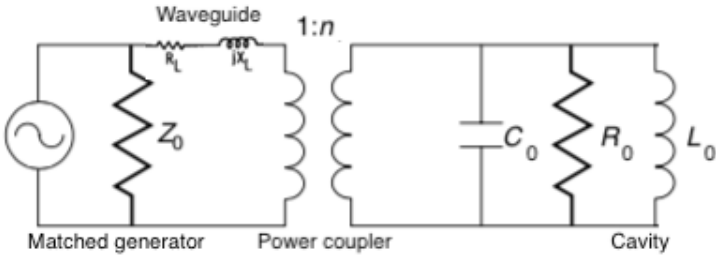

Figure 7.2: Equivalent circuit of a cavity coupled to an external circuit, which are transformer coupled to the cavity resonator.

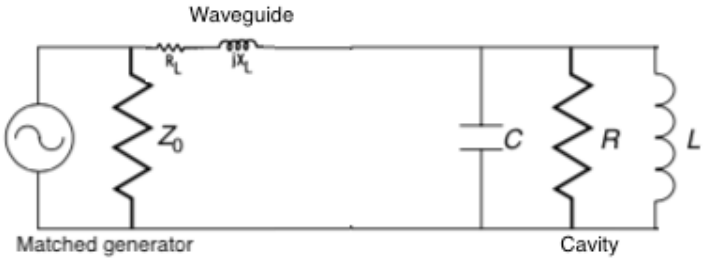

Figure 7.3: Equivalent circuit with all components reflected into the external circuit containing the generator where $R = \frac{R_0}{n^2}$, $L = \frac{L_0}{n^2}$, $C = \frac{C_0}{n^2}$.

$$= \frac{R_0 I_m^2}{2}. \tag{7.16}$$

Replacing Eq.s (7.15) and (7.16) into the Eq. (7.1) we can get the unloaded quality factor as follows,

$$Q_0 = \frac{\omega_0 U}{P} = \frac{\omega_0 \frac{I_m^2 R_0^2 C_0}{2}}{\frac{R_0 I_m^2}{2}} = \omega_0 R_0 C_0, \tag{7.17}$$

the loaded quality factor can be written as,

$$Q_L = Q_0/(1+\beta), \tag{7.18}$$

where β is referred to as the coupling coefficient.

We can express input shunt admittance in terms of the unloaded quality factor as follows:

$$Y_C = \frac{1}{R} + j\frac{1}{R}(\omega RC - \frac{R}{\omega L}), \tag{7.19}$$

$$= \frac{1}{R}[1 + j(\frac{\omega Q_0}{\omega_0} - \frac{Q_0 \omega_0}{\omega})],$$

$$= \frac{1}{R}[1 + jQ_0(\frac{\omega}{\omega_0} - \frac{\omega_0}{\omega})].$$

The corresponding shunt impedance can be written as,

$$Z_C = \frac{1}{Y} = \frac{R}{1 + jQ_0(\frac{\omega}{\omega_0} - \frac{\omega_0}{\omega})}. \tag{7.20}$$

We can simplify $(\frac{\omega}{\omega_0} - \frac{\omega_0}{\omega})$ as follows,

$$\delta = \frac{\omega}{\omega_0} - \frac{\omega_0}{\omega} = \frac{\omega^2 - \omega_0^2}{\omega\omega_0}, \tag{7.21}$$

we can expand the Taylor series of ω^2 at a fixed point ω_0,

$$\omega^2 = \omega_0^2 + 2\omega_0(\omega - \omega_0) + (\omega - \omega_0)^2, \tag{7.22}$$

ignoring the term $(\omega - \omega_0)^2$ and putting into the Eq. (7.21) we have,

$$\delta = \frac{\omega}{\omega_0} - \frac{\omega_0}{\omega} = \frac{\omega^2 - \omega_0^2}{\omega\omega_0} = \frac{2\omega_0(\omega - \omega_0)}{\omega\omega_0} = \frac{2(\omega - \omega_0)}{\omega} = 2\frac{\Delta\omega}{\omega}. \tag{7.23}$$

On the basis of the preceding equivalent circuit, the input impedance is

$$Z_L = Z_W + Z_C, \tag{7.24}$$

where Z_W is the shunt impedance of the waveguide which is composed of two components, the coupling loss, R_L and reactance of coupling system, X_L. Then the equation for the input shunt impedance can be written as,

$$Z_L = R_L + jX_L + \frac{\beta Z_0}{1 + jQ_0(\frac{\omega}{\omega_0} - \frac{\omega_0}{\omega})}. \tag{7.25}$$

The coupling reactance and coupling loss related have a small effect of the frequency shift and they can be ignored because the variation of the unloaded quality factor due to frequency shift is not insignificant. If we consider a wave that is emitted from the generator into the guide, the reflection coefficient produced by the cavity load impedance, becomes

$$\Gamma = \frac{Z_L - Z_0}{Z_L + Z_0}, \tag{7.26}$$

replacing the Eq. (7.25) into the equation above we have,

$$\Gamma = \frac{\frac{\beta Z_0}{1+jQ_0(\frac{\omega}{\omega_0} - \frac{\omega_0}{\omega})} - Z_0}{\frac{\beta Z_0}{1+jQ_0(\frac{\omega}{\omega_0} - \frac{\omega_0}{\omega})} + Z_0}, \tag{7.27}$$

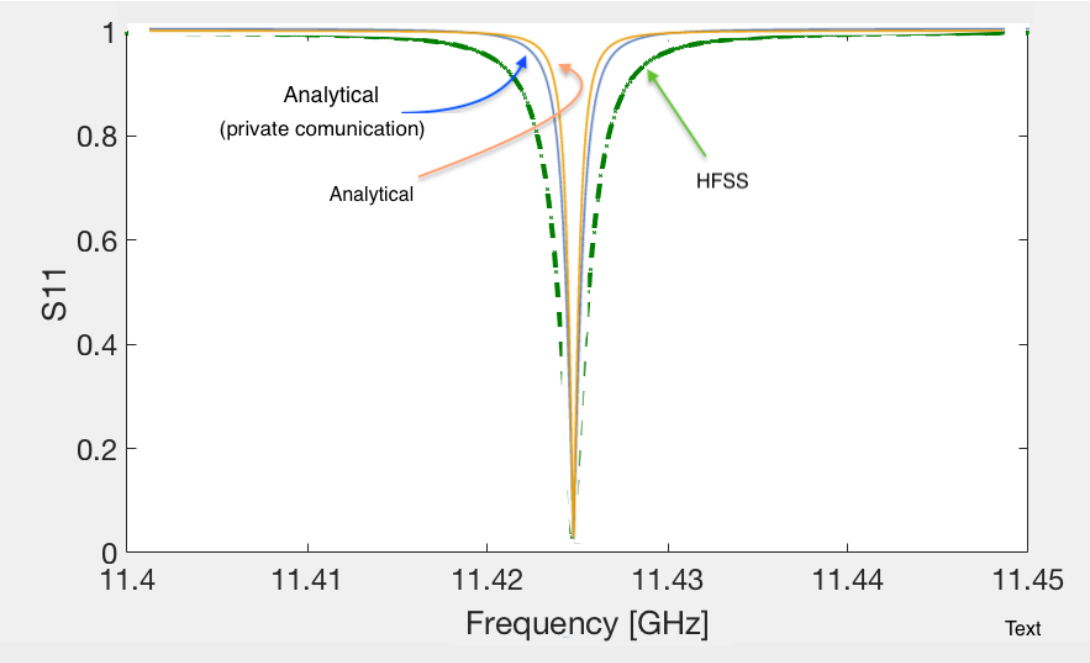

Figure 7.4: Comparison between Analytical and numerical of reflection coefficient calculation in a π mode accelerating structure .

$$= \frac{\beta Z_0 - Z_0(1 + jQ_0\delta)}{\beta Z_0 + Z_0(1 + jQ_0\delta)},$$

substituting $Q_L = Q_0/(1+\beta)$ into the equation above and canceling out Z_0 from the numerator and the denominator we have,

$$\Gamma = \frac{\beta - 1 - jQ_L(1 + \beta)\delta}{\beta + 1 + jQ_L(1 + \beta)\delta}, \tag{7.28}$$

by multiplication of all term at $\beta + 1$ the equation above turn to be,

$$\Gamma = \frac{\frac{\beta-1}{\beta+1} - jQ_L\delta}{1 + jQ_L\delta}, \tag{7.29}$$

multiplying the numerator and the denominator by the complex conjugate of the denominator and with some calculation we have,

$$\Gamma = \frac{\frac{\beta-1}{\beta+1} - (Q_L\delta)^2}{1 + (Q_L\delta)^2} - j\,\frac{Q_L\delta(1 + \frac{\beta-1}{\beta+1})}{1 + (Q_L\delta)^2}, \tag{7.30}$$

finally the amplitude of reflection coefficient can be written,

$$|\Gamma| = \sqrt{\frac{(\frac{\beta-1}{\beta+1})^2 + (Q_L\delta)^4 + (Q_L\delta)^2 + (Q_L\delta)^2(\frac{\beta-1}{\beta+1})^2}{1 + (Q_L\delta)^4 + 2(Q_L\delta)^2}}, \tag{7.31}$$

ignoring the high order term we get,

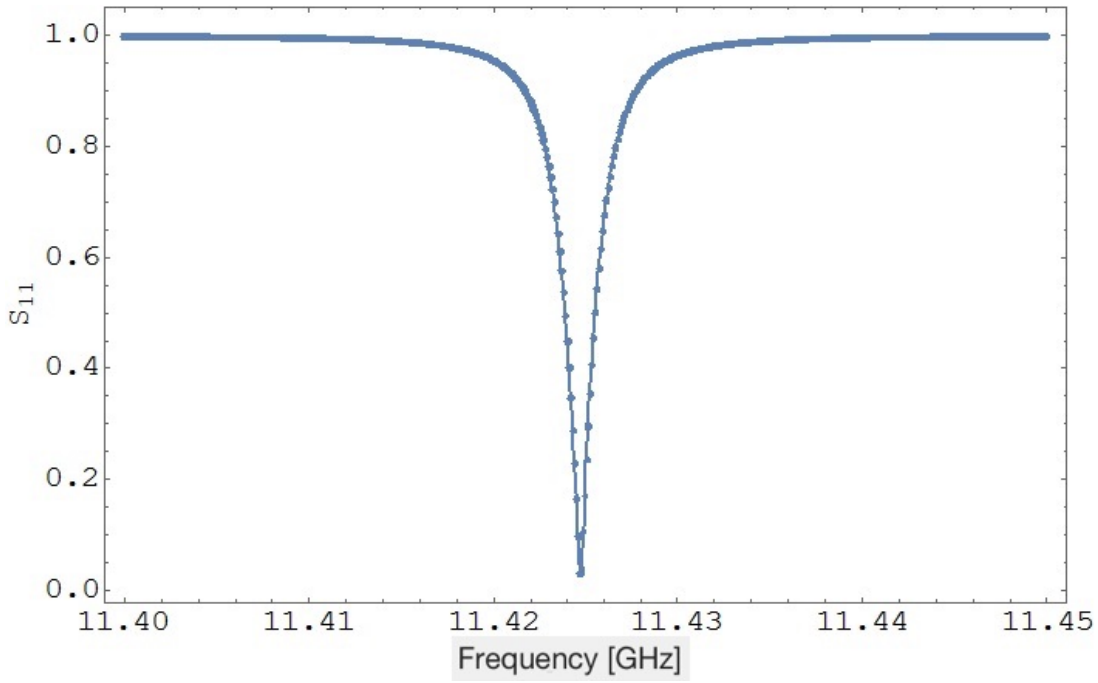

Figure 7.5: Comparison between Analytical and numerical of reflection coefficient calculation in a π mode accelerating structure .

$$\Gamma = \sqrt{\frac{(\frac{\beta-1}{\beta+1})^2 + (Q_L\delta)^2}{1 + 2(Q_L\delta)^2}}, \tag{7.32}$$

which is similar to the the equation taken from [34],

$$\Gamma = \sqrt{\frac{(\frac{\beta-1}{\beta+1})^2 + (Q_L\delta)^2}{1 + (Q_L\delta)^2}}. \tag{7.33}$$

Fig. (7.4) shows the comparison of analytical and numerical results of reflection coefficient calculation in a π mode accelerating structure. At $\beta = 1.05$ and $Q_0 = 7904$ analytical results have a good agreement with the numerical results as it has been shown in Fig. (7.5).

7.2 Reflection Coefficient Calculation by Modified Bethe's Theory

The concept of reflection coefficient is fundamental in high accelerating periodic structures. Electromagnetic energy may be coupled from one waveguide into another guide or into a cavity resonator by a small aperture located at a suitable position in the common wall. There is an approximate theory which states that the aperture is equivalent to an electric or/and magnetic dipole moments [8]. These dipole moments are respectively proportional to the normal electric

and tangential magnetic field of the incident wave. The theory originally stated by Bethe [8], developed by Collin [1] and modified by S. De Santis, L. Palumbo and A. Mostacci for small hole compared to the wavelength [7, 9] . The solution procedure was based on one of Schelkunoff's field equivalence principle. In his article the aperture is closed by a perfect magnetic wall. The incident field, which is chosen as the field in the absence of the aperture , will induce a magnetic current J_m and a magnetic charge ρ_m on the magnetic wall surface. These sources produce a scattered field that can be expressed as a field radiated by the dipole moment of the source distribution. After the field scattered into waveguide has been found the aperture is opened and a magnetic current $-J_m$ is placed in the aperture. The field radiated by this source into the waveguide and/or a cavity, together with the specified incident field and the scattered field in waveguide found earlier, represents the total unique solution to the coupling problem. In our case at the presence of a dielectric iris coupled between the waveguide and the cavity which supports by the thin perfectly conducting screen. Babinet's principle [17] allows us to relate the diffraction fields of one diffracting screen to those of complementary screen which is the iris in the current problem. The basic procedure is replacing the problem of diffraction conducting screen with a certain aperture by diffraction of the disk as a complementary screen. The presence of the screen gives rise to transmitted and reflected fields will be denoted as scattered fields. We applied the theory for TM_{010} mode cavities coupled by a small hole with a thickness size comparable to the wavelength. The amplitudes of forward and backward waves due to polarizabilites have been determined and we found equations for reflection and transmission coefficients.

Beth's diffraction theory states that the hole is equivalent to an electric and a magnetic dipole whose moments are given by

$$P(z) = \epsilon\alpha_e(E_0 + E_{sF} - E_{sB}), \tag{7.34}$$

$$M_\phi(z) = \alpha_m(H_0 + H_{sF} - H_{sB}), \tag{7.35}$$

where α_e and α_m are the polarizabilites of the hole and E_0, H_0 are the primary fields, E_{sF}, H_{sF} are the scattered field (radiation field) due to the polarizability of the iris, and E_{sB}, H_{sB} are the scattered field (radiation field) due to the polarizability of the iris from the field entered to the cavity, reflected with a phase reversal and propagated back to the iris where it becomes an incoming wave from the right with a certain amplitude which it can be polorize the iris and due to this polorization we have another radiation field. We will use these equations later.

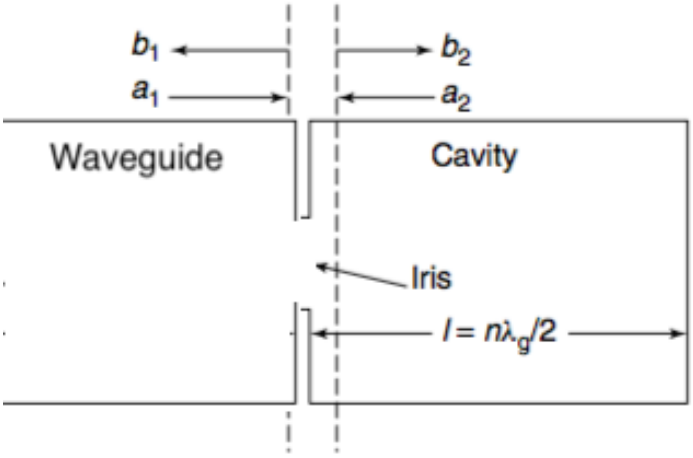

Figure 7.6: Waveguide and cavity section separated by a conducting plate with an iris.

7.2.1 Scattering Matrix

Fig. (7.6) shows a waveguide and resonant cavity separated by a conducting plate with an iris. We describe the iris by a 2×2 scattering,

$$\begin{bmatrix} b_1 \\ b_2 \end{bmatrix} = \begin{bmatrix} s_{11} & s_{12} \\ s_{21} & s_{22} \end{bmatrix} \begin{bmatrix} a_1 \\ a_2 \end{bmatrix} \tag{7.36}$$

We assumed that the iris has a left- right symmetry and to be free of energy dissipation and this property implies a well known reciprocity property that we can mathematically write $s_{11} = s_{22} = \Gamma$, and implying energy conservation for the iris and considering the symmetric of the iris wangler conclude in his book [4] that $s_{21} = s_{12} = j\sqrt{1 - |\Gamma|^2}$. Then scattering matrix can be written as,

$$\begin{bmatrix} b_1 \\ b_2 \end{bmatrix} = \begin{bmatrix} \Gamma & j\sqrt{1 - |\Gamma|^2} \\ j\sqrt{1 - |\Gamma|^2} & \Gamma \end{bmatrix} \begin{bmatrix} a_1 \\ a_2 \end{bmatrix} \tag{7.37}$$

A part of the wave coming from the generator going through the iris into the cavity and other fraction is incident upon the iris is reflected back into the waveguide. The transmitted wave will propagate in the cavity and at the end reflected back to the iris while some fraction transmitted into the waveguide and other fraction again reflected back into the cavity. The input waveguide will have both incident and outgoing traveling waves. If the generator frequency is varied, there will exist discrete resonant frequencies at which we will observe the build up of a high-field standing wave within the cavity region as a result of the constructive interference of the multiply reflected waves inside the cavity. Finally we have a steady state in which the energy entering

to the cavity is equal to the summation of the energy lost from ohmic power dissipation in the cavity walls, and wave energy propagating out of the iris.
Following the buildup of the waves, after N cycles one have found [4],

$$a_2(N) = -je^{-2\alpha\ell}\sqrt{1-\Gamma^2}a_1\Sigma_{n=0}^{N-1}x^n = -je^{-2\alpha\ell}\sqrt{1-\Gamma^2}a_1[\frac{1-x^N}{1-x}], \tag{7.38}$$

$$b_1(N) = a_1[\Gamma + (1-\Gamma^2)e^{-2\alpha\ell}\Sigma_{n=0}^{N-1}x^n] = a_1[\Gamma + (1-\Gamma^2)e^{-2\alpha\ell}\Sigma_{n=0}^{N-1}(\frac{1-x^N}{1-x})], \tag{7.39}$$

and

$$b_2(N) = je^{-2\alpha\ell}\sqrt{1-\Gamma^2}a_1\Sigma_{n=0}^{N}x^n = je^{-2\alpha\ell}\sqrt{1-\Gamma^2}a_1(\frac{1-x^N}{1-x}), \tag{7.40}$$

where $x = -\Gamma e^{-2\alpha\ell}$ is a positive number. The steady-state solution corresponds to $N \to \infty$, and since $|x| < 1$, $x^N \to 0$ and the steady-state solution is

$$a_2(\infty) = \frac{-je^{-2\alpha\ell}\sqrt{1-\Gamma^2}a_1}{1-x}, \tag{7.41}$$

$$b_1(\infty) = a_1[\Gamma + \frac{(1-\Gamma^2)e^{-2\alpha\ell}}{1-x}], \tag{7.42}$$

and

$$b_2(\infty) = j\frac{\sqrt{1-\Gamma^2}a_1}{1-x}, \tag{7.43}$$

considering Eqs. (7.41) and (7.43) we can write,

$$a_2(\infty) = -b_2(\infty)e^{-2\alpha\ell}. \tag{7.44}$$

We will use this result for construction of the field into the structure and $b_2(\infty)$ to be considered as an amplitude of backward wave.

7.2.2 The Fields into the Structure

The structure we are going to consider is a pillbox cavity coupled by the iris to the waveguide and the cavity will be excited in a TM_{010}-like standing-wave mode. For this mode, a particle is acted upon by the nonzero E_z and H_θ fields, and when holes are included in the end walls for the beam, a nonzero E_r component is also present as wangler has mentioned in his famous book "Principles of RF Linear Accelerators" [4]. Subsequent round-trip passes of the internal wave

will reinforce each other and produce resonance when $\phi = 2\pi n$, where n is a positive integer. The fields at resonance after N cycles can be written as,

$$E_n = E_0 + E_{sF} - E_{sB}, \tag{7.45}$$

$$= AJ_0(k_c\rho)e^{-j\beta z} + A_{01}^{-}(e_{t01}^{-} - \hat{z}e_{z01})e^{j\beta_n z} - jA_{01}^{+}(e_{t01}^{-} + \hat{z}e_{z01})\ e^{-(2\alpha\ell + j\beta z)},$$

$$E_t = H_0 + H_{sF} - H_{sB}, \tag{7.46}$$

$$= -\frac{A}{\eta_{01}}J_0'(k_c\rho)e^{-j\beta z} + A_{01}^{-}(-h_{t01}^{-} + \hat{z}h_{z01})\ e^{j\beta_n z} - jA_{01}^{+}(h_{t01}^{-} + \hat{z}h_{z01})\ e^{-(2\alpha\ell + j\beta z)},$$

where,

β: propagation constant,

Z_{01}: wave impedance of the TM_{010},

α: attenuation constant per unit length,

2ϕ: round-trip phase shift of the wave,

and

Γ= reflection coefficient,

these sources produce a scattered field that can be expressed as a field radiated by the dipole moment of the source distribution. After the field scattered into waveguide has been found, the aperture is opened and a magnetic current $-J_m$ is placed in the aperture. The field radiated by this source into the waveguide and/or a cavity, together with the specified incident field and the scattered field in waveguide found earlier, represents the total unique solution to the coupling problem.

The field radiated from the sources propagate in the negative z direction ($\bar{E}_-$ and $\bar{H}_-$) and in the positive direction ($\bar{E}_+$ and $\bar{H}_+$) and can be written as the superpositions of the waveguide modes [17, 19],

$$\bar{E_+} = \Sigma_n A_n^{+}\bar{E_n^{+}} = \Sigma_n A_n^{+}(\bar{e_n}\ +\ \hat{z}e_{zn})\ e^{-j\beta_n z}, \tag{7.47}$$

$$\bar{H_+} = \Sigma_n A_n^{+}\bar{H_n^{+}} = \Sigma_n A_n^{+}(\bar{h_n}\ +\ \hat{z}h_{zn})\ e^{-j\beta_n z}, \tag{7.48}$$

$$\bar{E_-} = \Sigma_n A_n^{-}\bar{E_n^{-}} = \Sigma_n A_n^{-}(\bar{e_n}\ -\ \hat{z}e_{zn})\ e^{j\beta_n z}, \tag{7.49}$$

$$\bar{H_-} = \Sigma_n A_n^{-}\bar{H_n^{-}} = \Sigma_n A_n^{-}(-\bar{h_n}\ +\ \hat{z}h_{zn})\ e^{j\beta_n z}, \tag{7.50}$$

where the single index n is used to represent any possible TE or TM modes. For a given current problem we can determine the amplitude A_n^+ and A_n^- Using Lorentz reciprocity theorem which is as follows,

$$\oint_S (E_1 \times H_2 \ - E_2 \times H_1).nds = \int_V (J \ . \ E_2 - M \ . \ H_2)dv, \tag{7.51}$$

where S is a closed surface enclosing the volume V. E_1, H_1 are the fields of the dominant-mode standing wave, TM_{010}, have shown in Eqs. (7.47) to (7.50). $\bar{J}$ is the source related to strength of electric polarization current (electric moment).

Primary fields for TM_{01} can be written as ,

$$E_0 = AJ_0(k_c\rho)e^{-j\beta z}, \tag{7.52}$$

$$H_0 = -\frac{A}{\eta_{01}}J_0'(k_c\rho)e^{-j\beta z}, \tag{7.53}$$

where,

β: propagation constant

η_{01}: wave impedance of the TM_{010},

The forward scattering fields (E_{sF} and H_{sF}) propagating in the negative z direction used in Eqs. (7.46) and (7.47) have been constructed from equation Eqs. (7.49) and (7.50) by considering that lowest TM mode (TM_{01}) only can propagate into the structure as follows,

$$E_{sF} = A_{01}^-(e_{t01}^- - \hat{z}e_{z01})e^{j\beta z}, \tag{7.54}$$

$$H_{sF} = A_{01}^-(-h_{t01}^- + \hat{z}h_{z01}) \ e^{j\beta z}, \tag{7.55}$$

where A_{01}^- is the TM_{01} mode amplitude of scattered field propagating in negative z direction, e_{t01} , h_{t01} are transverse electric and magnetic modal functions and finally e_{z01} , h_{z01} are longitudinal electric and magnetic modal functions for TM_{01}.

we recall the summary for circular waveguide in Table (7.1) to calculate the modal field for TM_{01} mode.

Transverse and longitudinal modal fields for TM from the table (Table (7.1)) can be written as,

$$e_{t01} = \frac{-j\beta}{k_c}J_0'(k_c\rho), \tag{7.56}$$

Quantity	TE_{nm} Mode	TM_{nm} Mode
k	$\omega\sqrt{\mu\epsilon}$	$\omega\sqrt{\mu\epsilon}$
k_c	$\frac{p'_{nm}}{a}$	$\frac{p'_{nm}}{a}$
β	$\sqrt{k^2 - k_c^2}$	$\sqrt{k^2 - k_c^2}$
λ_c	$\frac{2\pi}{k_c}$	$\frac{2\pi}{k_c}$
λ_g	$\frac{2\pi}{\beta}$	$\frac{2\pi}{\beta}$
ν_p	$\frac{\omega}{\beta}$	$\frac{\omega}{\beta}$
ν_g	$\frac{d\omega}{d\beta}$	$\frac{d\omega}{d\beta}$
α_d	$\frac{k^2 tan\delta}{2\beta}$	$\frac{k^2 tan\delta}{2\beta}$
E_z	0	$(Asinn\phi + Bcosn\phi)\ J_n(k_c\rho)\ e^{-j\beta z}$
H_z	$(Asinn\phi + Bcosn\phi)\ J_n(k_c\rho)\ e^{-j\beta z}$	0
E_ρ	$\frac{-j\omega\mu n}{k_c^2\rho}\ (Asinn\phi - Bcosn\phi)\ J_n(k_c\rho)\ e^{-j\beta z}$	$\frac{-j\beta}{k_c}\ (Asinn\phi + Bcosn\phi)\ J'_n(k_c\rho)\ e^{-j\beta z}$
E_ϕ	$\frac{j\omega\mu}{k_c}\ (Asinn\phi + Bcosn\phi)\ J_n(k_c\rho)\ e^{-j\beta z}$	$\frac{-j\beta n}{k_c^2\rho}\ (Asinn\phi - Bcosn\phi)\ J'_n(k_c\rho)\ e^{-j\beta z}$
H_ρ	$\frac{-j\beta}{k_c}\ (Asinn\phi + Bcosn\phi)\ J_n(k_c\rho)\ e^{-j\beta z}$	$\frac{-j\omega\epsilon n}{k_c^2\rho}\ (Asinn\phi - Bcosn\phi)\ J'_n(k_c\rho)\ e^{-j\beta z}$
H_ϕ	$\frac{-j\beta n}{k_c^2\rho}\ (Asinn\phi - Bcosn\phi)\ J_n(k_c\rho)\ e^{-j\beta z}$	$\frac{-j\omega\epsilon}{k_c}\ (Asinn\phi + Bcosn\phi)\ J'_n(k_c\rho)\ e^{-j\beta z}$
Z	$Z_{TE} = \frac{k\eta}{\beta}$	$Z_{TM} = \frac{\beta\eta}{k}$

Table 7.1: Summary of Results for for wave propagation in circular waveguide [19].

$$e_{z01} = J_0(k_c\rho), \tag{7.57}$$

$$h_{t01} = \frac{-j\omega\epsilon}{k_c} J_0'(k_c\rho) = \frac{-j\beta}{\eta_{01} k_c} J_0'(k_c\rho), \tag{7.58}$$

$$h_{z01} = 0, \tag{7.59}$$

where k_c is cutoff wavenumber, β is the propagation constant, n is the number of nulls in E_z along the radial direction, $J_n'(k_c\rho)$ is the derivative of the Bessel function of the first kind and η_{01} the impedance of free space and it's a physical constant relating the magnitudes of the electric and magnetic fields of electromagnetic radiation traveling through free space. That is, $\eta_0 = |E|/|H|$, where $|E|$ is the electric field strength and $|H|$ is the magnetic field strength for the TM_{010}. It has an exactly defined value $\eta_{01} = 376.73$.

Backward waves are constructed from equation Eqs. (7.47) and (7.48) by considering that only lowest TM mode (TM_{01}) propagating into the structure as follows,

$$E_{sB} = A_{01}^{+}(e_{t01}^{-} + \hat{z}e_{z01})e^{-(2\alpha\ell + j\beta z)}, \tag{7.60}$$

$$H_{sB} = A_{01}^{+}(h_{t01}^{-} + \hat{z}h_{z01})\ e^{-(2\alpha\ell + j\beta z)}, \tag{7.61}$$

where A_{01}^{+} is the TM_{01} mode amplitude of scattered field propagating in positive z direction, e_{t01} , h_{t01} are transverse electric and magnetic modal functions and finally e_{z01} , h_{01} are longitudinal electric and magnetic modal functions for TM_{01}.

Then putting all together, electric and magnetic dipole moments can be written,

$$P_r(z) = \epsilon\alpha_e(AJ_0(k_c\rho)e^{-j\beta z} + A_{01}^{-}(\frac{-j\beta}{k_c}J_0'(k_c\rho) - J_0(k_c\rho))e^{j\beta z} - jA_{01}^{+}(\frac{-j\beta}{k_c}J_0'(k_c\rho) + J_0(k_c\rho))e^{-(2\alpha\ell + j\beta z)}), \tag{7.62}$$

$$M_\phi(z) = \alpha_m(-\frac{A}{\eta_{01}}e^{-j\beta z} + A_{01}^{-}\frac{j\beta}{\eta_{01}k_c}e^{j\beta z} - jA_{01}^{+}\frac{j\beta}{\eta_{01}k_c}e^{-(2\alpha\ell + j\beta z)})J_0'(k_c\rho), \tag{7.63}$$

7.2.3 Relation between sources and electric and magnetic polarization

We now show that the electric and magnetic polarization currents , are related to electric and magnetic current sources, $\bar{J}$ and $\bar{M}$. respectively. From Maxwell's equations we have,

$$\nabla \times \bar{E} = -j\omega\mu\bar{H} - \bar{M}, \tag{7.64}$$

$$\nabla \times \bar{H} = j\omega\epsilon\bar{E} + \bar{J}, \tag{7.65}$$

where $\bar{J}$ and $\bar{M}$ are the electric current and fictitious magnetic current. In a linear medium, the electric polarization in related to the applied electric field, with some manipulation we can write,

$$\bar{D} = \epsilon_0\bar{E} + \bar{P}_e = \epsilon\bar{E}, \tag{7.66}$$

$$\bar{B} = \mu_0(\bar{H} + \bar{P_m}) = \mu\bar{H}, \tag{7.67}$$

then,

$$\nabla \times \bar{E} = -j\omega\mu_0\bar{H} - j\omega\mu_0\bar{P_m} - \bar{M}, \tag{7.68}$$

$$\nabla \times \bar{H} = j\omega\epsilon\bar{E} + j\omega\bar{P}_e + \bar{J}, \tag{7.69}$$

thus, since $\bar{J}$ and $\bar{M}$ has the same roles in these equations as $j\omega\bar{P}_e$ and $j\omega\mu_0\bar{P}_m$, the equivalent currents can be defined as,

$$\bar{J} = j\omega\bar{P}_e, \tag{7.70}$$

$$\bar{M} = j\omega\mu_0\bar{P}_m, \tag{7.71}$$

The electric and magnetic current sources, $\bar{J}$ and $\bar{M}$ are volume current densities with units A/m^3 and V/m^3, respectively. In many cases, however, the actual currents will be in the form of a current sheet, a line current, or an infinitesimal dipole current. These special types of current distributions can always be written as volume current densities through the use of delta functions. The strength of Electric polarization current and Magnetic polarization current in cartesian coordinates can be found as these equations are applicable in rectangular waveguide,

$$\bar{P}_e = \epsilon_0\alpha_e\hat{n}E_n\delta(x - x_0)\delta(y - y_0)\delta(z - z_0), \tag{7.72}$$

$$\bar{P_m} = -\alpha_m\bar{H}_t\delta(x - x_0)\delta(y - y_0)\delta(z - z_0), \tag{7.73}$$

we are going to find the strength of Electric polarization current and Magnetic polarization current in cylindrical coordinates because we want to work with circular waveguide and cavity. For this reason we should transform dirac delta function from cartesian coordinates to cylindrical coordinates.

$$\delta(x-x_0)\delta(y-y_0)\delta(z-z_0) = \frac{1}{|J|}\ \delta(r-r_0)\delta(\theta-\theta_0)\ \delta(z-z_0), \tag{7.74}$$

where J is Jacobian matrix .

recall that $x = f(r,\theta) = rcos\theta$ and $x = g(r,\theta) = rsin\theta$,

hence,

$f_r = cos\theta$, $f_\theta = -rsin\theta$, $g_r = sin\theta$ and $g_\theta = -rcos\theta$

the Jacobian is

$$J = |(cos\theta)(-rcos\theta) - (-rsin\theta)(sin\theta)| = r, \tag{7.75}$$

then the transformation would be,

$$\delta(x-x_0)\delta(y-y_0)\delta(z-z_0) = \frac{1}{r}\ \delta(r-r_0)\delta(\theta-\theta_0)\ \delta(z-z_0). \tag{7.76}$$

Knowing the transformation between two coordinates, the strength of Electric polarization current and Magnetic polarization current in cylindrical coordinates can be written as,

$$\bar{P_e} = \frac{1}{r}\epsilon_0\alpha_e\hat{n}E_n\delta(r-r_0)\ \delta(\theta-\theta_0)\ \delta(z-z_0), \tag{7.77}$$

$$\bar{P_m} = -\frac{1}{r}\alpha_m\bar{H_t}\delta(r-r_0)\ \delta(\theta-\theta_0)\ \delta(z-z_0), \tag{7.78}$$

where,

$\bar{P_e}$: infinitesimal electric polarization currents,

$\bar{P_m}$: infinitesimal magnetic polarization currents,

ϵ_0 : Electric conductivity,

α_e : electric polarizability of the aperture,

α_m : magnetic polarizability of the aperture,

The electric and magnetic polarizabilites are constants that depend on the size and shape of the aperture which we will talk about it in details in the section (7.2.6).

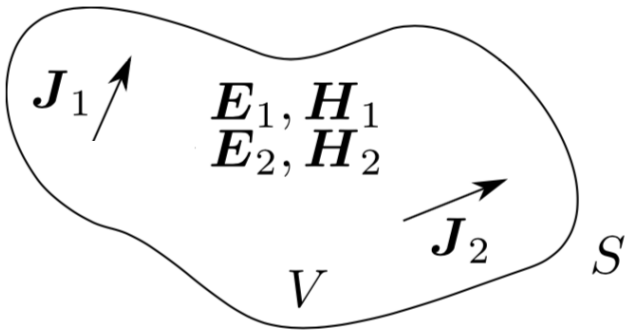

Figure 7.7: A volume containing two sets of sources, J_1 and J_2, which each produce fields E_1, H_1 and E_2, H_2, respectively.

7.2.4 Lorentz Reciprocity Theorem

A formal derivation of the Lorentz Reciprocity Theorem begins by considering a volume containing two sets of sources, J_1 and J_2, which each produce fields E_1, H_1 and E_2, H_2, respectively, as shown in Figure (7.7). Consider the quantity

$$\nabla \, . \, (E_1 \times H_2 \; - \; E_2 \times H_1), \tag{7.79}$$

which is expandable using a vector identity as

$$(\nabla \times E_1) \, . \, H_2 \; - \; (\nabla \times H_2) \, . \, E_1 \; - \; (\nabla \times E_2) \, . \, H_1 \; + \; (\nabla \times H_1) \, . \, E_2. \tag{7.80}$$

From Maxwell's equations,

$$\nabla \times E_1 = \; -j\omega\mu H_1 \; - \; M_1, \tag{7.81}$$

$$\nabla \times H_1 = \; j\omega\epsilon E_1 + J_1, \tag{7.82}$$

$$\nabla \times E_2 = \; -j\omega\mu H_2 \; - \; M_2, \tag{7.83}$$

$$\nabla \times H_2 = \; j\omega\epsilon E_2 + J_2, \tag{7.84}$$

therefore,

$$\nabla \, . \, (E_1 \times H_2 - E_2 \times H_1) = (\nabla \times E_1) \, . \, H_2 - (\nabla \times H_2) \, . \, E_1 - (\nabla \times E_2) \, . \, H_1 + (\nabla \times H_1) \, . \, E_2 \tag{7.85}$$

$$\nabla \cdot (E_1 \times H_2 \ - \ E_2 \times H_1) = -j\omega\mu H_1 \cdot H_2 - M_1 \cdot H_2 \ - \ j\omega\epsilon E_2 \cdot E_1 \ - \ J_2 \cdot E_1$$

$$+ j\omega\mu H_2 \cdot H_1 + M_2 \cdot H_1 \ + \ j\omega\epsilon E_1 \cdot E_2 \ + \ J_1 \cdot E_2,$$

$$= J_1 \cdot E_2 \ - \ J_2 \cdot E_1 + M_2 \cdot H_1 - M_1 \cdot H_2, \tag{7.86}$$

let us now integrate the divergence over the volume of interest:

$$\int_V \nabla \cdot (E_1 \times H_2 \ - \ E_2 \times H_1)dv' = \int_V (J_1 \cdot E_2 \ - \ J_2 \cdot E_1 + M_2 \cdot H_1 - M_1 \cdot H_2)dv', \tag{7.87}$$

applying the Divergence Theorem or Gauss's theorem to the left hand side:

$$\int_V \nabla \cdot (E_1 \times H_2 \ - \ E_2 \times H_1)dv' = \oint_S (E_1 \times H_2 \ - \ E_2 \times H_1)ds', \tag{7.88}$$

therefore the two side of the Eqs.(7.87) and (7.88) are equal,

$$\oint_S (E_1 \times H_2 \ - \ E_2 \times H_1)ds' = \int_V (J_1 \cdot E_2 \ - \ J_2 \cdot E_1 + M_2 \cdot H_1 - M_1 \cdot H_2)dv', \tag{7.89}$$

considering an electric current source,

$$\oint_S (E_1 \times H_2 \ - \ E_2 \times H_1)ds = \int_V (J_1 \cdot E_2 \ - \ J_2 \cdot E_1)dv. \tag{7.90}$$

7.2.5 Applying Lorentz Reciprocity Theorem to the Current Problem

We can apply reciprocity theorem considering the volume V being between the cavity walls, then let $\bar{E}_1 = \bar{E}^{\pm}$ and $\bar{H}_1 = \bar{H}^{\pm}$ when $z > z2$ for the wave propagating in positive direction and $z < z1$ for the wave propagating in negative direction .
Suppose $\bar{E}_2$, $\bar{H}_2$ be the nth cavity mode traveling in the positive z direction,

$$\bar{E}_2 = \bar{E}_{01}^{-} = (\bar{e_{t01}} \ + \ \hat{z}\bar{e}_{z01}) \ e^{-j\beta z}, \tag{7.91}$$

$$\bar{H}_2 = \bar{H}_{01}^{-} = (\bar{h_{t01}} \ + \ \hat{z}\bar{h}_{z01}) \ e^{-j\beta z}, \tag{7.92}$$

where β_n is the propagation constant for the mode n in the z direction and $\bar{e}_n$, $\bar{h}_n$ are electric and magnetic transverse fields and $\bar{e}_{zn}$, $\bar{h}_{zn}$ are electric and magnetic longitudinal fields propagating in the z direction. Then Eq. (7.51) turn out to be,

$$\oint_S [(\bar{E}^+ \times \bar{H}_{01}^+ \ - \bar{E}_{01}^+ \times \bar{H}^+) \\ + (\bar{E}^- \times \bar{H}_{01}^+ \ - \bar{E}_{01}^+ \times \bar{H}^-)] ds = \int_V (J \ . \ E_2 - M \ . \ H_2) dv, \tag{7.93}$$

substituting Eqs. (7.47) to (7.50) into the equation above and considering that the tangential electric field and normal magnetic field will be vanish on the waveguide and cavity walls so that surface integral of the *Eqs.*(7.93) will be reduced to just integration at z_1 and z_2 where z_1 and z_2 are the cross section of the waveguide or cavity. Then the equation can be written as follows,

$$A_{01}^+ \int_{z_2} (\bar{E}^+ \times \bar{H}_{01}^+ \ - \bar{E}_{01}^+ \times \bar{H}^+) \ . \ d\bar{s} \\ + A_{01}^- \int_{z_1} (\bar{E}^- \times \bar{H}_{01}^+ \ - \bar{E}_{01}^+ \times \bar{H}^-) \ . \ d\bar{s} = \int_V (J \ . \ E_2 - M \ . \ H_2) dv, \tag{7.94}$$

the first integral will be vanish because of the orthogonality of the modes,

$$A_{01}^- \oint_S (\bar{E}^- \times \bar{H}_{01}^+ \ - \bar{E}_{01}^+ \times \bar{H}^-) ds = \int_V (J \ . \ E_2 - M \ . \ H_2) dv, \tag{7.95}$$

this equation can be written explicitly as,

$$A_{01}^- \int_{z_1} [(\bar{e}_{t01} - \hat{z} e_{nz}) \times (\bar{h}_{t01} + \hat{z} h_{z01}) - (\bar{e}_n + \hat{z} e_{zn}) \times (-\bar{h}_n + \hat{z} h_{zn})] \ . \hat{z} ds \\ = \int_V (J \ . \ E_2 - M \ . \ H_2) dv, \tag{7.96}$$

we can simplify the equation,

$$- 2A_{01}^- \int_{z_2} \bar{e}_{t01} \times \bar{h}_{t01} \ . \hat{z} ds = \int_V (J \ . \ E_2 - M \ . \ H_2) dv, \tag{7.97}$$

then we have,

$$A_{01}^- = \frac{-1}{P_{01}} \int_V [(\bar{e}_{t01} + \hat{z} e_{z01}) \ . \ \bar{J} - (\bar{h}_{t01} + \hat{z} h_{z01}) \ . \ \bar{M}] e^{-j\beta_n z} dv, \tag{7.98}$$

where $P_{01} = 2 \int_{z_1} \bar{e}_{t01} \times \bar{h}_{z01} \ . \hat{z} ds$ is a normalization constant proportional to the power flow of the TM_{01} mode which we will calculate in the next section. Substituting $\bar{J} = j\omega \bar{P}_e$ and $\bar{M} = j\omega\mu_0 \bar{P}_m$ into the equation above we have,

$$A_{01}^- = \frac{-1}{P_{01}} \int_V [(\bar{e}_{t01} + \hat{z} e_{z01}) \ . \ (j\omega \bar{P}_e) - (\bar{h}_{t01} + \hat{z} h_{z01}) \ . \ (j\omega\mu_0 \bar{P}_m)] e^{-j\beta_n z} dv, \tag{7.99}$$

where $e_z(\rho,\phi) = (Asinn\phi + Bcosn\phi)J_n(k_c\rho)$ and $h_n(\rho,\phi) = \frac{-j\omega\epsilon}{k_c}(Asinn\phi + Bcosn\phi)J_n'(k_c\rho)$ are the modal fields for TM_{01} mode as we shows in Table. (7.1) . Replacing Eqs. (7.77) and (7.78) and introducing the modal fields into the Eq. (7.99) we have,

$$A_{01}^{-} = \frac{-1}{P_{01}} \int [(e_{t01} \; + \; \hat{z}e_{z01}) \; e^{-j\beta_n z}] \; . \; (\hat{z}\frac{j\omega}{r}\epsilon_0\alpha_e[AJ_0(k_c\rho)e^{-j\beta z} + A_{01}^{-}(\frac{-j\beta}{k_c}J_0'(k_c\rho) - J_0(k_c\rho))e^{j\beta z}$$
$$- jA_{01}^{+}(\frac{-j\beta}{k_c}J_0'(k_c\rho) + J_0(k_c\rho))e^{-(2\alpha\ell + j\beta z)}] - [(h_{t01}^{-} \; + \; \hat{z}h_{z01}) \; e^{-j\beta_n z}] \; . \; (\hat{t} \; \frac{j\omega}{r}\alpha_m[(-\frac{A}{\eta_{01}}e^{-j\beta z}$$
$$+ A_{01}^{-}\frac{j\beta}{\eta_{01}k_c}e^{j\beta z} - jA_{01}^{+}\frac{j\beta}{\eta_{01}k_c}e^{-(2\alpha\ell + j\beta z)})J_0'(k_c\rho)])\delta r \; \delta\theta \; \delta z)rdrd\theta dz. \tag{7.100}$$

We know that the integration of the convolution of a function is the quantity of the function at the point in which the convolution will end.

$$\int f(x)\delta(x - x_0)dx = f(x_0). \tag{7.101}$$

Finally considering the electric modal field for TM_{01} and some simplification the equation turn out to be,

$$A_{01}^{-} = \frac{-1}{P_{01}} j\omega\epsilon_0\alpha_e A$$
$$+ \frac{-1}{P_{01}} \int_0^b \int_0^{2\pi} \int_0^{\ell} j\omega\epsilon_0\alpha_e A_{01}^{-}(\frac{-j\beta}{k_c}J_0'(k_cr)J_0(k_cr) - J_0^2(k_cr))e^{j\beta z}\delta r\delta\theta\delta z dr \; d\theta \; dz$$
$$+ \frac{-1}{P_{01}} \int_0^b \int_0^{2\pi} \int_0^{\ell} j\omega\epsilon_0\alpha_e[-jA_{01}^{+}(\frac{-j\beta}{k_c}J_0'(k_cr)J_0(k_cr) + J_0^2(k_cr))e^{-2\alpha\ell - j\beta z}])\delta r\delta\theta\delta z dr \; d\theta \; dz. \tag{7.102}$$

Normalization constant proportional to the power flow of the nth mode

As we have mentioned earlier P_n is the normalization constant proportional to the power flow of the nth mode and in a special case P_{01} is a normalization constant proportional to the power flow of the TM_{010} mode and it's equal to $2\int_z \bar{e}_{01} \times \bar{h}_{01}^{*} \; .\hat{z}ds$. TM modal fields as we have shown in Table (7.1) can be written as,

$$e_n(\rho,\phi) = \frac{-j\beta}{k_c}(Asinn\phi + Bcosn\phi)J_n'(k_c\rho), \tag{7.103}$$

$$h_n(\rho,\phi) = \frac{-j\omega\epsilon}{k_c}(Asinn\phi + Bcosn\phi)J_n'(k_c\rho),$$

$$= \frac{-j\beta}{\eta_{01}k_c}(Asinn\phi + Bcosn\phi)J_n'(k_c\rho), \tag{7.104}$$

where K_c is cutoff wavenumber, β is the propagation constant, n is the number of nulls in E_z along the radial direction, $J'_n(k_c\rho)$ is the derivative of the Bessel function of the first kind and η_{01} the impedance of free space and it's a physical constant relating the magnitudes of the electric and magnetic fields of electromagnetic radiation traveling through free space. That is, $\eta_0 = |E|/|H|$, where $|E|$ is the electric field strength and $|H|$ is the magnetic field strength for the TM_{010}. It has an exactly defined value $\eta_{01} = 376.73$. For TM_{010} modal fields we can write,

$$e_{01} = \frac{-j\beta}{k_c} J'_0(k_c\rho), \tag{7.105}$$

$$h_{01} = \frac{-j\beta}{\eta_{01} k_c} J'_0(k_c\rho). \tag{7.106}$$

Finally normalization constant proportional to the power flow of the TM_{01} mode will be,

$$P_{01} = 2\int_z \bar{e}_{01} \times \bar{h}_{01} \,.\hat{z} ds = \frac{-2\pi b^2}{\eta_{01}} \, J_1^2(\chi_{01}). \tag{7.107}$$

7.2.6 Calculation of electric and magnetic polarizabilites

There is an electric polarization coefficient for electric moment, $P = -2a^3\epsilon_0 E_0/3$, where $\alpha = -2/3a^3$. This is the coefficient polarization obtained by Bethe, in his famous article "Theory of Diffraction by Small Holes"[5]. As we have mentioned in chapter 3, Bethe obtained the coefficient for small holes compare to the wavelength, he mentioned in his article that it is possible to extend to the holes comparable in size with the wavelength considering the E_0, normal electric field, contain factors of the type e^{ikr} in which the variation in the Green's function ϕ must be considered and he said that the correction for the holes comparable to the wavelength will be of relative order $(ka)^2$ rather than ka. Eggimann [16] solved the problem of diffraction of arbitrary electromagnetic field by a circular perfectly conducting disk using a series representation in powers of $k = 2\pi/\lambda$ and he obtained an expression for electric and magnetic moments using the results of generalized Babinet's principle [17] and considering that the disk problem and the aperture problem are equivalent if some consideration would be taken, the final results were the following expressions for the induced dipole moments: $P_z = \frac{4}{3}a^3\epsilon_0(E_z^0 - \frac{1}{10}(ka)^2[3E_z^0 + \frac{1}{k^2}\,\frac{\partial^2 E_z^0 l}{\partial z^2}] + j\frac{4}{9\pi}(ka)^3 E_z^0)$, in which taking first and second term of the equation we have a term that is proportional to $(ka)^2$ as Bethe was said about the hole size comparable with the wavelength. Considering the electric moment according to Eggimann, but taking two terms instead of the whole equation we have: $P_z = \frac{4}{3}a^3\epsilon_0 E_z^0(1 - \frac{3}{10}(ka)^2)$.

For the small irises all the modes of waveguide are below cut-off and their attenuation is exponential with respect to the length of the iris. McDonald [2] has derived an electric polarizability

in which the attenuation term can be considered and it is as follows,

$$\alpha_e = C_E\ \alpha_e^*\ e^{-2.405h/a} \quad with\ \ C_E = 0.83\ \ and\ \ \alpha_e^* = -\frac{2}{3}a^3, \tag{7.108}$$

$$\alpha_m = C_M\ \alpha_m^*\ e^{-1.841h/a} \quad with\ \ C_M = 0.84\ \ and\ \ \alpha_m^* = \frac{4}{3}a^3, \tag{7.109}$$

where h is the iris thickness, C_E and C_M are the numerical values calculated by McDonald [3]. Gluckstern has derived integral equations for the potential and field distribution within a circular hole in a plane conducting wall of finite thickness induced by uniform field. then he obtained variational expressions for the polarizability and susceptibility of the hole, from which one can obtain the electric and magnetic dipole moments induced on the inside (far field) and outside (no far field) boundaries of the hole [21]. His results had a good agreement with McDonald's results.

7.2.7 Reflection Coefficient

Finally we can calculate the amplitude for forward and backward waves due to dipole moments,

$$A_{01}^- = \frac{-1}{P_{01}} j\omega\epsilon_0\alpha_e A \tag{7.110}$$

$$+\frac{-1}{P_{01}}\int_0^b\int_0^{2\pi}\int_0^{\ell} j\omega\epsilon_0\alpha_e A_{01}^-\left(\frac{-j\beta}{k_c}J_0'(k_cr)J_0(k_cr) - J_0^2(k_cr)\right)e^{j\beta z}\delta r\delta\theta\delta z dr\ d\theta\ dz$$

$$+\frac{-1}{P_{01}}\int_0^b\int_0^{2\pi}\int_0^{\ell} j\omega\epsilon_0\alpha_e\left[-jA_{01}^+\left(\frac{-j\beta}{k_c}J_0'(k_cr)J_0(k_cr) + J_0^2(k_cr)\right)e^{-2\alpha\ell - j\beta z}\right]\delta r\delta\theta\delta z dr\ d\theta\ dz,$$

where $P_{01} = \frac{2\pi b^2}{\eta_{01}}\ J_1^2(\chi_{01})$ is the normalization constant proportional to the power flow of the TM_{01} mode and α_e is electric polarizability and it can be written as we have obtained before, $\alpha_e = C_E\ \alpha_e^*\ e^{-2.405h/a} \quad with\ \ C_E = 0.83\ \ and\ \ \alpha_e^* = -\frac{2}{3}a^3$.
We can simplify $e^{-2\alpha\ell}$as follows,

$$e^{-2\alpha\ell} = e^{-\frac{2(2.405)\ell}{b}} = e^{-\frac{4.81\ell}{b}}, \tag{7.111}$$

as $\ell = \lambda/2$ for π mode accelerating periodic structure,

$$e^{-2\alpha\ell} = e^{-\frac{4.81\lambda}{2b}} = e^{-\frac{2.405\lambda}{b}}, \tag{7.112}$$

replacing $\lambda = 2.61b$ in the equation above,

$$e^{-2\alpha\ell} = e^{-2.405(2.61)} = 0.001879 \approx 0.00188. \tag{7.113}$$

$$D = \frac{1}{P_{01}}\omega\epsilon_0\alpha_e = \frac{\alpha_e}{2.61b^3\ J_1^2(\chi_{01})}, \tag{7.114}$$

as $\alpha_e = \frac{-2}{3}a^3$, where a is iris radius, we have,

$$D = -0.964(\frac{a}{b})^3. \tag{7.115}$$

A_{01}^- and A_{01}^+ in the Eq. (7.110) are the amplitudes of the radiation fields due to iris as a dipole. They can be written as reflection and transmission coefficients.

$$A_{01}^- = \Gamma A, \tag{7.116}$$

$$A_{01}^+ = (1-\Gamma)A, \tag{7.117}$$

Replacing these equations into the equation above we get,

$$\Gamma = \frac{-1}{P_{01}}j\omega\epsilon_0\alpha_e(1+e^{-2\alpha\ell}) \tag{7.118}$$

$$+\frac{-1}{P_{01}}\int_0^b\int_0^{2\pi}\int_0^{\ell} j\omega\epsilon_0\alpha_e\Gamma(\frac{-j\beta}{k_c}J_0'(k_cr)J_0(k_cr)-J_0^2(k_cr))e^{j\beta z}(1-e^{-2\alpha\ell-2j\beta z})\ \delta r\ \delta\theta\ \delta z\ dr\ d\theta\ dz,$$

writing the equation above in a compact way we have,

$$\Gamma = \Gamma_0 + D\int_V \Gamma\ f(r)g(z)h(\theta)\delta r\ \delta\theta\ \delta z \quad dV, \tag{7.119}$$

where

$\Gamma_0 = \frac{-1}{P_{01}}j\omega\epsilon_0\alpha_e(1+e^{-2\alpha\ell})$,

$D = \frac{-\beta}{P_{01}k_c}j\omega\epsilon_0\alpha_e$,

$f(r) = (J_0'(k_cr)J_0(k_cr) - J_0^2(k_cr))$,

$g(z) = e^{j\beta z}(1-e^{-2\alpha\ell-2j\beta z})$,

$h(\theta) = 1$,

and

$dV = dr\ d\theta\ dz$.

We have obtained an equation that the solution can be found by "self consistent solution method" which because of complexity of this method we will solve it in the future work but before to end this chapter we make some notes about the equation above:

- to obtain equation above we assumed that the iris is at the center of the cross section of the cavity. This assumption simplify the equation of infinitesimal electric and magnetic polarization currents (see Eq.s (7.77) and (7.78) to the equations below,

$$\bar{P_e} = \frac{1}{r}\epsilon_0 \alpha_e \hat{n} E_n \delta(r)\ \delta(\theta)\ \delta(z), \tag{7.120}$$

$$\bar{P_m} = -\frac{1}{r}\alpha_m \bar{H_t} \delta(r)\ \delta(\theta)\ \delta(z), \tag{7.121}$$

these equations allow us make a convolution of the functions at the center and simplify the equation to obtain Eq. (7.100) from the Eq. (7.99) and then by further assumption which was nothing other that the consideration of that only we have electric moment for the TM_{01} mode at the center for the small iris compared with the wavelength we reach the Eq. (7.102) and finally with some calculation we obtained the Eq. (7.119).

- as Γ depends on the coordinate parameters we can take out it from the integral by calculation the Γ at the center of the iris and obtain the equation below,

$$\Gamma = \frac{\frac{-1}{P_{01}} j\omega\epsilon_0\alpha_e(1+e^{-2\alpha\ell})}{1 + jH(0)\frac{-\beta}{P_{01}k_c}\omega\epsilon_0\alpha_e(1-e^{-2\alpha\ell})}, \tag{7.122}$$

where H(0) is Heaviside function and

$$P_{01} = \frac{-2\pi b^2}{\eta_{01}}\ J_1^2(\chi_{01}), \tag{7.123}$$

this equation is an analogous of the reflection coefficient obtained by Collin for TE_{10} using the circuit theory which for a comparison we will write here [17],

$$1 - \frac{4j\alpha_m\beta_{10}/ab}{1 + jX + W}, \tag{7.124}$$

Where $X = 2\alpha_m\beta_{10}/ab$ and

$$W = -\frac{4\alpha_m k_0^2\pi^2}{k_{101}^2 abd^3[k_{101}^2 - k_0(1+\frac{1-j}{Q})]} \tag{7.125}$$

- as in the equation is a Heaviside function we can obtain a distribution as we need for s_{11}, so by a Fourier transformation and then using the transformation below we can have a distribution (sweep) around the resonant frequency,

$$\hat{H}(s) = \frac{1}{2}(\delta(s) - \frac{i}{\pi} p.v.\frac{1}{s}), \tag{7.126}$$

where $p.v.\frac{1}{s}$ is a distribution that relates the Cauchy principle value of $\int_{-\infty}^{\infty} \frac{\phi(s)}{s} ds$ to the test function ϕ for the distribution.

Chapter 8

Simulation codes

In this chapter, the numerical codes used for the various simulations, carried out in this thesis work, are briefly explained.

8.1 HFSS

HFSS (High Frequency Structures Simulator) is a user-friendly software package, initially released by ANSOFT [1], Pittsburg, that allows to evaluate the 3D electromagnetic field distribution inside a structure. In order to do this, it solves the Maxwell equations in the frequency domain, so only linear material can be simulated. The numerical method employed is the FEM (Finite Element Method). HFSS divides the 3D model into a relatively large number of small domains, tetrahedra, that represent the mesh. The following features can be obtained from simulations:

- main RF properties of the electromagnetic field, and also the near and far fields for open structures;
- propagation constants and impedance at specified ports;
- parameters of the scattering S-matrix;
- eigenvalues, or resonant frequencies, and eigenfunctions for a closed structure.

8.2 SuperFish

SuperFish [3] is the main solver program for calculating Radio-Frequency electromagnetic fields in either 2-D Cartesian coordinates or axially symmetric cylindrical coordinates. The program

generates a triangular mesh fitted to the boundaries of the material in the problem geometry. It is not a very user- friendly code, like HFSS, and the internal part of the structures is simulated independently from any kind of input source. This means that a coupling condition with outside inputs, such as RF waveguide, is not achievable. Nevertheless, the fast computational time of simulations and accuracy of the results make SuperFish a powerful tool for the design of RF accelerators.

Chapter 9

Conclusions

In this concluding chapter we summarize the contributions of this thesis and discuss the important directions of future work.

9.1 Summary of thesis contributions

The purpose of this thesis was to study on design and measurements of the high gradient accelerating structures. After introducing the main parameters to characterize Linacs we explained the application of the periodic accelerating structure. Then we studied TW accelerating structure operating at K-band frequency in order to linearize longitudinal space phase in the framework of the Compact Light XLS project. We estimated group velocity as a function of frequency both analytically and numerically. Analytical results have a good agreement with the numerical results. The main parameters such as shunt impedance, quality factor (Geometric factor) and R/Q independently from the operating frequency for the TM_{010}, TM_{110} and TM_{011} for a single cylindrical "pill-box" have been determined analytically as they provide accurate model for the accelerating structures.

In order to characterize a normal conducting high accelerating structure with maximum gradients operating at X-band with extremely low probability of RF breakdown, an electroformed SW structures has been fabricated and characterized by SLAC and INFN with collaboration of other institute around the world at 11.424 GHz, coated with Au-Ni. We designed a gold plate RF high gradient structure operating at the X- band coated with Au-Ni. Bench measurements have been performed in the Department of SBAI of the University of Rome "La Sapienza". The Slater method for the SW cavity has been employed in order to quantify the electric field inside the structure. Comparing the results with the results exposed from HFSS we report the features that have been quantified, showing good agreement.

We continued working on the perturbation effect due to the aperture coupled between a waveguide and a cavity but for our application in SW multi-cell high gradient accelerating structure we studied on theoretical approach for reflection coefficient calculation in a SW cavity coupled to a waveguide. One method was based on circuit theory in which we found the overall Q of a resonant circuit for a cavity coupled to an external waveguide containing the RF generator. Q calculation led to the determining of the shunt impedance and consequently the reflection coefficient calculation. Comparison of the results shows a good agreement with the numerical results carried out by using the numerical code, HFSS. Another method of reflection coefficient calculation has been accomplished. We applied the modified Bethe's theory presented by Collin and developed by De santis, Mostacci and L.Palumbo for TM_{01} mode cavities coupled by a small hole with a thickness size comparable to the wavelength. The amplitudes of forward and backward waves due to polarizabilites have been determined and we found equations for reflection and transmission coefficients. We demonstrated that our equation for reflection coefficient calculation is an analogous of the reflection coefficient obtained by Collin for TE10 using the circuit theory.

9.2 Direction for future work

9.2.1 Self Consistent Solution Method for Reflection Coefficient Calculation

We recall the equation obtained in chapter 7,

$$\Gamma = \Gamma_0 + D \int_V \Gamma \ f(r)g(z)h(\theta)\delta r \ \delta\theta \ \delta z \quad dV, \tag{9.1}$$

where

$\Gamma_0 = \frac{-1}{P_{01}} j\omega\epsilon_0\alpha_e(1 + e^{-2\alpha\ell})$,

$D = \frac{-\beta}{P_{01}k_c} j\omega\epsilon_0\alpha_e$,

$f(r) = (J_0'(k_c r)J_0(k_c r) - J_0^2(k_c r))$,

$g(z) = e^{j\beta z}(1 - e^{-2\alpha\ell - 2j\beta z})$,

$h(\theta) = 1$,

and

$dV = dr \ d\theta \ dz$.

As we mentioned at the end of chapter 7, we have obtained an equation that the solution can be found by "self consistent solution method" which because of complexity of this method we will solve it as a future work.

9.2.2 Emittance growth due to multipole transverse magnetic modes in an rf gun

Emittance growth of electron beams due to the cylindrical asymmetry of an rf gun have been studied in many works. The breaking of the cylindrical symmetry occurs by certain ports, such as laser ports, vacuum ports, and power-coupling ports in different cells of the photocathode rf gun, and the primary asymmetry usually lies in the cell with the biggest port [43]. Consequently, the lack of cylindrical symmetry excites multipole field components, such as the dipole, quadrupole, and octopole, which kick the beam time dependently, leading to the emittance growth[44]. Minimization of the multipole rf field has been investigated and implemented in many works to produce high-brightness electron beams in the photocathode rf gun [45,46, 47]. Eliminatin of the multipole rf field is a new demanding of electron beams for the high gradient accelerating structures and the study to eliminate the multipole field effect on electron beam emittance in an rf gun is already started in some cases [47]. Mode launcher is a matched devices that couples the rectangular TE_{01} mode waveguide to a TM_{01} mode in a circular waveguide. Generally speaking, it is used as a converter from rectangular waveguide to circulare waveguide and the application of the mode launcher are as follows,

- Photoinjectors and Linacs: To avoid a breakdown problem due to holes of coupling between the rectangular waveguide of rf source and accelerating structure, the mode launcher is utilized as we show in Fig. (9.1)

  It's been demonstrated experimentally that these holes are one of the main reason for the malfunctioning of the accelerators, specially for the high power accelerators. Furthermore, by coupling of accelerating structure in axial mode, it's possible to avoid multipole components of electromagnetic fields which cause damage for the particle accelerator beam.

- High power testing: Putting an internal coating on the surface of mode launcher, it could be increased the efficiency of the high power rf accelerator because of reducing the risk of breakdown probability.

- Industrial application: As the figure below, currently high energy industrial linac should be enclosed from the cone of dense material for the radio protection. Rectangular waveguide

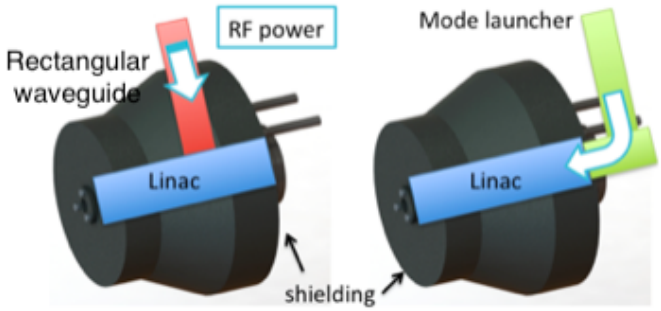

Figure 9.1: Mode launcher connected to the Linac.

of our supply is connected perpendicularly to the accelerating linac and it should pass through that cone, making the system less flexible from mechanical point of view. Using a mode launcher it could be possible to propagate the RF potential to the internal linac in the axial mode to avoid of touching of radio protection cone.

The mode launcher can be employed for military application, in particularly for all radar systems, for example, in which it needs the transportation of RF potential into the waveguide, making the system more flexible and linear from mechanical point of view, from momentum that the potential can be propagate axially.

Because the high brightness rf guns have a strong requirements on output beam properties, rf gun designers are attempting to eliminate the dipole or quadrupole or in general multipole rf fields [33, 48]. The authors in Ref. [47] have studied on a theoretical analysis and numerical simulations of the multipole field effect to the emittance growth (see Fig (9.2)). INFN in collaboration with SLAC designed a compact and symmetric mode launcher as shows in Fig. (9.3) with no multipolars fields. This mode launcher proposed by V. Dolgashev and couples the rectangular TM_{10} mode to a TM01 circular mode. A high brilliance beam can be produced because of the cancelation of dipolar and quadrupolar components by the four symmetrized arms of the device. The designs have been carried out for S-band and X-band [52,53]. In this work, we are studying for the analytical model to eliminate the multipole rf field in the case of four gun models with zero, one, two, and four holes at the cell cavity. An electron beam passing through a single cell near the axis with the light velocity in a zero, one, two, and four holes at the cell cavity.

The analytical mode for the effects of these multipoles on emittance growth is based on Panofsky wenzel theorem [49, 50] by which the transverse momentum imparted to an electron beam by the rf field in a single cell can be calculated as follows:

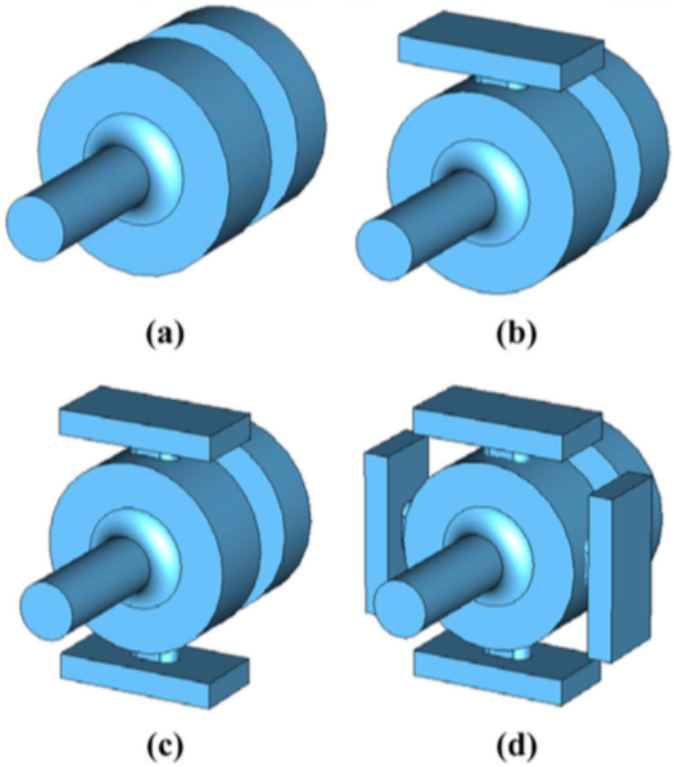

Figure 9.2: Simulation model of the rf gun with (a) one hole, (c) two holes, and (d) four holes in the full cell part [47].

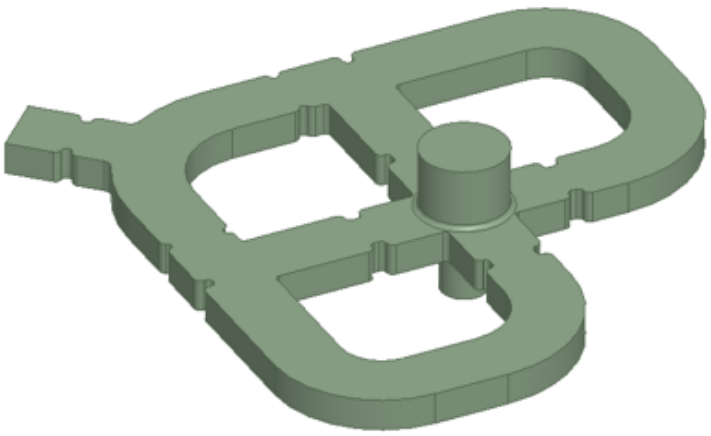

Figure 9.3: The mode launcher with compensated quadrupole components.

$$P_L = \frac{e}{\omega} Re(\int_{-\frac{L}{2}}^{\frac{L}{2}} i\nabla_\perp E_z dz), \tag{9.2}$$

where E_z is the electric field along the longitudinal axis, which can be expressed as the superposition of all the TM_{n10} modes [51],

$$E_z(r,\theta,z,t) = e^{i(\omega t+\phi_0)} \Sigma_{n=0}^{\infty} E_n cos(kz) J_n(k_c r) cos[n(\theta-\theta_0)], \tag{9.3}$$

where,

k_c: radial wave number

ϕ_0: rf phase

θ_0: polarization angle which will be determined by the position of the holes

k: rf wave number ($\frac{2\pi}{\lambda}$)

θ: azimuthal angle

We have obtained the monopole (TM_{010}), dipole TM_{110}, quadropole TM_{210} and octopole TM_{410} modes. The procedure for obtaining the longitudinal electric fields for the monopole and multipoles can be found in Appendix C,

$$E_z^{010} \simeq e^{i(\omega t+\phi_0)} E_0 cos(kz)(1 - \frac{k_c^2}{4}(x^2+y^2)), \tag{9.4}$$

$$E_z^{110} \simeq e^{i(\omega t+\phi_0)} a_1 E_0 cos(kz)\ y, \tag{9.5}$$

$$E_z^{210} \simeq -e^{i(\omega t+\phi_0)} a_2 E_0 cos(kz)(x^2-y^2), \tag{9.6}$$

$$E_z^{410} \simeq e^{i(\omega t+\phi_0)} a_4 E_0 cos(kz)(x^4 - 6x^2y^2 + y^4), \tag{9.7}$$

substituting the equations above into the Panofsky-Wenzel theorem we will calculate the transverse momentum imparted to an electron beam by the rf field in the case of four gun models with zero, one, two, and four holes at the cell cavity, respectively [Appendix D]. The results are as follows,

$$P_{n,\perp}^{010} = \frac{k_c^2}{2} \alpha L\ sin\phi_0\ (x\hat{x} + y\hat{y}), \tag{9.8}$$

$$P_{n,\perp}^{110} = -2\ a_1\ \alpha\ L\ sin\phi_0 \hat{y}, \tag{9.9}$$

$$P_{n,\perp}^{210} = 2a_2\alpha L sin\phi_0(x\hat{x} - y\hat{y}), \tag{9.10}$$

$$P_{n,\perp}^{410} = -4a_2\alpha L sin\phi_0[(x^3 - 3xy^2)\hat{x} + (y^3 - 3x^2y)\hat{y}]. \tag{9.11}$$

The normalized rms emittance growth can be calculated by

$$\epsilon_{n,x} = \sqrt{< (p_{n,x} - < p_{n,x} >)^2 >< (x - < x >)^2 > \; - \; < (p_{n,x} - < p_{n,x} >)(x - < x >) >^2}, \tag{9.12}$$

where the angle brackets mean statistical average. Substituting the previous results into the equation above we can obtained the normalized rms emittance growth due to the multipole fields.

For the next step we quantify the minimization of the multipole components though the Fourier analysis of the fields. The obtainable voltage from the multipole field can be written as follows: First, generally we write the field as an original continuous signal and we will call it $F(j\omega)$. Then we divide the original continuous signal to N samples. Obtaining the discrete form of the field we are able to perform a Discrete Fourier Transform to obtain a coefficient which in our case is the multipole voltage. The procedure is as follows,

$$F(j\omega) = \int_{-\infty}^{\infty} f(t)\ e^{-j\omega t}\ dt, \tag{9.13}$$

where f(t) is the original continuous signal. Let N samples be denoted f[0],f[1],f[2],..,f[k],..f[N-1] then we have,

$$F(j\omega) = \int_{0}^{(N-1)T} f(t)\ e^{-j\omega t}\ dt, \tag{9.14}$$

$$= f[0]\ e^{-j0} + f[1]\ e^{-j\omega t} + ... + f[k]\ e^{-j\omega kT} + ... + F[N-1]\ e^{-j\omega(N-1)T}, \tag{9.15}$$

$$= \Sigma_{k=0}^{N-1}\ f[k]\ e^{-j\omega kT}. \tag{9.16}$$

We evaluate the DFT equation for the fundamental frequency (one cycle per sequence, $\frac{1}{NT}Hz$, $\frac{2\pi}{NT}Hz$ rad/sec) and its harmonics.

$\omega = 0, \frac{2\pi}{NT}, \frac{2\pi}{NT} \times 2, ..., \frac{2\pi}{NT} \times n, ..., \frac{2\pi}{NT} \times (N-1)$,

then we get,

$$F[n] = \Sigma_{k=0}^{N-1}\ f[k]\ e^{-j\frac{2\pi}{N}nk}, \tag{9.17}$$

$$= \Sigma_{k=1}^{N}\ f[k]\ e^{-j\frac{2\pi}{N}(n-1)k}. \tag{9.18}$$

It is customary to write the equation above for our case as,

$$F[j] = \Sigma_{s=1}^{n}\ f[s]\ e^{-\frac{2\pi i}{n}(j-1)s}, \tag{9.19}$$

$$f[s] = \frac{1}{\sqrt{n}}\Sigma_{j=1}^{n}\ F[j]\ e^{\frac{2\pi i}{n}(j-1)s}, \tag{9.20}$$

as we know the equation for the voltage V_{-} is:

$$V_{\mp}(r,\theta) = \int_{z_i}^{z_f} E_z(r,\theta,z)\ e^{\mp ik_0 z}\ dz, \tag{9.21}$$

where θ is the azimuthal angle, k_0 is the wavenumber of the input rf power and z_i, z_f are the limits of integration on longitudinal axis. Then with the same procedure we have performed in the procedure above for DFT we can obtained,

$$M_{\mp,s}(r) = \frac{1}{\sqrt{n}}\Sigma_{j=1}^{n}\ V_{\mp}(r,\theta_j)\ e^{\frac{2\pi i}{n}(j-1)s}. \tag{9.22}$$

where n is the number of azimuthal variations of the voltage and s is the index of the modes and comparing this formula with the equation in ref. [45] we have obtained the Fourier transform coefficients for a multipole compensation. For the future work we will continue to work on analytical approach to eliminate multipole rf field to have less emittance growth due to the multipole transverse magnetic modes and consequently to construct a high brightness rf gun.

Chapter 10

Appendix

10.1 Appendix-A

Maxwell's equations predict the propagation of electromagnetic energy away from time-varying sources (current and charge) in the form of waves. Consider a linear, homogeneous, isotropic media characterized by (μ, ϵ, σ) in a source-free region.

We start with the source-free, instantaneous Maxwell's equations written in terms of E and H only. Note that conduction current in the source-free region is accounted for in the σE term.

$$\nabla \times \bar{E} = -\mu \frac{\partial \bar{H}}{\partial t}, \tag{10.1}$$

$$\nabla \times \bar{H} = \sigma \bar{E} + \epsilon \frac{\partial \bar{E}}{\partial t}, \tag{10.2}$$

$$\nabla \ . \ \bar{E} = 0, \tag{10.3}$$

$$\nabla \ . \ \bar{H} = 0, \tag{10.4}$$

taking the curl of $Eq.(10.1)$,

$$\nabla \times \nabla \times \bar{E} = -\mu \frac{\partial}{\partial t}(\nabla \times H), \tag{10.5}$$

and inserting $Eq.(10.2)$ gives

$$\nabla \times \nabla \times \bar{E} = -\mu \frac{\partial}{\partial t}(\sigma \bar{E} + \epsilon \frac{\partial \bar{E}}{\partial t}),$$

$$= -\mu\sigma\frac{\partial \bar{E}}{\partial t} - \mu\epsilon\frac{\partial^2 \bar{E}}{\partial t^2}, \tag{10.6}$$

taking the curl of $Eq.(10.2)$,

$$\nabla \times \nabla \times \bar{H} = \sigma(\nabla \times \bar{E}) + \epsilon\frac{\partial}{\partial t}(\nabla \times \bar{E}), \tag{10.7}$$

and inserting $Eq.(10.1)$ yields

$$\nabla \times \nabla \times \bar{H} = \sigma(-\mu\frac{\partial \bar{H}}{\partial t}) + \epsilon\frac{\partial}{\partial t}(-\mu\frac{\partial \bar{H}}{\partial t}),$$

$$= -\mu\sigma\frac{\partial \bar{H}}{\partial t} - \mu\epsilon\frac{\partial^2 \bar{H}}{\partial t^2}. \tag{10.8}$$

Using the vector identity for any vector A

$$\nabla \times \nabla \times \bar{A} = \nabla(\nabla \ . \ \bar{A}) - \nabla^2\bar{A}, \tag{10.9}$$

in $Eq.(10.6)$ and $Eq.(10.8)$ gives,

$$\nabla \times \nabla \times \bar{E} = \nabla(\nabla \ . \ \bar{E}) - \nabla^2\bar{E} = -\mu\sigma\frac{\partial \bar{E}}{\partial t} - \mu\epsilon\frac{\partial^2 \bar{E}}{\partial t^2}, \tag{10.10}$$

$$\nabla \times \nabla \times \bar{H} = \nabla(\nabla \ . \ \bar{H}) - \nabla^2\bar{H} = -\mu\sigma\frac{\partial \bar{H}}{\partial t} - \mu\epsilon\frac{\partial^2 \bar{H}}{\partial t^2}, \tag{10.11}$$

where from Maxwell's equation we have , $\nabla \ . \ E = 0$ and $\nabla \ . \ H = 0$, then the equations above turn out to be,

$$\nabla^2\bar{E} = \mu\sigma\frac{\partial \bar{E}}{\partial t} + \mu\epsilon\frac{\partial^2 \bar{E}}{\partial t^2}, \tag{10.12}$$

$$\nabla^2\bar{H} = \mu\sigma\frac{\partial \bar{H}}{\partial t} + \mu\epsilon\frac{\partial^2 \bar{H}}{\partial t^2}, \tag{10.13}$$

which are instantaneous vector wave equations known Helmholtz equations.

For time-harmonic fields, the instantaneous (time-domain) vector A is related to the phasor (frequency-domain) vector A_s by

$A \ <-> \ A_s$

$\frac{\partial A}{\partial t} \ <-> \ j\omega A_s$

$\frac{\partial^2 A}{\partial t^2} \ <-> \ (j\omega)^2 A_s$

Using these relationships, the instantaneous vector wave equations are transformed into the phasor vector wave equations:

$$\nabla^2 \bar{E} - k^2 \bar{E} = 0, \tag{10.14}$$

$$\nabla^2 \bar{H} - k^2 \bar{H} = 0, \tag{10.15}$$

where $k^2 = j\omega\mu(\sigma + j\omega\epsilon)$ and the complex constant k is defined as the propagation constant.

$$k = \alpha + j\beta = \sqrt{j\omega\mu(\sigma + j\omega\epsilon)}. \tag{10.16}$$

The Solutions of Wave Equation in Cylindrical Coordinates [40]:

The Helmholtz equation in cylindrical coordinates is

$$\frac{1}{\rho}\frac{\partial}{\partial\rho}(\rho\frac{\partial\psi}{\partial\rho}) + \frac{1}{\rho^2}\frac{\partial^\psi}{\partial^2} + \frac{\partial^2\psi}{\partial z^2} + k^2\psi = 0. \tag{10.17}$$

By separation of variables, assume $\psi = R(\rho)\Phi(\phi)Z(z)$. We have

$$\frac{1}{\rho R(\rho)}\frac{d}{d\rho}(\rho\frac{dR(\rho)}{d\rho}) + \frac{1}{\rho^2\Phi(\phi)}\frac{d2^\Phi}{d\Phi^2} + \frac{1}{Z(z)}\frac{\partial^2 Z(z)}{dz^2} + k^2 = 0, \tag{10.18}$$

the third term is independent of ϕ and ρ, so it must be constant:

$$\frac{1}{Z(z)}\frac{\partial^2 Z(z)}{dz^2} = -k_z^2, \tag{10.19}$$

This leaves,

$$\frac{1}{\rho R(\rho)}\frac{d}{d\rho}(\rho\frac{dR(\rho)}{d\rho}) + \frac{1}{\rho^2\Phi(\phi)}\frac{d^2\Phi}{d\Phi^2} + k^2 - k_z^2 = 0. \tag{10.20}$$

Now define the radial wavenumber as,

$$k_\rho^2 = k^2 - k_z^2, \tag{10.21}$$

and multiply the resulting equation by ρ^2 to find

$$\frac{\rho}{R(\rho)}\frac{d}{d\rho}(\rho\frac{dR(\rho)}{d\rho}) + \frac{1}{\Phi(\phi)}\frac{d^2\Phi}{d\phi^2} + k_\rho^2\rho^2 = 0, \tag{10.22}$$

the second term is independent of ρ and z, so we let

$$\frac{1}{\Phi(\phi)}\frac{d^2\Phi}{d\Phi^2} = -n^2. \tag{10.23}$$

This process leaves an ordinary differential equation in ρ alone. then we must have

$$\rho\frac{d}{d\rho}(\rho\frac{dR(\rho)}{d\rho}) + [k_\rho^2\rho^2 - n^2]R(\rho) = 0, \tag{10.24}$$

$$\frac{d^2\Phi}{d\phi^2} + n^2\Phi(\phi) = 0, \tag{10.25}$$

$$\frac{\partial^2 Z(z)}{dz^2} + k_z^2 Z = 0, \tag{10.26}$$

$$\frac{\partial^2 Z(z)}{dz^2} + k_z^2 Z = 0, \tag{10.27}$$

$$k_\rho^2 + k_z^2 = k^2, \tag{10.28}$$

the first of these equations is called Bessel's Equation; the others are familiar.

The second and third equations are the harmonic equations. We have already seen equations like those in the z and ϕ directions; the solutions are trigonometric or exponential. The only novelty is that ϕ is periodic or finite; it therefore is always expanded in a series and not an integral. If there is no limit in the ϕ direction we find $\Phi(\phi) = \Phi(\phi+2\pi)$ for the periodic boundary condition. This implies that $n\epsilon Z$ if the entire range is included.

The remaining equation to be solved is the radial equation, i.e. Bessel's Equation.Note that the problem simplifies considerably if $k_\rho = 0$. This case may be considered as a Bessel's functions for statics or stationary state. In this case, we have

$$\rho\frac{d}{d\rho}(\rho\frac{dR(\rho)}{d\rho}) - n^2R(\rho) = 0, \tag{10.29}$$

to solve it, let $\rho = e^x$ so $\frac{d\rho}{dx} = e^x = \rho$.This implies that,

$$\frac{d}{dx} = \frac{d\rho}{dx}\frac{d}{d\rho} = \rho\frac{d}{d\rho}, \tag{10.30}$$

then the equation for statics Bessel's function turn to be,

$$\frac{d^2R}{dx^2} - n^2R = 0, \tag{10.31}$$

the solutions to this are,

$$R(x) = \{^{A+Bln\rho \quad n=0}_{A\rho^n+B\rho^{-n} \quad n\neq 0}, \tag{10.32}$$

We are generally more interested in the dynamic case in which we must solve the full Bessel Equation:

$$\xi\frac{d}{d\xi}(\xi\frac{dR}{d\xi}) + [\xi^2 - n^2]R = 0, \tag{10.33}$$

one may be normalize $k_\rho = 1$, and rewrite the equation in terms of ρ instead of ξ to solve this equation, we suppose

$$R(\xi) = \xi^\alpha \Sigma_{m=0}^{\infty} c_m \xi^m, \tag{10.34}$$

now the derivative of $R(\xi)$ respect to ξ is,

$$\frac{dR}{\xi} = \Sigma_{m=0}^{\infty}(\alpha + m)c_m\xi^{\alpha+m-1}, \tag{10.35}$$

thus

$$\xi\frac{dR}{\xi} = \Sigma_{m=0}^{\infty}(\alpha + m)c_m\xi^{\alpha+m}, \tag{10.36}$$

and

$$\frac{d}{d\xi}(\xi\frac{dR}{\xi}) = \Sigma_{m=0}^{\infty}(\alpha + m)^2 c_m\xi^{\alpha+m-1}, \tag{10.37}$$

finally we construct the first term of the $Eq.(10.33)$ as,

$$\xi\frac{d}{d\xi}(\xi\frac{dR}{\xi}) = \Sigma_{m=0}^{\infty}(\alpha + m)^2 c_m\xi^{\alpha+m}, \tag{10.38}$$

now, we can plug in the second term of $Eq.(10.33)$ putting the $Eq.(10.34)$ for the $R(\xi)$,

$$\Sigma_{m=0}^{\infty}(\alpha + m)^2 c_m\xi^{\alpha+m} + [\xi^2 - n^2]\Sigma_{m=0}^{\infty} c_m\xi^{\alpha+m} = 0, \tag{10.39}$$

now we have

$$\Sigma_{m=0}^{\infty}[(\alpha + m)^2 - n^2]c_m\xi^{\alpha+m} + \Sigma_{m=0}^{\infty} c_m\xi^{\alpha+m} = 0, \tag{10.40}$$

we can proceed by forcing the coefficients of each term to vanish. We fixed $c_0 \neq 0$ because of the homogeneity of the equation.

For ξ^α we have $\alpha^2 - n^2 = 0$. Since $c_0 \neq 0$ by assumption, then $\alpha = \pm n$. For ξ^α we have instead $[(\alpha + 1)^2 - n^2]c_1 = 0$, thus $c_1 = 0$. Finally for all other $\xi^{\alpha+m}$:

$$[(\alpha + 1)^2 - n^2]c_m + c_{m-2} = 0, \tag{10.41}$$

assuming $\alpha = n$, then,

$$c_m = \frac{-1}{m(m+2n)} c_{m-2}, \tag{10.42}$$

thus, immediately for $p \in \mathbb{Z}$ we have: $c_{2p+1} = 0$.

Given that the odd coefficients vanish, we let $m = 2p$ and let $a_p = c_{2p}$, so we get

$$a_p = c_{2p} = \frac{-1}{4p(p+n)} c_{2p-2} = a_{p-1}, \tag{10.43}$$

and

$$a_1 = \frac{-1}{4(n+1)} a_0, \tag{10.44}$$

$$a_2 = \frac{-1}{4(n+2)(2)} \frac{-1}{4(n+1)} a_0, \tag{10.45}$$

$$a_3 = \frac{-1}{4(n+3)(3)} \frac{-1}{4(n+2)(2)} \frac{-1}{4(n+1)} a_0, \tag{10.46}$$

in general it can be written,

$$a_p = \frac{(-1)^p n!}{4^p p!(n+1)!} a_0, \tag{10.47}$$

if we choose $2^{-n} n! a_0 = 1$ and recall,

$$R(\xi) = \xi^\alpha \Sigma_{m=0}^{\infty} cm \xi^m = \Sigma_{p=0}^{\infty} a_p \xi^{2p+n}, \tag{10.48}$$

finally we can define the Bessel function of order n as a solution for our equation $R(\xi)$:

$$R(\xi) = J_n(\xi) = \Sigma_{p=0}^{\infty} \frac{(-1)^p}{p!(n+p)!} (\frac{\xi}{2})^{2p+n}, \tag{10.49}$$

this function is entire; it exists and is differentiable for all ξ, this is only one solution of the equation. The other solution is not regular at the origin since the coefficient of the second order derivative vanishes there.Note that the solution looks like the corresponding static ρ^n solution at the origin.we have to mention that also fractional orders are possible, but do not arise as commonly in applications.

Our original equation (normalized) was

$$\xi \frac{d}{d\xi} (\xi \frac{du}{d\xi}) + [\xi^2 - n^2] u = 0, \tag{10.50}$$

the other solution, v must be,

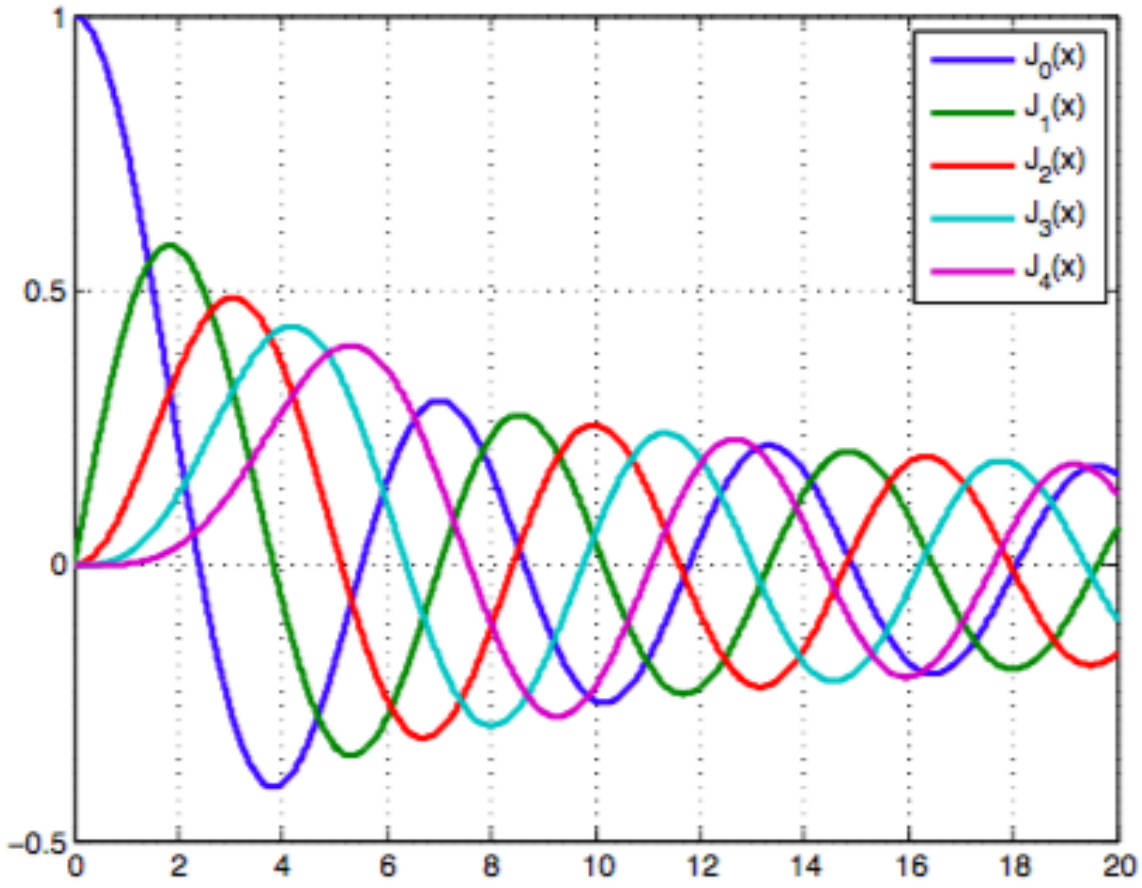

Figure 10.1: Bessel's Function

$$\xi\frac{d}{d\xi}(\xi\frac{dv}{d\xi}) + [\xi^2 - n^2]v = 0, \tag{10.51}$$

multiply the first equation by v and the second by u, subtract, and divide by ξ:

$$v\frac{d}{d\xi}(\xi\frac{du}{d\xi}) - u\frac{d}{d\xi}(\xi\frac{dv}{d\xi}) = 0 \tag{10.52}$$

expanding this out

$$\xi(u"v - uv") + u'v - uv' = 0. \tag{10.53}$$

or

$$\frac{d}{d\xi}[\xi(u'v - uv')] = 0. \tag{10.54}$$

It therefore stands to reason that $\xi(u'v - uv') = C$ or $\frac{(u'v-uv')}{v^2} = \frac{C_2}{\xi v^2}$. This of course implies $\frac{d}{d\xi}(\frac{u}{v}) = \frac{C_2}{\xi v^2}$. This can be integrated to give,

$$\frac{u}{v} = C_1 + C_2\int\frac{d\xi}{\xi v^2}, \tag{10.55}$$

or

$$u(\xi) = C_1 v(\xi) + C_2 v(\xi)\int\frac{d\xi}{\xi v(\xi)^2}, \tag{10.56}$$

setting $C_1 = 0$ and $v(\xi) = J_n(\xi)$ and expanding the series and integrating gives rise to the

$$Y_n(\xi) = J_n(\xi)\int\frac{d\xi}{\xi J_n^2(\xi)}, \tag{10.57}$$

which is the Neumann function.This function is also called the "Bessel function of the second kind".It is sometimes denoted by $N_n(\xi)$. This function is not defined for $\xi = 0$.
The J_n and Y_n are both real functions for real arguments.They must therefore represent standing waves. It should be noted that Hankel functions represent traveling waves which they can construct taking the real part from Bessel's function and the immaginary part from Neumann function.

$$H_n^{(1)}(x) = J_n(x) + jY_n(x), \tag{10.58}$$

$$H_n^{(1)}(x) = J_n(x) - jY_n(x), \tag{10.59}$$

these are called Hankel functions of the first and second kind, respectively.

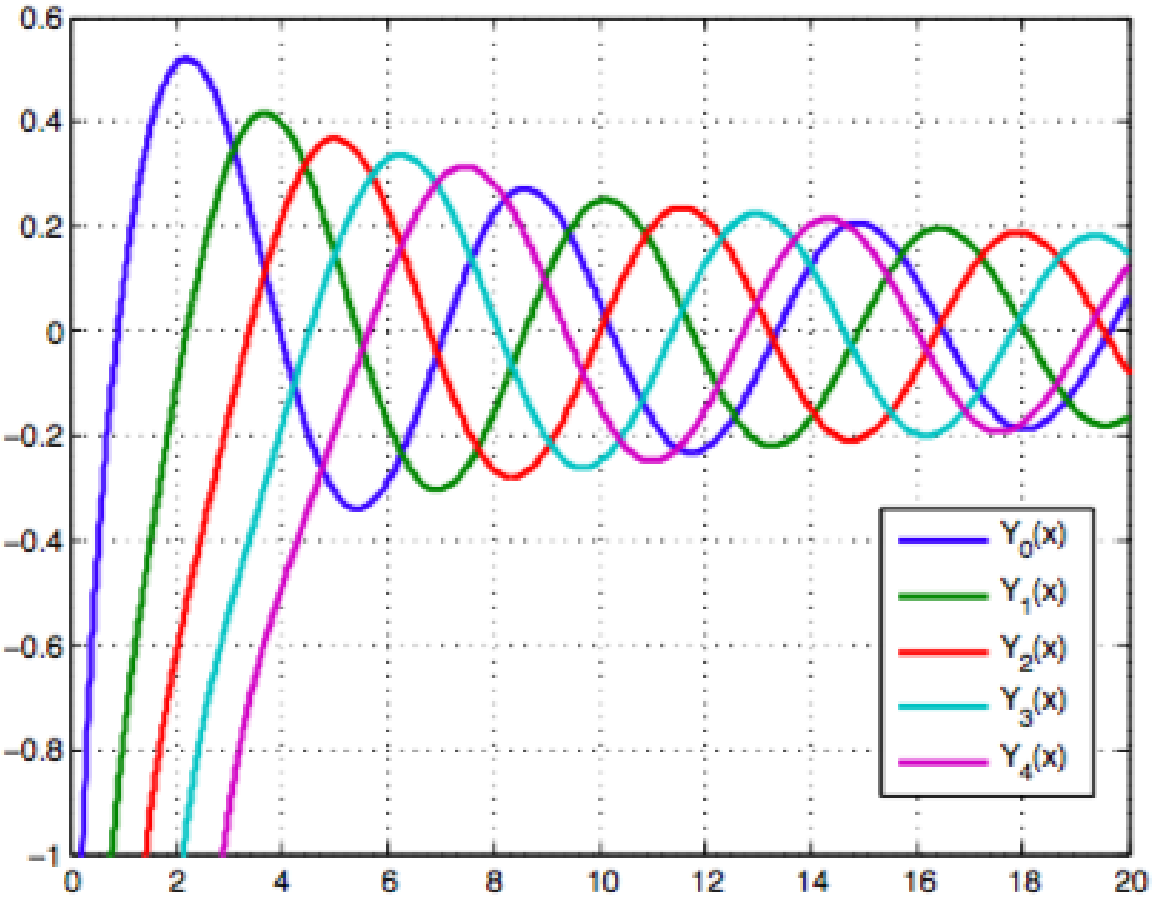

Figure 10.2: Neumann Function

Recalling the equation

$$\frac{d^2\Phi}{d\phi^2} + n^2\Phi(\phi) = 0, \tag{10.60}$$

let $\Phi = e^{r\phi}$ be a solution of the equation above, then substitute $\frac{d\Phi}{d\phi} = re^{r\phi}$ and $\frac{d^2\Phi}{d\phi^2} = r^2e^{r\phi}$ into the equation we get,

$$r^2e^{r\phi} + n^2e^{r\phi} = 0, \tag{10.61}$$

$$e^{r\phi}(r^2 + n^2) = 0, \tag{10.62}$$

since $e^{r\phi}$ is never zero, the above equation is satisfied (and therefore$e^{r\phi}$ is a solution if and only if $r^2+n^2 = 0$).This polynomial is called the characteristic polynomial of the differential equation and each and every root, sometimes called a characteristic root, r, and linear superposition of the. solution made by characteristic roots is also a solution of the differential equation.Therefore, a general solution is,

$$\Phi = A_1e^{r_1\phi} + A_2e^{r_2\phi}, \tag{10.63}$$

$$\Phi = A_1e^{jn\phi} + A_2e^{-jn\phi}, \tag{10.64}$$

$$\Phi = A_1(cos(n\phi) + jsin(n\phi)) + A_2(cos(n\phi) - jsin(n\phi)) = A_1cos(n\phi) + A_2cos(n\phi), \tag{10.65}$$

A_1 and A_2 can be obtained from the boundary conditions.
so for the $\phi(\phi)$ we can write,

$$\phi(\phi) = A_1cos(n\phi) + A_2cos(n\phi), \tag{10.66}$$

and recalling the last equation,

$$\frac{d^2Z(z)}{dz^2} + k_z^2Z = 0, \tag{10.67}$$

the same procedure has done for $\Phi(\phi)$ and the solution can be written as,

$$Z(z) = B_1cos(k_zz) + B_2cos(k_zz). \tag{10.68}$$

Replacing Eq.s (10.49), (10.66) and (10.68) in equation $\psi = R(\rho)\Phi(\phi)Z(z)$, we obtained complete solution of wave equation in cylindrical coordinates.

10.2 Appendix-B

Floquet Theory:

Consider the linear periodic system as follows.

$$\dot{x} = A(t)x, A(t+p) = A(t), p > 0, \tag{10.69}$$

where A(t) ∈ C(R). Lemma: If C is a $n \times n$ matrix with det C $\neq 0$, then, there exists a $n \times n$ (complex) matrix B such that $e^B = C$.

Proof: For any matrix C, there exists an invertible matrix P, s.t. $P^{?1}CP = J$, where J is a Jordan matrix.

If $e^B = C$,then, $e^{P^{-1}BP} = P^{-1}e^BP = P^{-1}CP = J$.Therefore, it is suffice to prove the result when C is in a canonical form.

Suppose that $C = diag(C_1, C_2, ..., C_s)$, $C_j = \lambda_j I_j + N_j$, where N_j is nilpotent, that is,

Since C is invertible for each $\lambda \neq 0$.

If we can show that for each C_j, there exists B_j s.t. $C_j = e^{B_j} \rightarrow C = e^B$. Since $C_j = \lambda_j(I_j + \frac{N_j}{\lambda_j})$, using the expansion of $ln(1+x) = \Sigma_{k=1}^{\infty}\frac{(-1)^{k+1}}{k}x^k$, $|x| < 1$, we have,

$$B_j = lnC_j = ln\{\lambda_j(I_j + \frac{N_j}{\lambda_j})\} = I_j ln\lambda_j + ln(I_j + \frac{N_j}{\lambda_j}),$$

$$= I_j ln\lambda_j + \Sigma_{k=1}^{\infty}\frac{(-1)^{k+1}}{k}(\frac{N^k}{\lambda^k}). \tag{10.70}$$

Since $N_j^{n_j} = 0$, we actually have

$$B_j = lnC_j = I_j ln\lambda_j + \Sigma_{k=1}^{n_j-1}\frac{(-1)^{k+1}}{k}(\frac{N^k}{\lambda^k}) = I_j ln\lambda_j + M_j, j = 1, 2, ..., s, \tag{10.71}$$

where $M_j = \Sigma_{k=1}^{n_j-1}\frac{(-1)^{k+1}}{k}(\frac{N^k}{\lambda^k})$. Therefore, we have,

$$e^{B_j} = exp\{I_j ln\lambda_j + M_j\} = exp\{ln\ C_j\} = C_j, \quad j = 1, 2, ..., s. \tag{10.72}$$

Let $B = diag(B_1, ..., B_s)$, where B_j is defined above. We have the desired result given by

$$e^B = diag(e^{B_1}, e^{B_2}, ..., e^{B_s}) = diag(C_1, C_2, ..., C_s) = C. \tag{10.73}$$

Clearly, B is not unique since $e^{B+2\pi kiI_n} = e^B e^{2\pi kiI_n} = e^B e^{2\pi ki} I_n = e^B e^{2\pi ki} = e^B$ for any integer k.

Floquet Theorem states that if $\Phi(t)$ is a fundamental matrix solution of the periodic system $\dot{x} = A(t)x$, then so is $\Phi(t+p)$. Moreover, there exists an invertible matrix P(t) with p-period such that

$$\Phi(t) = P(t)e^{Bt}. \tag{10.74}$$

Proof of the theory: Let $\Psi(t) = \Phi(t+p)$. Since $\Phi'(t) = A(t)\Phi(t)$, it follows that

$$\Psi(t) = \Phi'(t+p) = A(t+p)\Phi(t+p) = A(t)\Psi(t), \tag{10.75}$$

Hence, $\Psi(t)$ is also a matrix solution. Since $\Phi(t)$ is invertible for all t $\in$ R , so is $\Phi(t+p) \Rightarrow \Psi(t)$ is also a fundamental matrix solution. Therefore, there exists an invertible matrix C (for example, if $\Phi(t)$ satisfies $\Phi(0) = I_n$, then $C = \Phi(p)$. Depends on solutions. It is a point of difficulty for computation) s.t.

$$\Phi(t+p) = \Phi(t)C \quad for \quad all \quad t \ \in \ R \tag{10.76}$$

By the results above there exists a matrix B such that $e^{Bp} = C$. For such a matrix B, we take $P(t) := \Phi(t)e^{-Bt}$, that is, $\Phi(t) = P(t)e^{Bt}$. Then

$$P(t+p) = \Phi(t+p)e^{-B(t+p)} = \Phi(t)Ce^{-B(t+p)} = \Phi(t)e^{-Bt} = P(t). \tag{10.77}$$

Therefore $P(t)$ is invertible for all t $\in$ R and p-periodic. This concludes the proof.

10.3 Appendix-C

The main mode is monopole (TM_{010}) mode:

$$E_z^{010} = e^{i(\omega t+\phi_0)}E_0 cos(kz)J_0(k_c r). \tag{10.78}$$

We can write the definition of the Bessel function,

$$J_\nu(x) = (\frac{x}{2})^\nu \Sigma_{k=0}^{\infty} \frac{(-1)^k}{\Gamma(k+1)\Gamma(\nu+k+1)}(\frac{x}{2})^(2k), \tag{10.79}$$

taking the first two terms we have,

$$J_0(k_c r) = 1 - \frac{k_c^2}{4}r^2, \tag{10.80}$$

substituting the equation above inside the Eq. (10.78),

$$E_z^{010} \simeq e^{i(\omega t+\phi_0)}E_0 cos(kz)(1 - \frac{k_c^2}{4}r^2) \tag{10.81}$$

Writing the equation above in the cartessian coordinate,

$$E_z^{010} \simeq e^{i(\omega t+\phi_0)} E_0 cos(kz)(1 - \frac{k_c^2}{4}(x^2 + y^2)). \tag{10.82}$$

The equation for the dipole TM_{110} mode is,

$$E_z^{110} = e^{i(\omega t+\phi_0)} E_1 cos(kz) J_1(k_c r) cos(\theta - \frac{\pi}{2}), \tag{10.83}$$

$$\simeq e^{i(\omega t+\phi_0)} E_1 cos(kz) \frac{k_c r}{2} sin\theta, \tag{10.84}$$

replacing $E_1 = \frac{2a_1 E_0}{k_c}$ into the equation above where a_1 is the relative strength of the dipole field to the monopole field and it can be written as,

$$a_1 = \frac{E_1}{E_0} \times \frac{k_c}{2}, \tag{10.85}$$

then the Eq. (10.83) can be written as,

$$E_z^{110} \simeq e^{i(\omega t+\phi_0)} a_1 E_0 cos(kz)\ y. \tag{10.86}$$

The quadropole TM_{210} mode is as follows,

$$E_z^{210} = e^{i(\omega t+\phi_0)} E_2 cos(kz) J_2(k_c r) cos[2(\theta - \frac{\pi}{2})], \tag{10.87}$$

$$= e^{i(\omega t+\phi_0)} E_2 cos(kz) J_2(k_c r)(cos^2\theta - sin^2\theta), \tag{10.88}$$

where,

$$J_2(k_c r) \simeq -\frac{k_c^2 r^2}{8}, \tag{10.89}$$

$$E_z^{210} \simeq -e^{i(\omega t+\phi_0)} E_2 cos(kz) \frac{k_c^2 r^2}{8}(cos^2\theta - sin^2\theta), \tag{10.90}$$

$$\simeq -e^{i(\omega t+\phi_0)} a_2 E_0 cos(kz)(x^2 - y^2), \tag{10.91}$$

where,

a_2 : relative strength of the quadropole field to the monopole field,

$a_2 E_0 = \frac{k_c^2}{8} E_2$,

$a_2 = \frac{E_2}{E_0} \times \frac{k_c^2}{8}$.

Octopole TM_{410} mode:

$$E_z^{410} = e^{i(\omega t+\phi_0)} E_2 cos(kz) J_4(k_c r) cos[4(\theta - \frac{\pi}{2})], \tag{10.92}$$

$$\simeq e^{i(\omega t+\phi_0)} E_4 cos(kz) J_4(k_c r) [\frac{1}{4!}(\frac{k_c r}{2})^4] cos4\theta, \tag{10.93}$$

where, $J_4(k_c r) \simeq \frac{1}{4}(\frac{k_c r}{2})^4$,

$$\simeq e^{i(\omega t+\phi_0)} a_4 E_0 cos(kz)(x^4 - 6x^2y^2 + y^4), \tag{10.94}$$

where,

$r^4 cos4\theta = r^4 cos(2\theta + 2\theta) = r^4[cos^2 2\theta - sin^2 2\theta]$,

$= r^4[(cos^2\theta - sin^2\theta)^2 - (2sin\theta cos\theta)^2]$,

$= r^4[cos^4\theta + sin^4\theta - 6sin^2\theta cos^2\theta]$,

$= r^4 cos^4\theta + r^4 sin^4\theta - 6r^4 sin^2\theta cos^2\theta$,

$= x^4 - 6x^2y^2 + y^4$,

$a_4 E_0 = E_4 \times \frac{1}{4!} \times \frac{k_c^4}{16}$,

$a_4 = \frac{E_4}{E_0} \times \frac{k_c^4}{4! \times 16}$,

a_4 : relative strength of the octopole field to the monopole field,

then,

$$E_z^{410} \simeq e^{i(\omega t+\phi_0)} a_4 E_0 cos(kz)(x^4 - 6x^2y^2 + y^4). \tag{10.95}$$

10.4 Appendix-D

The normalized transverse monopole kick for an electron beam is,

$$P_{n,\perp} = \frac{mv}{mc}, \tag{10.96}$$

where mv is the transverse momentum imparted to the electron,

$$P_{n,\perp}^{010} = \frac{1}{mc} P_{\perp}^{010}, \tag{10.97}$$

then the equation can be calculated by the Panofsky-Wenzel theorem for a single electron as,

$$P^{010}_{n,\perp} = \frac{1}{mc} Re(\frac{e}{\omega} \int_{-\frac{L}{2}}^{\frac{L}{2}} i\nabla_\perp E^{010}_z \; dz), \tag{10.98}$$

$$= \frac{1}{mc} Re(\frac{e}{\omega} \int_{-\frac{L}{2}}^{\frac{L}{2}} [i\frac{\partial}{\partial x} E^{010}_z + i\frac{\partial}{,}\partial y E^{010}_z] dz) \tag{10.99}$$

substituting the results from the appendix C we have,

$$P^{010}_{n,\perp} = \frac{1}{mc} Re(\frac{e}{\omega} \int_{-\frac{L}{2}}^{\frac{L}{2}} i\frac{\partial}{\partial x}[E_0 e^{i\phi}(1-\frac{k_c^2}{4}(x^2+y^2))]dz) + \frac{1}{mc} Re(\frac{e}{\omega} \int_{-\frac{L}{2}}^{\frac{L}{2}} i\frac{\partial}{\partial y}[E_0 e^{i\phi}(1-\frac{k_c^2}{4}(x^2+y^2))]dz), \tag{10.100}$$

$$= \frac{1}{mc} Re(\frac{e}{\omega} \int_{-\frac{L}{2}}^{\frac{L}{2}} [-iE_0 e^{i\phi} \frac{k_c^2}{2} \; x]dz) + \frac{1}{mc} Re(\frac{e}{\omega} \int_{-\frac{L}{2}}^{\frac{L}{2}} [-iE_0 e^{i\phi} \frac{k_c^2}{2} \; y]dz), \tag{10.101}$$

$$= \frac{1}{mc} Re(\frac{e}{\omega} \int_{-\frac{L}{2}}^{\frac{L}{2}} [-iE_0 \; (cos\phi + isin\phi) \frac{k_c^2}{2} \; x]dz) + \frac{1}{mc} Re(\frac{e}{\omega} \int_{-\frac{L}{2}}^{\frac{L}{2}} [-iE_0 \; (cos\phi + isin\phi) \frac{k_c^2}{2} \; y]dz), \tag{10.102}$$

we only need to consider the real part of integral,

$$P^{010}_{n,\perp} = \frac{1}{mc} Re(\frac{e}{\omega} \int_{-\frac{L}{2}}^{\frac{L}{2}} E_0 \; sin\phi \frac{k_c^2}{2} \; x \; dz) + \frac{1}{mc} Re(\frac{e}{\omega} \int_{-\frac{L}{2}}^{\frac{L}{2}} E_0 \; sin\phi \frac{k_c^2}{2} \; y \; dz), \tag{10.103}$$

$$= \frac{1}{mc} \frac{e}{\omega} E_0 \; sin\phi \frac{k_c^2}{2} \; L \; x + \; \frac{1}{mc} \frac{e}{\omega} E_0 \; sin\phi \frac{k_c^2}{2} \; L \; y, \tag{10.104}$$

$$= \frac{1}{mc} \frac{e}{\omega} E_0 \; sin\phi_0 \frac{k_c^2}{2} \; L \; (x\hat{x} + y\hat{y}), \tag{10.105}$$

with some simplification it can be written as,

$$P^{010}_{n,\perp} = \frac{1}{mc^2} \frac{e}{k} E_0 \; sin\phi_0 \frac{k_c^2}{2} \; L \; (x\hat{x} + y\hat{y}), \tag{10.106}$$

where α is the normalized rf field strength

$$\alpha = \frac{eE_0}{mc^2 k}, \tag{10.107}$$

finally for the normalized transverse monopole kick for a single electron we have,

$$P^{010}_{n,\perp} = \frac{k_c^2}{2} \alpha L \; sin\phi_0 \; (x\hat{x} + y\hat{y}). \tag{10.108}$$

The normalized transverse dipole kick for a single electron is:

$$P_{n,\perp}^{110} = \frac{1}{mc}\ Re(\frac{e}{\omega}\int_{-\frac{L}{2}}^{\frac{L}{2}} i\nabla_\perp E_z dz), \tag{10.109}$$

$$= \frac{1}{mc}Re(\frac{e}{\omega}\int_{-\frac{L}{2}}^{\frac{L}{2}}[i\frac{\partial}{\partial x}E_z^{110}]dz) + \frac{1}{mc}Re(\frac{e}{\omega}\int_{-\frac{L}{2}}^{\frac{L}{2}}[i\frac{\partial}{\partial y}E_z^{110}]dz), \tag{10.110}$$

taking the results for the dipole TM110 mode from the appendix C and substituting inside the equation above,

$$P_{n,\perp}^{110} = \frac{1}{mc}Re(\frac{e}{\omega}\int_{-\frac{L}{2}}^{\frac{L}{2}}[i\frac{\partial}{\partial x}(e^{i(\omega t+\phi)}a_1 E_0 cos(kz)\ y]dz) + \frac{1}{mc}Re(\frac{e}{\omega}\int_{-\frac{L}{2}}^{\frac{L}{2}}[i\frac{\partial}{\partial y}(e^{i(\omega t+\phi)}a_1 E_0 cos(kz)\ y]dz), \tag{10.111}$$

taking the real part of integral

$$= -\frac{1}{mc}Re(\frac{e}{\omega}\int_{-\frac{L}{2}}^{\frac{L}{2}} a_1 E_0 cos\phi_0 dz), \tag{10.112}$$

$$= -2\frac{1}{mc}\frac{e}{\omega}a_1 E_0 sin\phi_0 L, \tag{10.113}$$

finally the normalized transverse monopole kick for an electron beam can be written

$$P_{n,\perp}^{110} = -2\ a_1\ \alpha\ L\ sin\phi_0 \hat{y}. \tag{10.114}$$

The normalized transverse quadrupole kick for a single electron is

$$P_{n,\perp}^{210} = \frac{1}{mc}Re(\frac{e}{\omega}\int_{-\frac{L}{2}}^{\frac{L}{2}} i\nabla_\perp E_z^{210}\ dz), \tag{10.115}$$

following the same procedure as for the normalized transverse dipole kick for a single electron that we have obtained for the normalized transverse quadrupole kick we can obtain,

$$P_{n,\perp}^{210} = 2a_2\alpha L sin\phi_0(x\hat{x} - y\hat{y}). \tag{10.116}$$

The normalized transverse octopole kick can be written according to the Panofsky-Wenzel theorem for a single electron as

$$P_{n,\perp}^{410} = \frac{1}{mc}Re(\frac{e}{\omega}\int_{-\frac{L}{2}}^{\frac{L}{2}} i\nabla_\perp E_z^{410}\ dz), \tag{10.117}$$

$$= \frac{1}{mc} Re(\frac{e}{\omega} \int_{-\frac{L}{2}}^{\frac{L}{2}} [i\frac{\partial}{\partial x} E_z^{410}]dz) + \frac{1}{mc} Re(\frac{e}{\omega} \int_{-\frac{L}{2}}^{\frac{L}{2}} [i\frac{\partial}{\partial y} E_z^{410}]dz), \tag{10.118}$$

substituting the results from the appendix C and some simplification it can be written as

$$P_{n,\perp}^{410} = \frac{1}{mc} Re(\frac{e}{\omega} \int_{-\frac{L}{2}}^{\frac{L}{2}} [i\frac{\partial}{\partial x}(e^{i(\omega t+\phi)} a_4 E_0 cos(kz)(x^4 - 6x^2y^2 + y^4)]dz)$$

$$+ \frac{1}{mc} Re(\frac{e}{\omega} \int_{-\frac{L}{2}}^{\frac{L}{2}} [i\frac{\partial}{\partial y}(e^{i(\omega t+\phi)} a_4 E_0 cos(kz)(x^4 - 6x^2y^2 + y^4)]dz) \tag{10.119}$$

$$= +\frac{1}{mc}\frac{e}{\omega} a_4 E_0 sin\phi_0 \int_{-\frac{L}{2}}^{\frac{L}{2}} [i\frac{\partial}{\partial x}(x^4 - 6x^2y^2 + y^4) + i\frac{\partial}{\partial y}(x^4 - 6x^2y^2 + y^4)]dz, \tag{10.120}$$

$$= +\frac{1}{mc}\frac{e}{\omega} a_4 E_0 sin\phi_0 [4x^3 - 12xy^2 - 12x^2y + 4y^3], \tag{10.121}$$

$$= +\frac{-4}{mc}\frac{e\lambda}{2\pi c} a_4 E_0 sin\phi_0 [(x^3 - 3xy^2)\hat{x} + (y^3 - 3x^2y)\hat{y}], \tag{10.122}$$

finally for the normalized transverse ocopole kick for a single electron we have,

$$P_{n,\perp}^{410} = -4a_2 \alpha L sin\phi_0 [(x^3 - 3xy^2)\hat{x} + (y^3 - 3x^2y)\hat{y}]. \tag{10.123}$$

Chapter 11

Bibliography

[1] R. E. Collin, Foundations for Microwave Engineering, McGraw-Hill Book Co., New York, 1992.

[2] M. Weiss, Fundamentals of ion Linacs, CAS Cern Accelerator School.

[3] M. Weiss, Introduction to RF linear accelerators, CAS Cern Accelerator School.

[4] T. Wangler, Principles of RF Linear Accelerators, Wiley, New York, 1998.

[5] R. H. Miller, Comparison of standing-wave and traveling-wave structures, 2003.

[6] J. D. Jackson, Classical Electrodynamics, Third Edition.

[7] S. De Santis, M. Migliorati, L. Palumbo, and M. Zobov, Phys. Rev. E 54, 800 (1996).

[8] H. Bethe, Theory of diffraction by small holes Phys. Rev. 66, 163-182 (1944).

[9] S. De Santis, A. Mostacci, and L. Palumbo, Phys. Rev. E 56, 1997, pp.5990-5995.

[10] P.Emma, LCLS-TN-01-1,SLAC 2001.

[11] D. Alesini, A. Falone, M. Migliorati, A. Mostacci, F. Palpini, L. Palumbo, and B. Spataro, "Design and RF measurements of an X-band accelerating structure for linearizing the longitudinal emittance at SPARC." Nucl. Instrum. Methods Phys. Res. A 554, 1-12 2005.

[12] J. W. S. Strutt Lord Rayleigh , The Theory of Sound, Vol. 1, 2nd. ed. Dover, New York, 1945.

[13] B. Auld, Acoustic Fields and Waves in Solids, Wiley-Interscience, New York, 1973.

[14] L. Brillouin, Wave Propagation in Periodic Structures, Dover, New York, 1953.

[15] www.ansoft.com.

[16] W. H. Eggimann, "Higher-Order Evaluation of Electromagnetic Diffraction by Circular Disks," IRE Trans. Microwave Theory and Tech., Vol. MTT-9, pp. 408-18, September 1961.

[17] R. E. Collin, "Field Theory of Guided Waves", McGraw-Hill Book Company , Inc., New York, 1960.

[18] E. Jensen, RF Cavity Design, CERN, Geneva, Switzerland.

[19] D. M. Pozar, Microwave Engineering, 3rd edition, Wiley, New York, 2005.

[20] N.A. McDonald, Electric and magnetic coupling through small apertures in shield walls of any thickness, IEEE Trans. Microwave Theory Tech., MTT-20, no. 10, 1972, pp.689-695.

[21] R. L. Gluckstem and J. A. Diamond, "Penetration of Fields Through a Circular Hole in a Wall of Finite Thickness", IEEE Trans. Microwave Theory Tech., vol. 39, no. 2, 1991.

[22] V. Dolgashev etal., Advances in X-band TW accelerator structures operating in the 100MV/m regime, proceedings of International Particle Accelerator Conference (IPAC 2010), May 23-28, Kyoto, Japan, 2010.

[23] V. Dolgashev, Recent progress in high gradient accelerating structures, seminar held at LNF (Sept., 2010).

[24] Pompili, R., Anania, M. P., Bellaveglia, M., Biagioni, A., Castorina, G., Chiadroni, E. Fil-

ippi, F. (2016). Femtosecond timing-jitter between photo-cathode laser and ultra-short electron bunches by means of hybrid compression. New Journal of Physics, 18(8), 083033.

[25] V. Dolgashev et al., Geometric dependence of radio-frequency breakdown in normal conducting accelerating structures , Appl. Phys. Lett. 97 (2010) 171501.

[26] B. Spataro et al., Technological issues and high gradient test results on X-band molybdenum accelerating structures, Nucl. Instrum. Meth. A 657 (2011) 114.

[27] B. Spataro etal., High-power comparison among brazed, clamped and electroformed X-band cavities, Nucl. Instrum. Meth. A 657 (2011) 88.

[28] R. Pompili, G. Castorina et al., Experimental characterization of the active plasma lens device (subm. 2016).

[29] A. W. Kraszewski, and S. O. Nelson, Observations on resonant cavity perturbation by dielectric objects, IEEE Transactions on Microwave Theory and Techniques, Vo.40, pp.151-155, January 1992.

[30] J.C. Slater, L.C. Maier, J. Appl. Phys. 23 (1) (1952) 68.

[31] P.J. Petersana, S.M. Anlage, J. Appl. Phys. 84 (6) (1998) 3392.

[32] E. Jensen, RF Cavity Design, CERN BE/RF CERN Accelerator School Accelerator Physics Chios, 2011.

[33] L. Faillace, Ph.D dissertation, Universita degli Studi di Roma “La Sapienza”, 2009.

[34] L. Faillace, Private communication, INFN-LNF, Italy.

[35] C. G. Montgomery, Technique of Microwave Measurements (MIT Radiation Laboratory Series 11). New York: McGraw-Hill, 1951.

[36] Romanofsky, R.R.: Analytical and Experimental Procedures for Determining Propagation

Characteristics of mm-Wave Ga As Microstrip Lines. NASA TP-2899, 1989.

[37] R. S. Kwok and J-F Liang, "Characterization of High-Q Resonators for Microwave-Filter Applications", IEEE Trans. Microwave Theory Tech., vol. 47, no. 1, 1999.

[38] A. Khanna and Y.Garault, "Determination of Loaded, Unloaded, and External Quality Factors of a Dielectric Resonator Coupled to a Microstrip Line", IEEE Trans. Microwave Theory Tech., vol. MTT-31, no. 3, 1983.

[39] J. C. Slater, "Microwave Electronics." Reviews of Modern Physics 18 (1946).

[40] Daniel S. Weile, Department of Electrical and Computer Engineering University of Delaware, ELEG 648-Waves in Cylindrical Coordinates.

[41] D. P. Pritzkau, "RF Pulsed Heating", SLAC-Report-577 ,Ph.D. Dissertation, Stanford University, 2001.

[42] M. Dal Forno, E. Nanni, V. Dolgashev, private communication (2016).

[43] X. Guan, C. Tang, H. Chen, W. Huang, X. He, P. Xu, and R. Li, Nucl. Instrum. Methods Phys. Res., Sect. A 574, 17 (2007).

[44] K.J. Kim, Nucl. Instrum. Methods Phys. Res., Sect. A 275, 201 (1989).

[45] D. T. Palmer, R. H. Miller, H. Winick, X. J. Wang, K. Batchelor, M. Woodle, and I. Ben-Zvi, in Proceedings of the Particle Accelerator Conference, Dallas, TX, 1995 (IEEE, Piscataway, 1995), pp. 982?984.

[46] D.H. Dowell, E. Jongewaard, J. Lewandowski, C. Limborg, Z. Li, J. Schmerge, A. Vlieks, J. Wang, and L. Xiao, SLAC Report No. SLAC-PUB-13401, 2008.

[47] M. S. Chae etal., Phys. Rev. ST Accel. Beams 14, 104203 (2011).

[48] B. Spataro etal., RF design for the TOPGUN photogun: A cryogenic normal conducting

copper electron gun, Nucl. Instrum. Meth. A 865 (2017) 105-108.

[49] W. K. H. Panofsky and W. A. Wenzel, Rev. Sci. Instrum. 27, 967 (1956).

[50] M.J. Browman, in Proceedings of the 1993 Particle Accelerator Conference, Washington, DC, 1993 (IEEE, Piscataway, NJ, 1993), pp. 800?802.

[51] J.B. Rosenzweig, S. Anderson, X. Ding, and D. Yu, in Proceedings of the 1999 Particle Accelerator Conference, New York, New York, 1999 (IEEE, Piscataway, NJ, 1999), pp. 2042?2044.

[52] G. Castorina etal., INFN, Demetra Activity Report, 2017.

[53] G. Castorina,. etal, A novel highly symmetric TM_{01} mode launcher for ultimate brightness applications, INFN-LNF-18-01, 2018.

[54] A. Cahill, V. Dolgashev, and M. Dal Forno. "TM_{01} mode launcher for use in high brightness photoguns." (2016): MOPMW039.

[55] D. Alesini etal., INFN, Demetra Activity Report, 2016.

[56] V. Dolgashev etal., (2016). High power tests of an electroforming cavity operating at 11.424 GHz. Journal of Instrumentation, 11(03), P03010.

[57] G. Gatti et al., "X-band accelerator structures", Nuclear Instruments and Methods in Physics Research Section A: Accelerators, Spectrometers, Detectors and Associated Equipment 829 (2016): 206-212.

[58] A. Brynes, G. Castorina, O. Frasciello, A. Marcelli and B. Spataro, Studies of geometric wakefields and impedances due to collimators, INFN-16-10/LNF, June 30, 2016.

[59] A. Grudiev, S. Calatroni, and W. Wuensch, Phys. Rev. ST Accel. Beams 12, 102001 (2009).

[60] S. Doebert, et al., High gradient performance of nlc/glc x-band accelerating structures, in:

Proceedings of the 21st Particle Accelerator Conference, Knox- ville, TN, 2005.

[61] A. Grudiev, S. Calatroni, W. Wuensch, New local field quantity describing the high gradient limit of accelerating structures, Phys. Rev. ST-Accel. Beams 12 (1020) (2009) 01.

[62] A. Yariv and P. Yeh, Phys. Lett. 28, 735 (1976).

[63] L. Brillouin, Wave Propagation and Group Velocity (Academic Press, New York, 1960).

[64] J. W. Wang, Ph.D. Dissertation, Stanford Linear Accelerator Center, Stanford, California, 94309, 1989.